



## City Research Online

### City, University of London Institutional Repository

---

**Citation:** Patil, S. (2023). Research in Profiling and Development of a New Screw Rotor Profile. (Unpublished Doctoral thesis, City, University of London)

This is the accepted version of the paper.

This version of the publication may differ from the final published version.

---

**Permanent repository link:** <https://openaccess.city.ac.uk/id/eprint/31012/>

**Link to published version:**

**Copyright:** City Research Online aims to make research outputs of City, University of London available to a wider audience. Copyright and Moral Rights remain with the author(s) and/or copyright holders. URLs from City Research Online may be freely distributed and linked to.

**Reuse:** Copies of full items can be used for personal research or study, educational, or not-for-profit purposes without prior permission or charge. Provided that the authors, title and full bibliographic details are credited, a hyperlink and/or URL is given for the original metadata page and the content is not changed in any way.

# Research in Profiling and Development of a New Screw Rotor Profile



**Sumit J Patil**

Doctor of Philosophy in Mechanical Engineering

**Centre for Compressor Technology  
School of Science and Technology  
City, University of London**

July 2023



*I dedicate this thesis to my beloved late grandmother who taught me everything from reading and counting to being a good man. . . .*



# Contents

<b>Contents</b>	<b>v</b>
<b>List of Figures</b>	<b>ix</b>
<b>List of Tables</b>	<b>xiii</b>
<b>List of Symbols</b>	<b>xv</b>
<b>Acknowledgments</b>	<b>xvii</b>
<b>Declaration</b>	<b>xix</b>
<b>Abstract</b>	<b>xxi</b>
<b>1 Introduction</b>	<b>1</b>
1.1 Screw Compressors . . . . .	2
1.2 Rotor Profiles . . . . .	4
1.3 Important Definitions . . . . .	4
1.3.1 Main Rotor, Gate Rotor and Rack . . . . .	5
1.3.2 Throughput Area / Displacement . . . . .	6
1.3.3 Clearances - Axial, Radial and Interlobe . . . . .	6
1.3.4 Interlobe Sealing Line . . . . .	7
1.3.5 Blow Hole . . . . .	8
1.4 Motivation for New Profile Development . . . . .	9
<b>2 Literature Review</b>	<b>11</b>
2.1 General Review . . . . .	12
2.2 Review of Methods . . . . .	18
2.3 On the Manufacturability of Rotor Profiles . . . . .	26
2.4 Study of N-Rack Characteristics and its Curves . . . . .	29
2.4.1 Rack Section D-E . . . . .	31
2.4.2 Rack Section D-C, E-F and A-H (Rotor Tips) . . . . .	32
2.4.3 Rack Section A-B-C (Long Edge) . . . . .	33
2.4.4 Rack Section F-G-H-A (Short Edge) . . . . .	35
2.5 Review of Performance Calculations in Screw Compressors . . . . .	36
2.6 Summary of the Literature Review . . . . .	38

<b>3</b>	<b>Methods and Approach</b>	<b>41</b>
3.1	Better Profiles, but how much? . . . . .	42
3.2	New Profile Development . . . . .	47
3.2.1	Conception . . . . .	47
3.2.1.1	Three Concepts for the New Profile . . . . .	47
3.2.1.2	The Concept of Homotopy . . . . .	48
3.2.2	Evaluation . . . . .	50
3.2.2.1	Methods to Evaluate Profile Geometry and Thermodynamic Performance . . . . .	50
3.2.2.2	Method to Evaluate Manufacturability (Stosic, 2006b) . . . . .	51
3.2.3	Validation . . . . .	56
3.3	Expected Contributions . . . . .	56
<b>4</b>	<b>Path Homotopy</b>	<b>59</b>
4.1	Homotopy in Rotor Profiling . . . . .	60
4.2	Rack Generated Homotopy Profiles . . . . .	64
4.2.1	Homotopic curves on long edge of the rack . . . . .	65
4.2.2	Homotopic curves on tips of the rack . . . . .	73
4.3	Summary of Homotopic Curves for the New Profile . . . . .	81
<b>5</b>	<b>Experiments with Further Profile Modifications</b>	<b>83</b>
5.1	Profile Generation to Minimize Oil Drag Loss . . . . .	84
5.2	Profiles Generated with Wide Gate Rotor Lobes . . . . .	88
5.3	Profile Generated by Combining Features of K-BETA1 and K-BETA2 . . . . .	91
5.4	Experimental Setup to Test K-BETA Profiles . . . . .	93
5.5	Results and Discussion . . . . .	94
5.5.1	Comparison of N and K-BETA1 Results . . . . .	95
5.5.2	Comparison of N and K-BETA2 Results . . . . .	96
5.5.3	Comparison of N and K-BETA3 Results . . . . .	97
5.5.4	Accuracy and Uncertainty Analysis . . . . .	98
5.6	Summary . . . . .	99
<b>6</b>	<b>Manufacturability</b>	<b>101</b>
6.1	Quantifying Manufacturability . . . . .	102
6.2	Modifying Relative Tool Wear Model with Considerations to Relative Speed between Tool and Rotor . . . . .	104
6.3	Manufacturability of Developed Profiles . . . . .	107
6.3.1	Comparison of H-Rack Profiles and N-Profile . . . . .	108
6.3.2	Comparison of K-BETA Profiles and N-Profile . . . . .	110
6.4	Summary . . . . .	111
<b>7</b>	<b>Conclusions and Future Scope</b>	<b>113</b>
7.1	Total Improvements in the New Profile . . . . .	114
7.2	Contributions of this Study . . . . .	117

7.3 Future Scope . . . . .	118
<b>A Euler-Lagrange Approach to Profile Optimization</b>	<b>121</b>
<b>B Application of Artificial Intelligence in Rotor Profiling</b>	<b>125</b>
<b>List of Publications</b>	<b>131</b>
<b>Bibliography</b>	<b>133</b>



# List of Figures

1.1	Illustration for the working principle of screw compressor (generated using SCORG) . . . . .	2
1.2	A screw compressor assembly (model by Kirloskar Pneumatic Co. Ltd.)	3
1.3	A typical rotor pair for twin-screw compressor plotted along with an imaginary rack, pitch circles and pitch line . . . . .	5
1.4	Illustration of various clearances in a twin-screw compressor . . . . .	6
1.5	Interlobe sealing line or the 3-D contact path of rotors . . . . .	7
1.6	Projections of interlobe sealing line on various planes . . . . .	7
1.7	3-D representation of blow-hole (Chapter 5, Svígler (2010)) . . . . .	8
1.8	A crude illustration of the blow-hole area projected on the profile plane	8
2.1	Early Symmetric Profiles . . . . .	14
2.2	The first efficient and fairly manufacturable asymmetric rotor profile, SRM-A (Schibbye, 1970) . . . . .	15
2.3	Later Asymmetric Profiles with Improved Manufacturability . . . . .	16
2.4	Rotor profile with ellipse and involute curve patented by Bowman (1983)	17
2.5	N-Profile Rack (Stosic, 1997) . . . . .	17
2.6	Demonstration of the envelope principle; conjugate curves on rotor pairs	19
2.7	Early Profiles Based on the Principle of Rack Generation . . . . .	21
2.8	Rack Profiles Closely Based on N-Rack . . . . .	21
2.9	A general rack profile along with its main and gate rotor profiles . . . . .	22
2.10	Optimized rotor profiles generated using bezier curves (Kauder et al., 2002) . . . . .	24
2.11	Illustration of the rack profile generating rotor virtually like a tool . . . . .	28
2.12	N-Rack with 7 curve sections on the rack profile . . . . .	30
2.13	The conjugate main and gate rotor profile sections generated from the respective N-Rack profile sections . . . . .	30
2.14	The representation of flat and inclined gate tip face . . . . .	32
2.15	Depiction of flatness characteristic of the arc at section A-B w.r.t parameter ‘n’ . . . . .	33
2.16	Influence of ‘n’ on Displacement area . . . . .	34
2.17	Influence of ‘n’ on Sealing line length . . . . .	34
3.1	4/6 Symmetric Circular Profile with center distance 100 mm . . . . .	43

3.2	4/6 SRM-A Profile with center distance 100 mm . . . . .	44
3.3	4/6 N-Profile with center distance 100 mm . . . . .	44
3.4	Retrofitted Profiles- Fu Sheng, Gardner Denver and N with 5/6 lobe combination and $\sim 100$ mm center distance . . . . .	45
3.5	Zoomed in view of the profiles in Figure 3.4 . . . . .	46
3.6	Profile development over the years Vs. improvements in energy efficiency	47
3.7	Demonstration of the homotopic deformations across any two curves defined in between fixed endpoints . . . . .	49
3.8	Homotopic deformations between a circle and an ellipse . . . . .	50
3.9	The rotor and tool coordinate system and orientation (Stosic, 2006b) . .	52
3.10	Rotor and tool Profiles for the benchmark N-Profile . . . . .	53
3.11	Rotor and tool profiles with and without stock metal ( $\delta$ enlarged to 1 mm for visualization) . . . . .	55
4.1	Example of the application of homotopy in a typical rotor profile (Patil et al., 2021) . . . . .	61
4.2	Two adjacent Homotopies $\mathcal{H}_1$ and $\mathcal{H}_2$ constructed within points $a-b$ and $c-d$ respectively with curves as depicted. . . . .	62
4.3	N-Rack profile for reference . . . . .	65
4.4	Algorithm for finding good combinations of curve parameters for homo- topies tested in H-Rack at $A - B$ . . . . .	68
4.5	H-Rack profile with $\mathcal{H}(Hyperbola, Parabola)$ at $A - B$ section in N-Rack	70
4.6	H-Rack profile with $\mathcal{H}(Hyperbola, Parabola)$ and $q = 0.8$ having same displacement as N-Rack but 0.9% shorter sealing line length . . . . .	72
4.7	N-Profiles generated by N-Racks with tip radii for $E - F$ as 2.5 mm and 1.5 mm . . . . .	74
4.8	N-Profile generated by omitting line $F - G$ in N-Rack retrofitted over the benchmark N-Profile with $F - G$ . . . . .	76
4.9	The application of homotopy constructed with an ellipse and a line to flatten(b) or sharpen(a) the gate rotor tips . . . . .	78
4.10	Profile generated with $\mathcal{H}(Ellipse, Line)$ at $E - F$ retrofitted with the benchmark N-profile which has a circle of radius 2.5 mm at $E - F$ . . .	79
4.11	Profile generated with $\mathcal{H}(Ellipse, Line)$ at $E - F$ retrofitted with bench- mark N-profile if it had 1 mm smaller radius at $E - F$ . . . . .	80
4.12	Homotopic curve constructed with a hyperbola and a parabola proposed for the long edge of the new profile rack . . . . .	81
4.13	Homotopic curve constructed with an ellipse and a line proposed for the high pressure side tip of the new profile rack . . . . .	82
5.1	141 mm benchmark N-profile used as a reference for profile modifications and comparisons . . . . .	84

5.2	141 mm benchmark N-profile gate rotor top land area of minimum clearance (marked red) that slides along rotor casing to create oil drag power loss . . . . .	85
5.3	The modified N-Profile with an inclined gate rotor top land (K-BETA1), plotted along with the benchmark 141 mm N-Profile . . . . .	85
5.4	141 mm BETA-1 profile (Figure 5.3) reduced gate rotor top land area of minimum clearance (marked red) that slides along the rotor casing . . .	86
5.5	Minimizing rotor casing - gate rotor top land sliding area by imposing variable clearance distribution on a regular profile . . . . .	86
5.6	N-Profile rack and K-BETA1 rack comparison . . . . .	87
5.7	The 141 mm K-BETA1 rotors manufactured at KPCL for testing . . . .	88
5.8	N-Profile optimized by box complex algorithm (Stosic et al., 2003b) for maximum adiabatic efficiency . . . . .	89
5.9	The modified N-Profile with wide gate rotor lobes (K-BETA1), plotted along with the benchmark 141 mm N-Profile . . . . .	90
5.10	141 mm K-BETA2 larger gate rotor top land area of minimum clearance (marked red) that slides along the rotor casing . . . . .	90
5.11	The 141 mm K-BETA2 rotors manufactured at KPCL for testing . . . .	91
5.12	The modified N-Profile with wide gate rotor lobes having inclined top land (K-BETA3), plotted along with the benchmark 141 mm N-Profile .	92
5.13	K-BETA2 and K-BETA3 rack comparison . . . . .	92
5.14	The K-BETA3 gate rotor manufactured at KPCL for testing . . . . .	93
5.15	A Kirloskar 55 kW oil-flooded, twin-screw, air compressor package used for testing K-BETA profiles . . . . .	93
5.16	The interlobe sealing lines of N and K-BETA1 profiles projected on the plane perpendicular to the rotor axes; marked portion indicates region of sealing line generated by the gate rotor top land . . . . .	95
5.17	The interlobe sealing lines of K-BETA2 and K-BETA3 profiles projected on the plane perpendicular to the rotor axes; marked portion indicates region of sealing line generated by the gate rotor top land . . . . .	98
6.1	Relative speeds between benchmark N-Profile rotors and their respective tools with setting $\Sigma=45^\circ$ , $C=200$ mm, $\omega_t=1500$ rpm, $\omega_r=15$ rpm . . . .	106
6.2	Relative tool wear indicators ( $TW_{ind}$ , Equation 6.7) for benchmark N-Profile rotors with $\delta=0.1$ mm, represented across the rotor profile coordinates . . . . .	106
6.3	Relative tool wear ( $TW_{rel}$ ) for benchmark N-Profile rotors with $\delta=0.1$ mm, represented across the rotor profile coordinates . . . . .	107
6.4	Relative tool wear indicators ( $TW_{ind}$ , Equation 6.7) for homotopy profile (Figure 4.6) with $\delta=0.1$ mm, represented across the rotor profile coordinates . . . . .	108

6.5	Relative tool wear indicators ( $TW_{ind}$ , Equation 6.7) for N-Profile with radius of $E - F$ 1.5 mm (Figure 4.7) with $\delta=0.1$ mm, represented across the rotor profile coordinates . . . . .	109
6.6	Relative tool wear indicators ( $TW_{ind}$ , Equation 6.7) for H-Profile with homotopy at $E - F$ (Figure 4.10) with $\delta=0.1$ mm, represented across the rotor profile coordinates . . . . .	110
6.7	Relative tool wear indicators ( $TW_{ind}$ , Equation 6.7) for K-BETA1 profile (Figure 5.3) with $\delta=0.1$ mm, represented across the rotor profile coordinates . . . . .	110
7.1	The complete K-Rack (H-Rack plus K-BETA1 features) sketch . . . . .	115
B.1	Three retrofitted 4/5 N-Profiles with different set of profile input parameters ( $R1, R2, R3, R4$ & $n$ ) . . . . .	126
B.2	The general framework and steps of setting up an artificial neural network model . . . . .	126
B.3	Plot of the specific powers predicted by ANN against those calculated by solving the chamber model for all the profiles in testing data-set . . .	128

# List of Tables

2.1	The curves constituting N-Rack and the respective conjugate curves on main and gate rotors . . . . .	31
3.1	Geometric profile characteristics for retrofitted Symmetric Profile, SRM-A and N-Profile . . . . .	43
3.2	Thermodynamic profile characteristics for retrofitted Symmetric Profile, SRM-A and N-Profile (oil injected air application, ambient suction and 8.5 bar discharge) . . . . .	44
3.3	Geometric profile characteristics for retrofitted Fu Sheng Profile, Gardner Denver Profile and N-Profile . . . . .	46
3.4	Thermodynamic profile characteristics for retrofitted Fu Sheng Profile, Gardner Denver Profile and N-Profile (oil injected air application, ambient suction and 8.5 bar discharge) . . . . .	46
4.1	Homotopic curves experimented in section $A - B$ of the N-Rack . . . . .	69
4.2	Percentage improvements in the H-Rack profiles based on geometric evaluation parameter- ratio of displacement to sealing line leakage area w.r.t benchmark N-Rack . . . . .	69
4.3	% improvements in H-Rack in Figure 4.5 w.r.t benchmark N-Profile . . . . .	70
4.4	% improvements in H-Rack in Figure 4.5 w.r.t benchmark N-Profile when more oil is present in the machine and clearances are even smaller . . . . .	71
4.5	% improvements in H-Rack in Figure 4.5 w.r.t benchmark N-Profile when less oil is present in the machine and clearances are larger . . . . .	71
4.6	% improvements in H-Rack in Figure 4.6 w.r.t benchmark N-Profile . . . . .	72
4.7	Comparison of geometric profile characteristics for N-Profiles generated from N-Racks with tip $E - F$ radii 2.5 mm and 1.5 mm . . . . .	73
4.8	% improvements in thermodynamic efficiencies of N-Profile with sharper tip (1.5 mm) at $E - F$ on rack in comparison to the benchmark profile (2.5 mm) . . . . .	74
4.9	Comparison of geometric characteristics of the profiles generated with and without the line $F - G$ in N-Rack . . . . .	75
4.10	% improvements in thermodynamic efficiencies of N-Profile generated without $F - G$ on rack in comparison to the benchmark profile (with $F - G$ ) . . . . .	76

4.11	Comparison of geometric profile characteristics for N-Rack with homotopy $\mathcal{H}(Ellipse, Line)$ at $E - F$ and the benchmark profile with circle at $E - F$ . . . . .	77
4.12	% improvements in thermodynamic efficiencies of N-Profile generated with homotopy $\mathcal{H}(Ellipse, Line)$ at $E - F$ on rack in comparison to the benchmark profile (with circle at $E - F$ ) . . . . .	77
5.1	Comparison of the experimental results of 141 mm benchmark N-Profile with the new K-BETA1 profile . . . . .	95
5.2	Comparison of the experimental results of 141 mm benchmark N-Profile with the new K-BETA2 profile . . . . .	96
5.3	Comparison of the experimental results of 141 mm benchmark N-Profile with the new K-BETA3 profile . . . . .	97
5.4	Accuracy of the instruments used in the experiments . . . . .	99
7.1	Adiabatic efficiencies of K-Profile in comparison to the retrofitted benchmark N-Profile; 1 bar suction and 6.5 bar discharge with internal clearances set to 35 micron . . . . .	116
7.2	Adiabatic efficiencies of K-Profile in comparison to the retrofitted benchmark N-Profile; 1 bar suction and 8.5 bar discharge with internal clearances set to 35 micron . . . . .	116
7.3	Adiabatic efficiencies of K-Profile in comparison to the retrofitted benchmark N-Profile; 1 bar suction and 14.5 bar discharge with internal clearances set to 35 micron . . . . .	116

# List of Symbols

$a$	Curve parameter
$b$	Curve parameter
$C$	Centre distance between tool and rotor
$\mathcal{C}$	A general mathematical curve
$f$	A general mathematical function mapping real numbers to real numbers
$h$	Rotor helicoid surface coordinates
$hn$	Coordinates normal to the rotor helicoidal surface
$\mathcal{H}$	A path homotopy
$\mathcal{H}(\mathcal{C}_1, \mathcal{C}_2)$	A homotopic construction between curves $\mathcal{C}_1$ and $\mathcal{C}_2$
$\hat{i}, \hat{j}, \hat{k}$	Unit vectors along principal orthogonal axes
$L/D$	Ratio of rotor's length to rotor's diameter
$\mathcal{L}$	An Euler-Lagrange integrand
$m$	Slope of a line
$n$	Curve parameter associated with the general arc in N-Profile
$O$	Objective function for optimization
$p$	Rotor lead per unit angle
$q$	Homotopy deformation parameter
$r$	General radius as a curve parameter OR rotor coordinates
$R$	General radii as a profile parameters OR main rotor addendum
$R0$	Gate rotor addendum
$t$	Curve parameter OR tool coordinates
$TW_{rel}$	Relative tool wear
$TW_{ind}$	Relative tool wear indicator/index
$V_{rel}$	Relative velocity
$x$	x-coordinate
$y$	y-coordinate
$z$	z-coordinate
$\delta$	Small distance normal to rotor helicoidal surface
$\omega$	Angular velocity
$\phi$	Profile parameter
$\Sigma$	Angle between tool and rotor axes
$\theta$	Angle of rotation



# Acknowledgments

The thesis presented is an outcome of a one-of-a-kind opportunity provided by the collaboration between my employer, Kirloskar Pneumatic Company Limited (KPCL), Pune, India and the Centre for Compressor Technology, City, University of London, London, U.K. where I enrolled as a part-time, external student in January 2020. Later in 2022, I converted the mode of my studies to full-time, external on account of the progress I was able to make with the support of my supervisors and employer.

I could not ask for a better supervisor to study rotor profiling than Prof. Stosic. He is the world's leading expert on screw compressors as well as the inventor of the renowned N-Profile. It is a matter of pride for me that I could pursue development of a new rotor profile under his supervision. His patience, motivation and constant guidance kept me focused during the work. I feel very honored to be his student.

I would also like to thank my second supervisor Prof. Kovacevic for his guidance and giving me valuable inputs on the study. He always motivated me to aim for the best results, do collaborations and supported me in all situations. I am truly grateful to have had the opportunity to work closely with him and have him as my supervisor.

Without the support of my manager Suraj Abdan and my team in Kirloskar who always allowed me to spend additional time on my PhD studies by sharing my responsibilities at work, doing this research effectively and efficiently would not have been possible. Herein, I wish to thank my external supervisor Neeraj Asati for always motivating me, keeping my spirits high and supporting in all the ways possible to make sure that I could conduct my research and experiments as smoothly as possible.

I wish to extend my gratitude to Prof. Smith for his valuable inputs regarding technical writing in multiple progress reports and research papers generated in the course of this study.

I wish to thank the management team of Kirloskar for believing in me to take up this challenging research and providing this opportunity. KPCL's higher management team-Aditya Kowshik, Srinivasan K, Aman Kirloskar, Sadashib Padhee, Neeraj Bhargava, Deepak Lokras, Neeraj Asati and Ganesh Chaudhari provided me with useful support in many ways.

Many thanks to my colleagues and friends who provided the necessary help and advice. Especially Suraj Abdan who happened to be a fellow PhD student and his work on oil drag losses triggered many important new profile concepts. Special thanks to Suraj Shelke who worked with me on his internship at KPCL and later became my colleague for helping me with developing multiple useful python programs for new profile

development. I would also like to highlight efforts and support from KPCL's manufacturing (Kalyan Mundhe, Amit Mahamuni, Vijay Sable, Swapnil Zinzurde, Nikhil Devade), packaging (Sethuraman K, Ashish Mundhe, Noor Khan, Shubham Dhokale) and quality assurance (Manishkumar Bhamare, Sharad Shirke) teams for new profile experiments and testing.

I learned a lot from my colleagues- Sagar Dundagekar, Ajinkya Shelke, Akash Dagar, Ajay Amle, fellow PhD students- Nausheen Basha, Yang Lu, Thibault Tam, Brijeshkumar Patel, Abhishek Kumar, research fellows and post docs- Sham Rane, Gursharanjit Singh, Thibaud Plantagenet. They not only gave technical inputs during our many discussions but also made this journey joyous and created lasting memories.

I also wish to thank Mr. Jack Sauls, Dr. Chris Holmes and Prof. Brummer for their valuable technical inputs during our discussions at various events and conferences. Their observations and inputs to my study have proven to be valuable for me.

Finally, I am highly indebted to my family and friends who offered a constant emotional support during this journey.

**Sumit J Patil**  
**London, 18<sup>th</sup> November 2022**

# Declaration

I confirm that this work is my own except where indicated by reference in the text. I agree for this work to be submitted to the Institutional Repository of City, University of London for use in accordance with the Thesis Deposit Agreement and the agreement between Kirloskar Pneumatic Co. Ltd. and City, University of London over confidentiality of the intellectual property which are outcome of their joint collaborative project.

**Sumit J Patil**  
**London, 18<sup>th</sup> November 2022**



# Abstract

Screw rotor profile impacts the overall performance of screw compressor to a large extent. Its improvement will directly impact the screw compressor efficiency and reduce the power consumption for unit flow of compressed gas under given conditions as well as manufacturing cost in comparison with a less efficient compressor; and thus reduce its environmental influence. In times where efforts to improve performance are taken at every level, it is only natural to take up research in the direction of improving rotor profiles for better energy efficiencies. Hence, this research is aimed at developing a new screw rotor profile in anticipation to improve the adiabatic efficiency of screw compressor while being equally or more manufacturable than existing well known profiles. A comprehensive literature review of the history and methods of rotor profiling along with their manufacturability aspect has been conducted. Based on this review, rack generated profiles comprising of analytical curves such as N-Profile seem to provide a strong basis for further improvements. Investigation into mathematical formalisms that can enable a wider search space for analytically represented curves on rack could pave the way to better rotor profiles. With better control and exploration of the profile curves, the best possible shape of profile for a given application can be designed. One such method from topology called ‘Path Homotopy’ which enables continuous morphing of one analytical curve into another is shown to be suitable and quite useful for designing more energy efficient rotor profiles. A mathematical basis to successfully use this idea in profiling has been developed and is used to design profiles having up to 2% better energy efficiency than the state of the art rotor profiles. The scope of this method adopted for profiling may have a wider reach into domain of shape optimization problems in mechanical engineering. The understanding of drag losses in screw machines was adopted to adjust profiles to have minimum drag losses. It is experimentally demonstrated to lead to substantial improvements in the overall energy efficiency of oil-injected screw compressors. The combined homotopy and drag minimizing profile generation results in 1.5-2.5% improvement in energy efficiency over benchmark N-Profile. Considering the maturity of the field of rotor profiling, improvement of this order on top of a good profile is quite significant. On the manufacturability aspect of profiles, methods from literature which quantify it in terms of relative tool wear across profiles have been modified to devise a scale which can be used to compare two profiles. Using this method, it is found that the new profile improvements in energy efficiency come at a minimal compromise in manufacturability. This method is not only useful to evaluate manufacturability of various profile designs but it can also be used to trigger fine tuning of certain profile features to strike a balance between efficiency and manufacturability.



# Chapter 1

## Introduction

**I**N this opening chapter, the history and working principle of screw compressors are presented. Along with that, rotor profiles are introduced with the motivation for a new profile development. Some of the crucial definitions of rotor profiling jargon such as essential rotor geometric parameters, rack and various leakage paths are also presented with illustrations.

### Contents

1.1	Screw Compressors . . . . .	2
1.2	Rotor Profiles . . . . .	4
1.3	Important Definitions . . . . .	4
1.3.1	Main Rotor, Gate Rotor and Rack . . . . .	5
1.3.2	Throughput Area / Displacement . . . . .	6
1.3.3	Clearances - Axial, Radial and Interlobe . . . . .	6
1.3.4	Interlobe Sealing Line . . . . .	7
1.3.5	Blow Hole . . . . .	8
1.4	Motivation for New Profile Development . . . . .	9

## 1.1 Screw Compressors

Compressor is a machine which delivers any gaseous fluid at an increased pressure than at its current state. There exist various designs and mechanical principles of performing this task. That is how different types of compressors come to be. The simplest of the principles is that of reducing the volume of gas in a closed space (chamber) to increase the pressure. Compressor types based on this principle are termed ‘positive displacement type’. If the principle of converting kinetic energy of high speed gas stream into static pressure is used for compression, it is termed as the ‘dynamic type’.

Screw compressors work on the positive displacement type principle. The helical screw rotors in these machines are designed and positioned to generate closed volumes (chambers) confined by the housing and intricate ports. As these rotors mesh, chamber volumes tend to progressively reduce on account of the screw motion. The desired internal pressure rise can be attained by designing the ports appropriately. The compressed gas is discharged out of each chamber as the rotors rotate and the empty chambers are filled again with new gas as they repeat the same process cyclically.

It is presented in Figure 1.1, how the pressure of gas increases in subsequent chambers as the rotors rotate and their volume reduces. Each chamber is confined by three boundaries- the rotor lobes, the casing around the rotors and the line of contact between rotors. As the rotors rotate, the line of contact between rotors also known as interlobe sealing line travels along to the axis of rotors which results in progressive reduction of the total chamber volume.

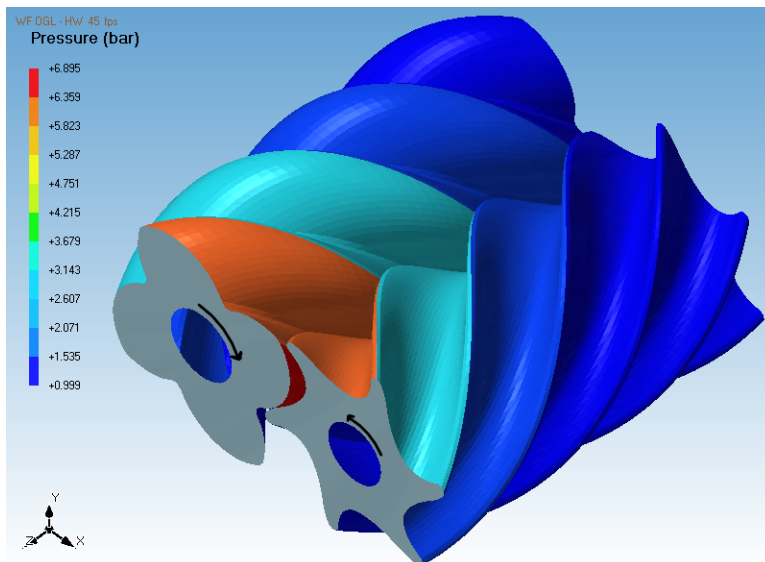


**Figure 1.1:** Illustration for the working principle of screw compressor (generated using SCORG)

A screw compressor with all its elements is presented in Figure 1.2. One can observe the round suction port from where the gas is taken inside the compressor and in a quarter section of the assembly, other elements such as bearings and seals are also visible.

The screw compressor requires to do thermodynamic work in order to compress the

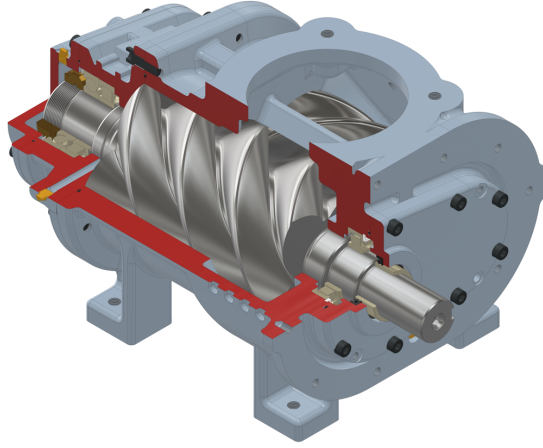


**Figure 1.2:** A screw compressor assembly (model by Kirloskar Pneumatic Co. Ltd.)

gas. The energy to perform this work is transferred to one of the rotors by a prime mover such as an electric motor or a diesel engine. The other rotor is either driven by the rotor to which prime mover is connected or they mesh without physical contact through the timing gears.

The idea of using two meshing helical screw rotors to compress a gas was first patented by Krigar (1878), an old German patent which claims to have generated up to 1.26 bar pressure of air at the outlet. This was more precisely a blower and ran slowly at 500 rpm. Later, Lysholm (1943) reports successful development and testing of a screw compressor in late 1930's capable of running up to maximum speed of 9000 rpm and suitable to generate pressure ratio of 3.6 with fairly good efficiency. It also talks about control methods for screw compressors and manufacturing of rotors.

In the following times, Swedish company Svenska Rotor Maskiner (SRM), continued developing this technology and they also licensed it to other manufacturers. In 1956, SRM patented the idea of oil-injection in screw compressor working chambers to eliminate timing gears, improve reliability and also achieve higher efficiency and pressure ratios in a single stage (Wilfred and Robert, 1963). Oil-injected screw compressors are more popular than the dry compressors.

With advancements in manufacturing technology to produce screw rotors with good accuracy as well as ability to maintain small clearances in machines, led to further improvements in efficiency of screw compressors. This led to their popularity especially in last 50 years. Contributions to the field by dedicated academic research groups such as Centre for Compressor Technology, City, University of London in UK and Chair of Fluidics, TU Dortmund in Germany which work in close collaborations with the compressors industry across the world, continue to drive the innovations in screw compressors.

The main advantage of this technology is its rotating operation which eliminates large inertial forces, allows smooth operation with low vibrations and it also enables attaining high speeds. Lower number of parts in their construction make screw compressors generally very reliable and they also require less maintenance. The simplicity of their working principle is the biggest advantage of screw compressors. However, the

complexity of their design (especially rotors) and criticality of assembly are also very peculiar on the other hand. Efficiency wise, modern screw compressors are preferred for moderate flows at pressure demands up to 15 bar.

The oil-injected twin screw compressor is the focus of this study. However, multiple other layouts of screw compressors such as single screw compressors, tri-screw compressors, variable geometry screw compressors, etc. have been studied and explored over the years and can be found in literature.

## 1.2 Rotor Profiles

The most essential design aspect of a screw compressor is the shape of its rotors. Rotors determine not only how energy efficient the compressor would be but also how reliable, cost efficient and silent it would be. They are essentially a pair of helical gears designed with an objective to trap a large enough volume of gas and reliably compress it according to the principle explained in the last section.

Complete rotor geometry is defined by two types of features. One of them is the rotor profile which is a the geometry or shape of the rotor in a plane perpendicular to its axis of rotation. It can be visualized by looking at the end planes of rotors in Figure 1.1. The other feature is three dimensional which actually gives the rotor profile a helical extrusion. This can be defined by the length of rotor along with either the wrap angle or the helix angle.

The rotor profile is a critical aspect of design as it dictates all the elements of screw compressor operation. This includes working chamber volume, leakage path areas and torque characteristics (which influences noise). The first aspect of rotor profile design is deciding the number of lobes. The lobe combination is referred to the number lobes on two rotors. 4/5, 4/6, 5/6 (main rotor lobes/gate rotor lobes) are some of the most common lobe combinations for oil injected screw compressors. Lobe combinations such as 6/8 are useful in high pressure applications since they are sturdier on account of their larger root diameters. Whereas, lobe combinations such as 3/5 are useful in oil-free as well as low pressure applications. All the lobes of one rotor are same, hence profile needs to be defined over a single lobe.

A rotor profile is designed by defining different curves and placing them side by side. The methods of rotor profiling and details of this art are discussed in depth in the next chapter. Historically, innovations and improvements in rotor profiles have always driven the success of screw compressor technology.

## 1.3 Important Definitions

This section has a specific purpose of defining important terms and jargon of screw rotor profiling. This would serve the reader to follow the technical discussion in upcoming chapters with ease and familiarity.

### 1.3.1 Main Rotor, Gate Rotor and Rack

Main rotor is also commonly referred to as the ‘Male rotor’. Refer Figure 1.3 for an illustration of main rotor, gate rotor as well as rack along with pitch circles for the respective rotors. Pitch circles for a pair of meshing gears/rotors are defined as the virtual circles concentric to the respective gears/rotors which may be supposed to perform pure rolling against each other.

Out of two rotors in a twin-screw compressor, the main rotor is the one whose major portion is outside of its own pitch circle. The difference between maximum radius and the pitch circle radius of the rotor is known as the addendum of the rotor. Similarly, the difference between minimum radius and the pitch circle radius of the rotor is known as the dedendum of the rotor. Usually the main rotor is the rotor whose addendum is larger than the dedendum.

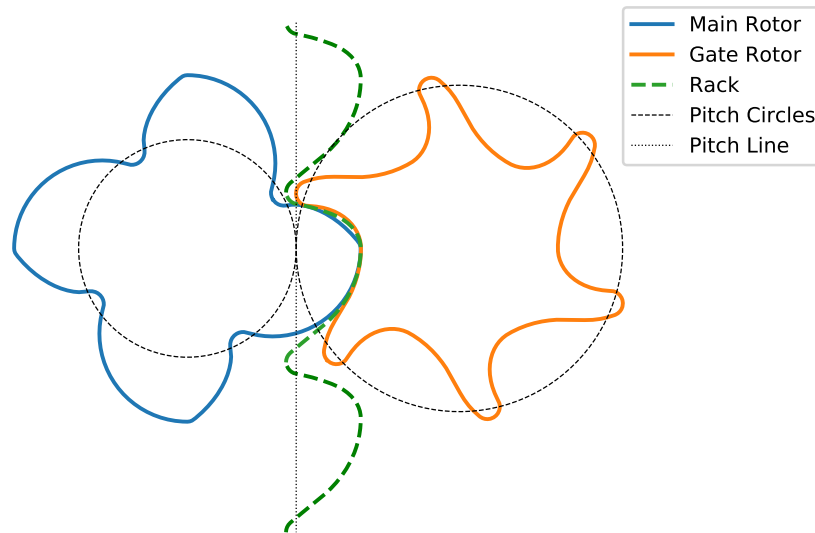


**Figure 1.3:** A typical rotor pair for twin-screw compressor plotted along with an imaginary rack, pitch circles and pitch line

Gate rotor is also commonly referred to as the ‘Female rotor’. It is also identified with respect to pitch circle. Out of two rotors in a twin-screw compressor, the gate rotor is the one whose major portion is inside of its own pitch circle (refer Figure 1.3). Usually the gate rotor’s dedendum is larger than its addendum.

Using Figure 1.3, one can visualize how the rotors would mesh. If the main rotor rotates clockwise, the gate rotor would rotate counter-clockwise. Whereas, the rack would mesh with both main and gate rotor by moving vertically in a linear motion. The rack could be imagined as a rotor of infinite radius in which case its rotational motion looks like linear motion. Similar to the pitch circle for rotors, rack has a pitch line which passes through the pitch point (point of contact of two pitch circles) perpendicular to the line joining centers of two rotors in the same plane.

### 1.3.2 Throughput Area / Displacement

The total volume of gas rotors can trap and compress during one cycle depends on the space available between teeth of the rotors. To get a higher flow output per unit time, it is desirable to contain as large as possible volume of gas between the teeth. However, this would weaken the rotor teeth and structure. Also, such an adjustment also affects other aspects of profile such as leakage areas and hence might always be beneficial. The throughput area is the combined area between teeth of main and gate rotor also considering the overlap between them.

When this area is multiplied by the helical length of the chambers, the maximum working volume of a chamber can be obtained. This is referred to as the ‘displacement volume’ or simply ‘displacement’ of the compressor. It is indicative of the theoretical volume of gas that can be trapped and delivered at the discharge, if zero volumetric losses are assumed to occur during the compression.

It is an important geometric feature of the profile which needs to be weighed against other features for obtaining a desirable profile.

### 1.3.3 Clearances - Axial, Radial and Interlobe

Various clearances in a screw compressor assembly are shown in Figure 1.4. They are in place for practical reasons and smooth operation of the machine. The axial clearance is between the rotor discharge end plane and the casing. Radial clearance is a circumferential gap between rotor periphery and the casing. Interlobe clearance lies between two rotors to facilitate their smooth rotation.

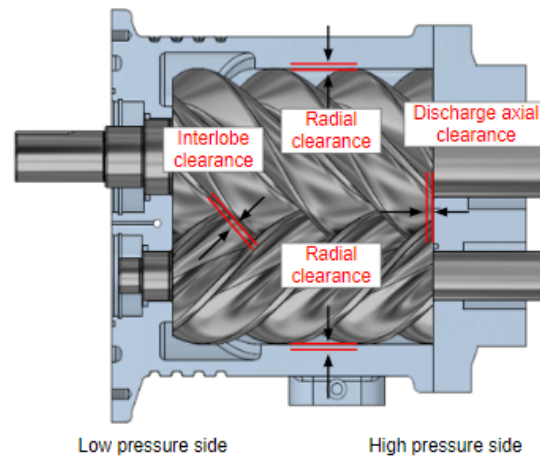


**Figure 1.4:** Illustration of various clearances in a twin-screw compressor

Clearances protect the machine from failing by accommodating thermal expansions and sudden shocks to the components. However, clearances are also leakage paths for the gas being compressed. These clearances connect working chambers of screw compressor which accommodate gas at different pressures depending upon their position in the compression cycle. This leads to leakage from high pressure chambers to low pressure chambers via these clearances and it results in loss of volumetric efficiency of the compressor.

Maintaining minimum clearances is desirable from the performance point of view but this is limited by practical constraints in manufacturing and assembly.

### 1.3.4 Interlobe Sealing Line

The rotors are three dimensional bodies which while meshing create a path of minimum distance between them. This is referred to as the ‘interlobe sealing line’ for a pair of rotors. It can be imagined as the locus along which theoretical rotor surfaces are in contact with each other. This is directly a feature of rotor profile. Different rotor profiles have different interlobe sealing lines.

It is also one of the leakage paths which along with interlobe clearance makes a crucial leakage area that affects screw compressor performance significantly. Arc length of this three dimensional (3-D) curve is called interlobe sealing line length. It is desirable to have a rotor profile that has small sealing line length as it would reflect in a smaller internal leakage area.

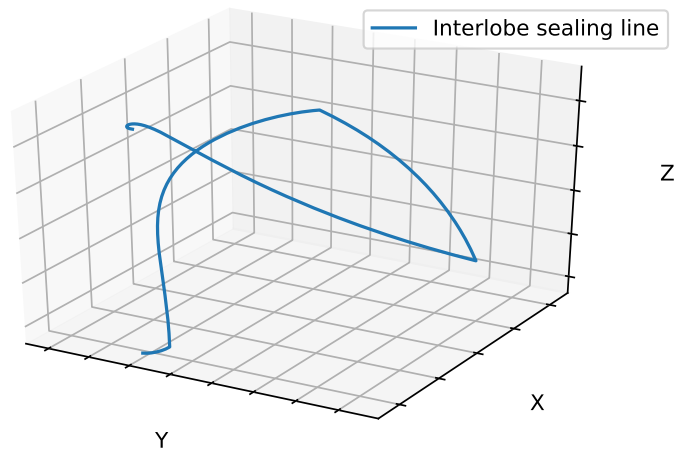


**Figure 1.5:** Interlobe sealing line or the 3-D contact path of rotors

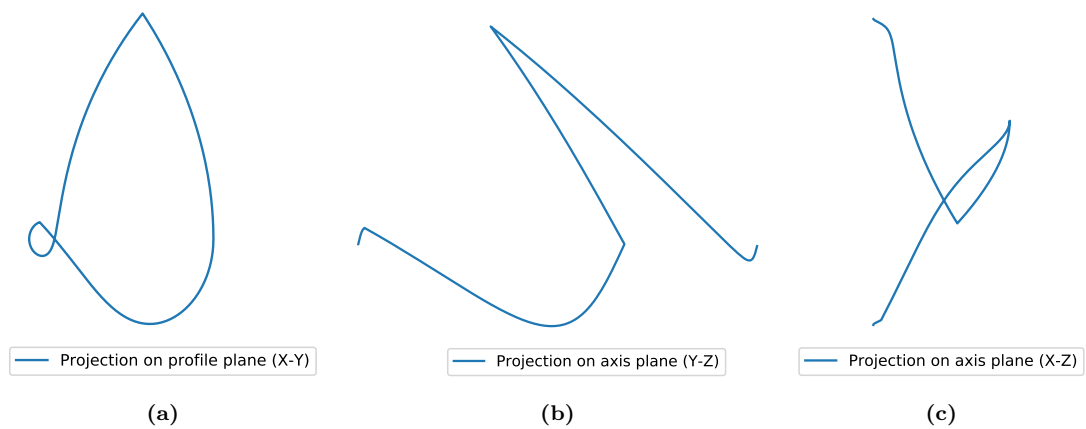


**Figure 1.6:** Projections of interlobe sealing line on various planes

It is presented in Figure 1.5, the 3-D shape of an interlobe sealing line for the rotor pair presented in Figure 1.3. The rotors axes are aligned to the Z-axis while profile lies

in the end plane or X-Y plane of this 3-D plot. For a better visualization of the sealing line, it can be projected on various planes, such as profile plane or a plane perpendicular to that as viewed from side of the rotors. Such projections are depicted in Figure 1.6.

The interlobe sealing line length calculated as an arc length of this 3-D curve is often referred while comparing two rotor profiles geometrically.

### 1.3.5 Blow Hole

Blow hole is an another leakage path peculiar to twin-screw compressors. They are formed between rotor tips at the cusps of the casing. There are two blow-holes on account of two cusps of the casing (the intersections of rotor bore circles in the casing). The cusp on high pressure side is crucial from operational point of view, hence unless specified or mentioned otherwise, ‘blow-hole’ refers to the high pressure side blow-hole.

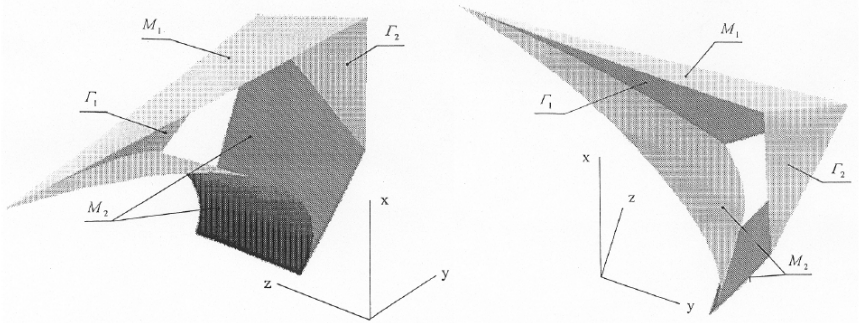


Figure 1.7: 3-D representation of blow-hole (Chapter 5, Svígler (2010))

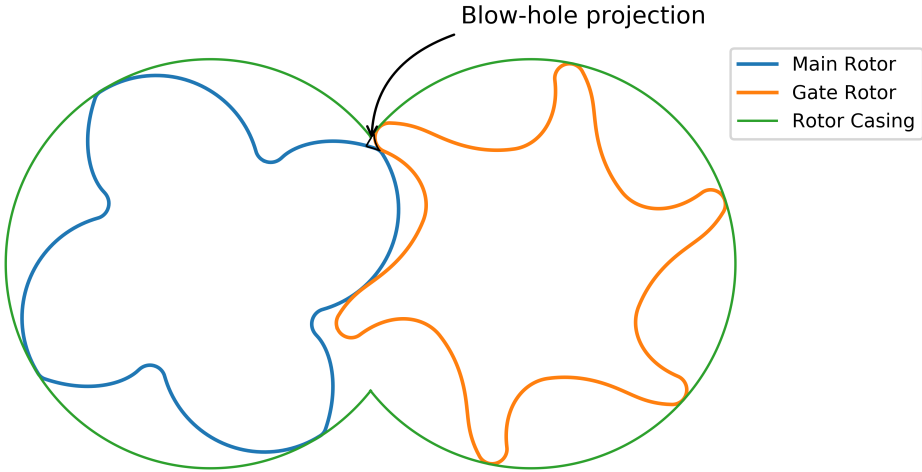


Figure 1.8: A crude illustration of the blow-hole area projected on the profile plane

When the interlobe sealing line of the rotor pair does not extend all the way up to high pressure side cusp, an opening is created whose boundaries are rotor tips and the cusp line. This is in fact a three dimensional shape which is slightly difficult to visualize. However, Svígler (2010) has generated a 3-D plot of blow-hole presented in Figure 1.7. For practical purpose, taking a cross section of this blow-hole in an

appropriate plane and measuring its area referred to as the ‘blow-hole area’ is a good enough approximation to judge its influence on the leakage.

It can be looked at in the profile plane (X-Y), as presented crudely in Figure 1.8. But for the best results, taking cross-section along the plane perpendicular to the leakage flow from one chamber to other through blow-hole which is known to follow gate rotor helix direction is recommended. Commercial software such as SCORG and SCORPATH enable these complex calculation for any general profile. Hence, two profiles can be geometrically compared based on their blow-hole area. Like any leakage area, smaller blow-hole area is desirable for better performance.

## 1.4 Motivation for New Profile Development

This study is a part of a research collaboration between Kirloskar Pneumatic Company Limited, Pune, India and City, University of London, London, UK. During this collaboration, a family of twin-screw air compressors are designed, developed and tested. Improvement of rotor profiles would further improve the energy efficiency of the range of compressors developed under this collaboration and further.

The policy of City, University of London Compressor Centre is to distribute knowledge and skills in profiling of screw compressor rotors to their customers and partners. As a part of this activity, this research is aimed at developing a new rotor profile for Kirloskar Pneumatic Co. Ltd. to get the best compressor performance for given operational conditions adjusted to the market demands.

Improvements in rotor profiles directly impact the screw compressor efficiency and reduce the power consumption for unit flow of compressed gas under given conditions; as well as manufacturing cost in comparison with less efficient compressors and, thus reduce their environmental influence. This has direct impact upon the economy and social relations at all layers of contemporary communities. Author believes this to be a key motivation for this study.

City University’s N Rotor profile patent (Stosic, 1997) based on pioneering work published in Stosic (1998) introduces screw compressor rotor profiles based on Euler envelope theory described in Litvin (1989) resulted in compact and more efficient screw compressors. This made substantial impact upon the screw compressor industry in last 25 years that not less than half of the world screw compressor production is assisted today and use all or some of this patent features in profiling, calculation, design and manufacturing of screw compressors. This study too is based on N-Profile and works towards the new profile by trying to improve the N-Profile features.

In this pursuit, first the literature on screw rotor profiling has been studied to identify the scope of improvement in state of the art profiles. It includes looking at profiling from different perspectives such as influence of constituent curves on performance as well as profile manufacturability. Contribution in both of these aspects is expected to substantially improve the rotor profiles. Hence, literature review has been structured to first chronologically summarize profiling relevant progress over the last century. Thereafter principles and methods of profile generation as well as manufac-

turability have been reviewed to clearly identify gap for contributions that would lead to further improvements.

## Chapter 2

# Literature Review

THE literature review is organized in four major sections- first of which briefly reviews all relevant literature in a chronological order whereas the second goes into detailed review of the methods of rotor profile generation and designs throughout the available literature. The third section specifically dives into the review of literature on manufacturing of rotor profiles and their manufacturability. The last section is a study of the N-Profile features and a road-map to how the new profile could evolve from it following the findings of literature review.

### Contents

2.1	General Review . . . . .	12
2.2	Review of Methods . . . . .	18
2.3	On the Manufacturability of Rotor Profiles . . . . .	26
2.4	Study of N-Rack Characteristics and its Curves . . . . .	29
2.4.1	Rack Section D-E . . . . .	31
2.4.2	Rack Section D-C, E-F and A-H (Rotor Tips) . . . . .	32
2.4.3	Rack Section A-B-C (Long Edge) . . . . .	33
2.4.4	Rack Section F-G-H-A (Short Edge) . . . . .	35
2.5	Review of Performance Calculations in Screw Compressors . . . . .	36
2.6	Summary of the Literature Review . . . . .	38

## 2.1 General Review

The available literature on screw compressors is in multiple languages where early textbooks are found in Russian and German whereas the more recent textbooks are found majorly in English and Chinese. However, there are many papers in English and other languages which preceded the textbooks. A good comprehensive review of all the information available on screw compressors has been published in the book Stosic et al. (2005) and in the review paper by Stosic et al. (2011b) which covers almost all the essential literature published till 2011. Stosic et al. (2002) is another review article that covers screw compressors and their development from an industrial point of view. Similarly, a comprehensive review of the screw compressor rotor geometry and their tools has been presented in Stosic et al. (2011a). The latest account of some of the most modern rotor profiles can be found in Patil et al. (2022).

An overview of the developments in the field of screw compressors based on published literature presents 4 major stages of evolution. First of these starts with the very first patent on rotary positive displacement compressor by Lysholm and William (1938) whose rotors had several difficulties in manufacturing w.r.t. technology of those times. The second stage in development came with the major improvements in rotor profiles around 1970's as seen in the patents by Lysholm (1967), Persson (1968) and Schibbye (1970). This was accompanied by advancements in manufacturing techniques which made it possible to cut the rotors to desired accuracy and at acceptable costs (Stosic et al., 2011a). Performance and cost effectiveness of screw machines scored high during these stages.

The use of computers in engineering marked the third stage of development in the field. During mid 1980's, using computer programs, mathematical models and suitable simulation tools were developed by Sangfors (1984), Singh and Onuschak (1984), Fujiwara et al. (1984) and Stosic et al. (1986). Further contributions by Singh and Bowman (1988), Tang (1995), Hanjalic and Stosic (1997), Stosic and Hanjalic (1997) and Fleming et al. (1998) enabled easy generation of screw rotor profiles as well as accurate prediction of the overall screw compressor performance using computers. Unprecedented flexibility in design that came with quick, accurate and reliable simulations of rotor generation as well as cutting processes marked the end of third stage in development of screw compressors.

Later and more recent contributions to the field of rotor profiling came through applications of finer design principles such as variable clearance distributions on rotors, controlling torque characteristics of the gate rotor (Stosic et al., 2005) and an extensive work on optimization techniques applied to rotor profile designs (Su and Tseng, 2000) (Kauder et al., 2002) (Stosic et al., 2003b) (Wu and Fong, 2009). Further gain in computer computational powers at hand also led to exploration of newer ways to generate screw rotor profiles based on previously untouched methods such as use of bezier curves by Helpertz (2003), b-splines by Hauser et al. (2008), sealing line by Zaytsev and Ferreira (2005) and deviation function method by Huang (2015). This is the current and fourth stage where improved manufacturing technologies combined with

computational capabilities will drive the further developments in the field. To mention a few - 3-dimensional CFD of screw compressors by Kovacevic et al. (2007), higher pressure applications of screw compressors by Hauser et al. (2016) and Vaidya (2019), internally geared screw compressors by Read et al. (2017) and Dmitriev et al. (2015), highly complex screw rotors by Gray et al. (2018) and Utri et al. (2018), etc.

A concurrent look at the literature on manufacturability of rotor profiles shows that the earliest work was done by rotor manufacturing frontiers such as Holroyd. With the advent of computer aided manufacturing in 1980's, we see work by Mould et al. (1982) that described a computer based method to generate milling or grinding tool cutter templates right from rotor profiles. Using manufacturing simulation tools, Sauls (1998) and Sauls (2000) evaluated the effect of manufacturing variations on rotor profile clearances that directly affect the performance since they form leakage paths. A more comprehensive study of screw rotor manufacturability is found in Guo and Tang (2003b) and Guo and Tang (2003a). These works provide a sound guidance on what can be regarded as a good profile on the manufacturability criteria. Still it is found that there is some scope for further research on quantifying the manufacturability of rotor profiles. The manufacturing aspects and its related literature is reviewed in depth in the third section of this chapter.

Since this research is more focused on rotor profiling; following few pages have been dedicated to the detailed review of the development of rotor profiles in the chronological order taking a more microscopic look into the art. A significant share of the relevant literature in rotor profiles lies in patents issued to compressor manufacturers across the globe. The number of patents granted in screw compressor field are estimated by Stosic et al. (2011b) to be in thousands where SRM alone has more than 1000 patents most of which are related to profiles. Hence, a comprehensive review of literature in screw rotor profiling will look into the most relevant patent documents while parallelly looking into published articles and textbooks for principles of generating and designing these profiles.

The very first screw rotor profile appeared with first patent in the field by Lysholm and William (1938) was a simple circular symmetric profile. It had very large blow hole area, lower displacement volume and was not easy to manufacture. Whereas, SRM's symmetric profile (Figure 2.1a) patented by Robert (1952) was more practical from manufacturing point of view though inefficient due to symmetry. These profiles were designed and generated by precise mathematical rules and procedures but no literature on theory of profile generation was published until Sakun (1960) who introduced the envelope method from differential geometry to screw rotor profile generation. Following this, Andreev (1961) published his work that elaborated on tooling and manufacturing aspects of screw rotor profiles. Soon after, Lysholm (1967) patented a modified circular arc symmetric profile (Figure 2.1b) which had features that hinted at asymmetric profiles to come later. The major problems with traditional circular arc profiles were large blow hole areas, large inner diameters of male rotor to ensure thick female lobes (this leads to reduction in displacement volume), pocket areas formation within lobes,

etc. Lysholm’s profile apparently came over these problems to a significant degree with the help of peculiar features of this profile such as separate curve for male rotor tip and possibility to incorporate ellipse or parabola on male rotor leading edge.

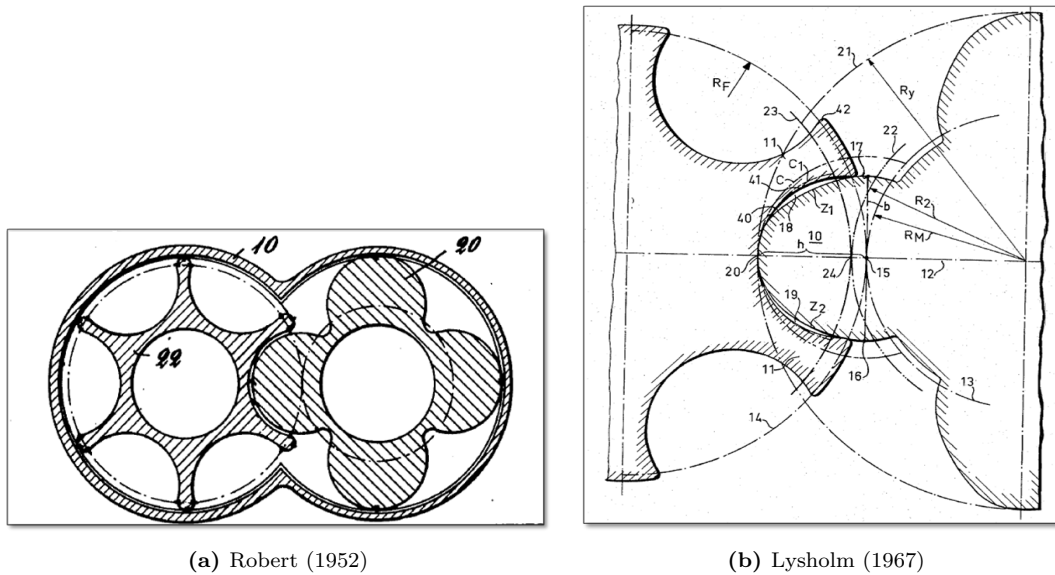
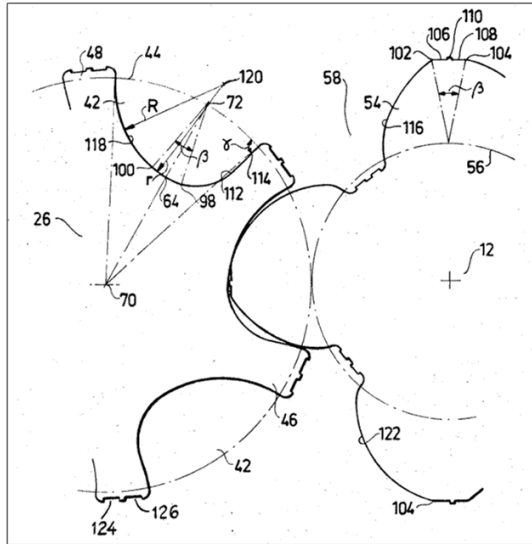


Figure 2.1: Early Symmetric Profiles

One of the earliest asymmetric profiles was patented by Persson (1968) which was entirely constructed out of circles and lines. Characteristics of sealing between rotor pair has been an important feature of this profile. One of the earliest accounts of unequal clearance distribution to ensure smooth and seize free running of screw machines is found in this invention. But it remained largely impractical due to point generated portions and close to zero pressure angles on circular arcs defined with centers on pitch circle. A truly practical to manufacture and efficient asymmetric profile was patented soon by Schibbye (1970) which is widely known as “SRM-A” (Figure 2.2). Stosic et al. (2011b) commends SRM-A for making screw compressors commercially viable for the first time.

Menssen (1977) came up with a new method of profiling previously unseen in literature on screw rotors; using an imaginary rack (essentially a rotor with infinite radius) to generate curves on both main and gate rotors. This method called “rack generation” will be discussed at length in next section but this particular profile though ingenious in technique, was not practical for various reasons. In the same year, another important text in screw rotor profiling by Amosov et al. (1977) presented methods to reproduce all important profiles to the date namely Lysholm’s profile, SRM-A and SKBK. This was followed by the publication of German textbook by Rinder (1979) which reproduced SRM profiles using profile generation method based on gearing theory. In the same year, one of the good screw rotor profiles known till date as “Sigma Profile” (Figure 2.3a) was patented by Bammert (1982). Rinder (1979) compared Sigma with SRM-A and found a drawback of SRM-A to be not very milling-friendly whereas Sigma is praised for overcoming it. Sigma profile is designed with minute details and constraints put on every aspect of rotor geometry make it highly efficient as well as manufacturable.

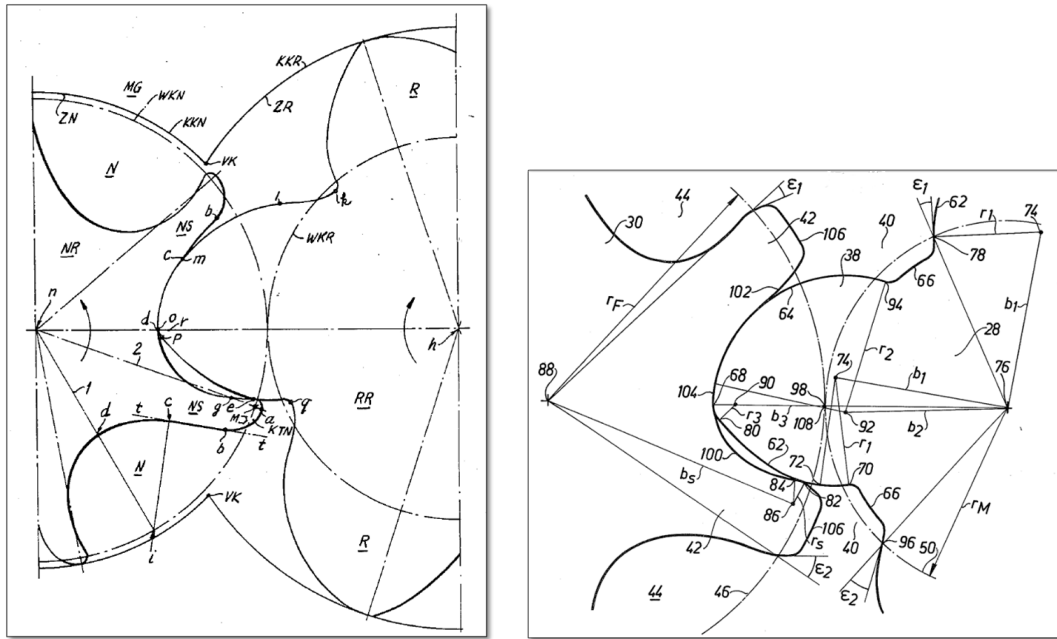


**Figure 2.2:** The first efficient and fairly manufacturable asymmetric rotor profile, SRM-A (Schibbye, 1970)

Soon after Sigma profile, SRM patented its most famous “D” Profile invented by Astberg (1984) (Figure 2.3b). This rotor generated profile is entirely defined using circular arcs all of which are placed off the pitch circle unlike SRM-A. SRM-D technically has better manufacturability, better sealing characteristics, built in flexibility for optimization but at the same time it is more complicated than SRM-A (especially the tip design). Regarding the types of curves used in profiling, Bowman (1983) took an interesting turn with introduction of conic sections and involutes whereas traditionally only circles and lines were commonplace for profile definitions. He patented a profile (Figure 2.4) very similar to Sigma for Ingersoll-Rand. The invention claimed to have beaten the best-in-class compressors of early 80’s with this rotor profile. Trailing edge of gate rotor lobe is of major interest here for it uses an involute section to ensure good sealing (wide practice in good profiles) and a small elliptical curve is put on the tip as it touches the addendum circle to maintain high pressure angle in the region.

By and large, most of the major screw compressor manufacturers had their own profile patents by late 1980’s. All these profiles were based on principles similar to SRM-A profile, wherein curves of choice were defined on either rotor to derive the conjugate curves on the other rotor using gearing condition. Efforts were put into choosing most suitable curves which would facilitate larger throughput area and minimize the leakage areas keeping manufacturability in consideration. As Soren Edstrom puts it very aptly- “rotor profiles are some kind of ‘recipe’, wherein lines, points and mathematical curves serve as ‘ingredients’ which are mixed in suitable proportions” – Edstrom (1992).

Rinder (1987) patented the first practical to use rack generated profile based on the principle introduced by Menssen (1977). Rinder entails that the use of circular arcs in rack profile ensures closure of sealing line and makes use of the fact that straight lines on rack map as involute curves on rotors which when meshed, create straight lines of sealing line along the rotor length. As a straight line is the shortest path between two points in space, the shortest possible sealing line length and hence the shortest leakage



(a) SIGMA Profile (Bammert, 1982)

(b) SRM-D Profile (Astberg, 1984)

**Figure 2.3:** Later Asymmetric Profiles with Improved Manufacturability

path is obtained in those parts of the profile. This profile, though an important step in the direction of rack generated profiles, had a problem of slightly larger blow hole area and poor sealing on the portion of rotors generated by the high pressure side of the rack; compared to the contemporary rotor generated profiles.

In the same year, Hough et al. (1987) patented a profile known as “Cyclon Profile” for Compair Broomwade. It is one of the famous and efficient profiles in history of screw rotor profiles. Relatively strong gate rotor lobes as well as good manufacturability of rotors had been the key features of this invention. Use of parabolic curves on tips of both main and gate rotor lobes to improve sealing characteristics is a peculiarity of this profile. At this point of time (late 1980’s) in development of new profiles of those times, one can see a shift in choice of curves where designs are exploring several other options (ellipses, parabolas, involutes) than only circles and lines peculiar to older profiles. This leaves one to wonder what curves will be best suited for various sections of profile (tips, leading and trailing edges). Around the same time, Litvin (1989) published his work that extended the mathematical basis of envelope theory which could be used for generation of screw rotor profiles of more complex curves too. This surely buttressed the further development in profiling.

Later in the 1990’s, Chen (1995) invented “Hyper Profile” which employed the curve hyperbola in profile design. The main objectives of this invention were reduction of blow hole area and minimization of mechanical losses in meshing as compared to the prior arts. Around the same time, introduction of CAD into profile design (Stosic et al., 1986) and availability of complete mathematical basis of profile generation through Litvin (1989)’s work led to important works such as Tang (1995), Stosic and Hanjalic (1997) and Stosic (1998). Culmination of this phase of development came with patent

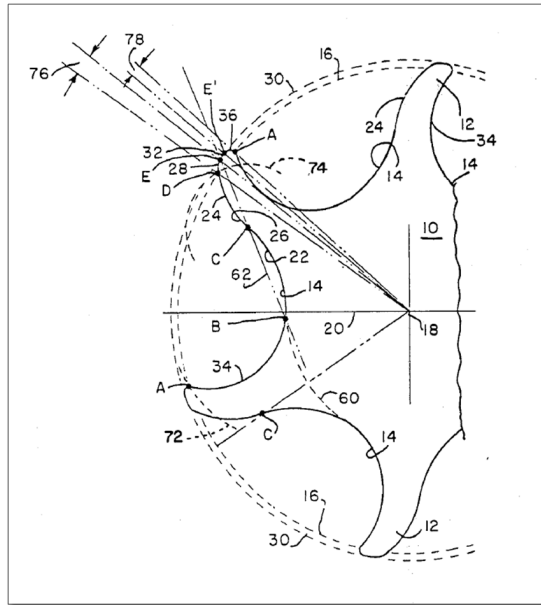


**Figure 2.4:** Rotor profile with ellipse and involute curve patented by Bowman (1983)

of the “N-Profile” by Stosic (1997) (Figure 2.5).

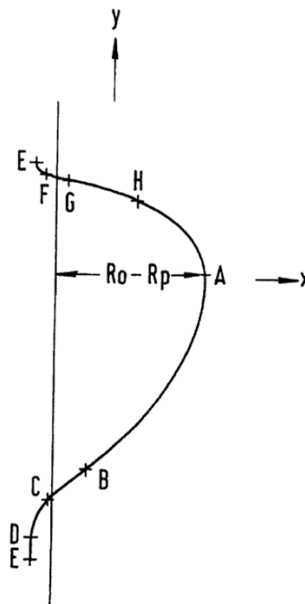


**Figure 2.5:** N-Profile Rack (Stosic, 1997)

It turned out to be one of the best profiles for screw compressor rotors with distinguishing features such as perfected rack-generation, cycloidal curves on high pressure sides of lobes and extreme flexibility in design. N-rotors are stronger yet lighter and also facilitate high throughput to leakage area ratio resulting in a higher energy efficiency of the machine. The best thing about N-profile and the main features because of which it stands above all the prior arts are the scope it has for additional control over curves, curve refinement, inclusion of the good prior-profile-features and optimization capabilities it offers with integrated thermodynamic calculation tool in software form (Hanjalic and Stosic, 1993).

Exploring new frontiers in rotor profiling/generation methods, Kauder et al. (2002) and Helpertz (2003) proposed representation of rotor profiles in the cross section with bezier curves and optimizing the profile shape by deploying genetic algorithms that weigh desirable geometric features of generated rotors and choose the best among them. These works are reviewed in depth in the next section. Stosic et al. (2003b) followed a more practical approach to optimization of profile shapes using thermodynamic performance criteria along with utilization of the flexibility that N-Profile offers. Based on applications and use case, optimized N-rotor profiles could be proposed with this work.

Meanwhile, companies continued to secure patents based on tweaking some or the other curves and features of prior art profiles. Examples of these are found in a Korean patent on rotor profiles by Kim and Lee (2004) wherein the female rotor tip is modified to influence blow hole area and manufacturing feasibility of the tips, Lee et al. (2006) wherein all the features of N-Profile are replicated, Tang (2007)’s patent for Carrier Corporation that intelligently incorporated elliptical curves to ensure lower contact stresses and sharper tips in desired regions. This insightful patent by Tang (2007) hints one to explore into a more efficient way of analytically representing a family of continuously changing curves (that change radii of curvature continuously as in between ellipse’s two ends) for particular sections of profile. Such representation of curves can give a significant advantage in designing new and better profiles. This hint is particularly of interest from the point of view of this study.

In another rack generated profile similar to N-Profile, patented by Cavatorta and Tomei (2014) improvised the flat side of rack to be a hyperbola which has an advantage that it cuts deeper into gate rotor blank while minimizing the sealing line length. Counting the most recent influential patents in rotor profiling, Stosic (2017) invented a variant of N-Profile for reducing noise in screw machines. Weih (2019) fine tuned old Sigma profile and all the other aspects of rotor and profile geometry by carrying out an extensive multi-variate optimization to set general design constraints on rotor inner and outer diameters, addendum, dedendum, center distance, relative profile depth, wrap angle, L/D, offset of female tip, tip radii and their relative ratios, lobe thickness, etc. This is evident of the shift in methods and objectives of rotor profiling over time.

## 2.2 Review of Methods

The mathematical basis for generation of even the most simple rotor profiles was not published in open literature until as late as 1960s. Prior to that, though profiles were designed according to strict mathematical procedures, methods were not made public by manufacturers or patentees. Though screw rotors are basically a pair of helical gears, as rightly pointed out by Rinder (1987), the traditional gear design principles are formulated and premised on factors many of which are essentially unlike and unrelated to the factors which are significant in the design of rotary screw compressors.

The prime theoretical challenge in screw rotor profile design lies in calculation of conjugate shapes generated on the paired rotor when one chooses curves on one of the rotors based on design needs. A classic concept of “Envelope Theory” formulated by

Euler in a branch of mathematics called differential geometry (Guggenheimer, 1977) proves helpful to tackle this challenge. Earliest reference to adoption of envelope approach in gear profiling is found in Gohman (1886). In modern times, it is proposed and generalized for all types of gear profiling including non-circular gears by the phenomenal work of Litvin (1989). The crux of this concept is that it enables mathematically to calculate an equation of a curve that envelopes a family of curves (‘enveloping’ simply refers to the condition of tangency at every instance, see Figure 2.6b). Thinking of the subsequent positions of a curve chosen on one rotor as family of curves and the generated rotor to be an envelope of this family of curves, the theory can be successfully applied to generate equations of conjugate shapes on paired rotors (Figure 2.6).

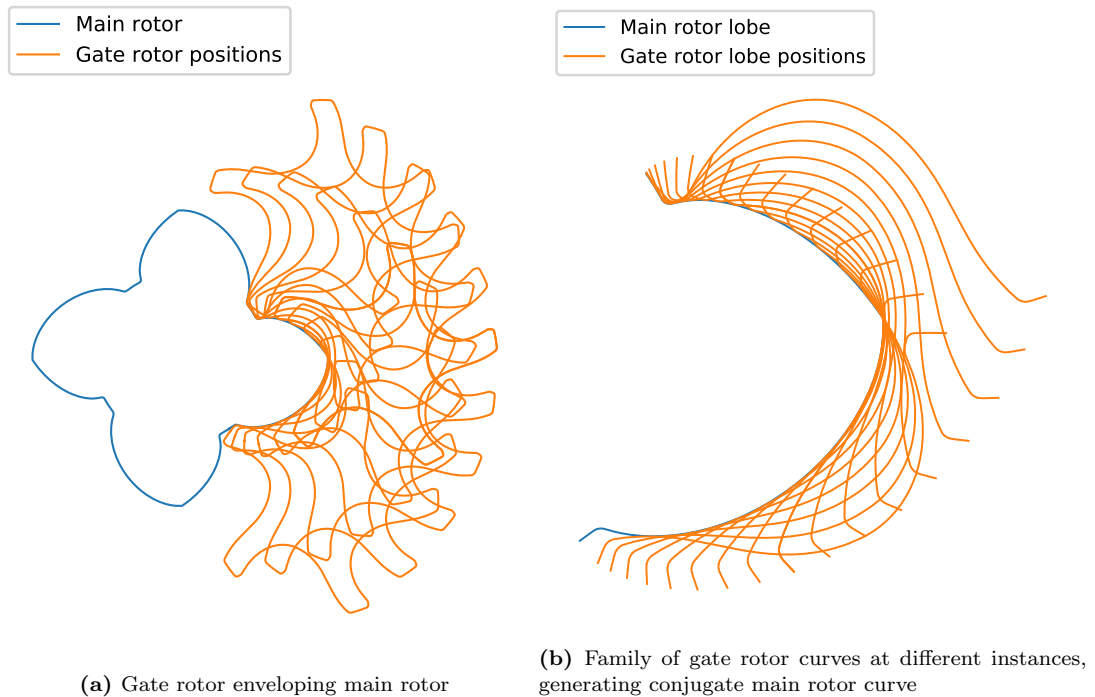


**Figure 2.6:** Demonstration of the envelope principle; conjugate curves on rotor pairs

Use of this method in screw rotor profile generation was first introduced by Sakun (1960). A mathematical equation that the chosen (or defined) and the generated (or conjugate) meshing curves on a pair of rotors must satisfy is termed as the “meshing condition”. Sakun (1960) derived a meshing condition for parametric curves defined on one rotor conjugate to curves on other rotor under a pre-specified relative motion of rolling over pitch circles. But Sakun’s practice was limited to deriving analytical meshing conditions which gave analytically representable conjugates of chosen analytical curves like circles, lines and points. This practice was later modified by Stosic and Hanjalic (1997) to significantly simplify the design procedure. Stosic’s method makes use of the capability to solve the envelope meshing condition numerically (using computers), hence not to limit the primary curves to only those which result in explicit analytical solutions of meshing condition. With this generalization, conjugate shapes of any analytical curve and even profiles defined with discrete points can be calculated. Stosic’s method also derives the meshing condition in a form which is suitable for easy

computer programming and more general in nature which can accommodate calculations of crossed axis rotors and tool profiles to cut the desired rotor profiles (Stosic, 1998).

Other meshing conditions which can be equally useful for gear profiling are found in literature such as “Willis meshing condition” based on the general notion that perfect transmission of power occurs when contact normal of the meshing gear teeth passes through pitch point (second law of gearing). But Stosic (1998) showed that it is just a special case of a more general meshing condition derived using envelope approach on two parallel non-intersecting helical gears. Rinder (1979) in his textbook has reproduced SRM asymmetric profile based on traditional laws of gearing. Though the analysis and profiles generated are perfectly equivalent, the envelope approach and specifically the one proposed by Stosic is most suited for screw rotor profile generation because of its simplicity and generality.

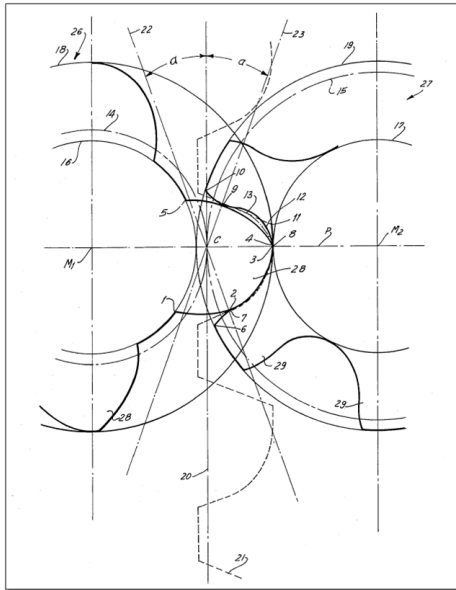
The second immanent theoretical challenge in rotor profiling is the choice of co-ordinate system to define the curves. It may look like a trivial thing but while specifying the curves on one or the other rotor; the profile designer can not know beforehand if the shapes of profiles formed on either rotors will be loop-free, conveniently representable in the current co-ordinate system and perfectly smooth (at least first order tangency at connecting points of two curves on profile). This challenge can be conveniently tackled by bringing in an imaginary rotor like a rack (rotor of infinite radius) to define the profile independent of two rotor co-ordinate systems and in a single convenient co-ordinate system as a result. Incorporation of the rack also ensures that the curves transformed onto either rotors will be loop-free; because rack-profile has the shortest profile length.

One of the earliest reference on using principle of rack-generation in screw rotor profiling is found in Menssen (1977) (Figure 2.7a). Later Rinder (1987) (Figure 2.7b) improved upon it and finally Stosic (1997) (Figure 2.5) perfected the rack-generated profiles by introducing cycloids on round side of the rack to replicate undercutting action of main and gate lobes in that portion to create perfect sealing- as practiced in rotor-generated profiles. The superiority and usefulness of this method of generation is evident in multiple later patents which cloned this feature in their designs such as Lee et al. (2006) and Cavatorta and Tomei (2014) (Figure 2.8).

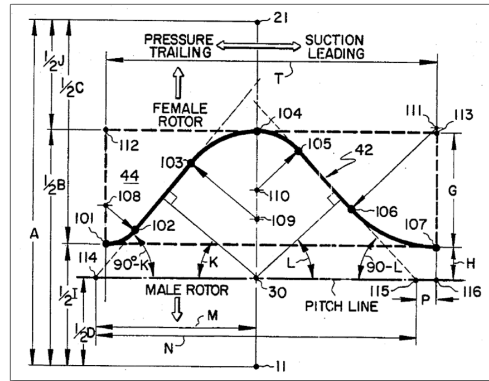
A typical rack generated profile is presented in Figure 2.9, wherein curves are defined on rack profile ( $A - E$ ) and the curves on main and gate rotor profiles ( $A1 - E1$  and  $A2 - E2$ ) are generated by solving a meshing condition in an explicit form which further simplifies the computation of generating these profiles.

In summary, the definite advantages of the principle of rack generation are as follows (Stosic and Hanjalic, 1997)-

- Rack profile is the shortest profiling which avoids reversals on the transformed main or gate rotor profiles.
- Straight lines on rack transform as involutes on the rotors. Positioned near the contact region, it ensures close to pure rolling contact between the rotors.

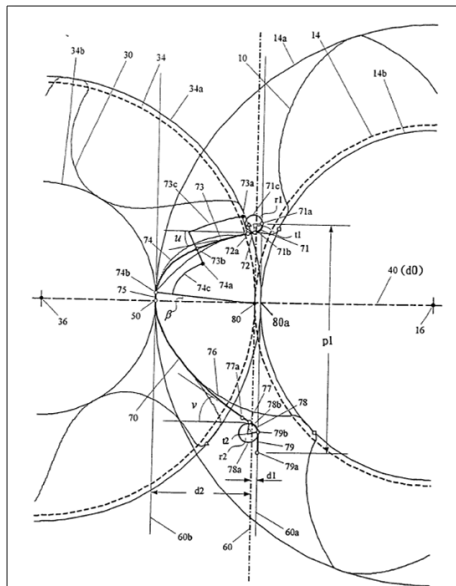


(a) Menssen (1977)'s Rack Generated Profile

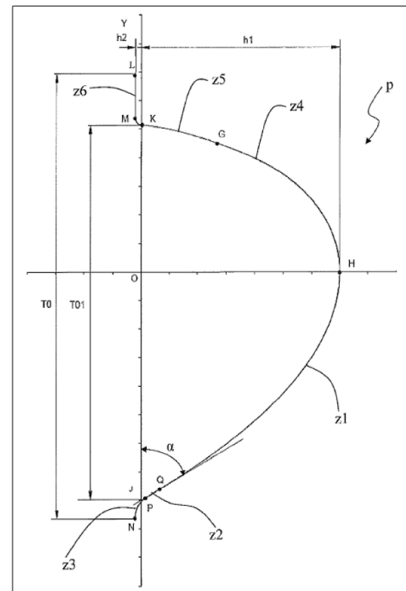


(b) Rinder (1987)'s Rack

**Figure 2.7:** Early Profiles Based on the Principle of Rack Generation



(a) Lee et al. (2006)'s Rack Generated Profile



(b) Cavatorta and Tomei (2014)'s Rack

**Figure 2.8:** Rack Profiles Closely Based on N-Rack

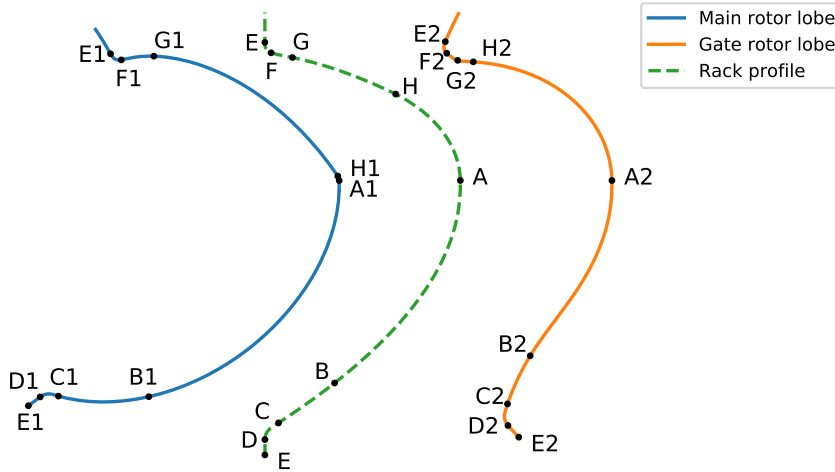


**Figure 2.9:** A general rack profile along with its main and gate rotor profiles

- Rack generated rotors are usually easier to manufacture.
- Main and gate rotors can be independently generated. Hence a single rack generated rotor can be matched with multiple sizes and lobes of the conjugate rotor.
- Rack-to-rotor transformation can be derived in an explicit form which is computationally faster and easier to solve.

The third challenge in design of a good rotor profile is the perfect choice of curves to make-up the shape of rotors best suited for desired application. From solely a thermodynamic performance point of view, a profile must have maximum throughput area and minimum leakage areas such as blow hole area and interlobe sealing line. But in a practical setting, rotors have to be manufacturable at a feasible cost and they must be strong enough to endure high pressures generated inside to bear a long life. The choice of curves is constrained by these factors too. All these factors are highly interrelated and often inversely correlated, hence making these decisions regarding choice of curves—a game of trade-offs between performance, cost and reliability.

In the most early days of rotor profiling, this issue of right choice of curves was sidelined simply because, even if there was any wish to test new types of curves in profiles, the formalism to calculate conjugate shapes of complex curves was not in place which made entire process a trial and error way to incremental improvement. For this reason, only the most simple curves such as circles, lines and single points are used in most of the earliest profiles in literature. Only after a fairly decent formalism at place established by Sakun (1960), Litvin (1989), Stosic and Hanjalic (1997) and others, one can see the use of curves like ellipses, parabolas, hyperbolas and cycloids in rotor profiles used either for their own benefits or simply to obtain a patent. Still the range of analytical curves used in rotor profiling are limited to conic sections, involutes and trochoids.

The reason for this limited use might be either that the profiles generated with these curves alone are sufficiently good or that the inherent challenges with incorporating

analytical curves into design procedure that searches best suitable shape of profile outweigh the ease at doing the same thing with numerical shape functions such as splines or bezier curves. Kauder et al. (2002) and Helpertz (2003) explored the efficacy of later approach wherein bezier curves were used whose shape can be manipulated by tweaking control points (Figure 2.10). Looking at this problem of finding the best shape of profile as an optimization problem, they proposed genetic algorithm with selection criteria on simple geometric features such as blow hole area, sealing line length and rotor inertia to quicken the calculations and convergence. Though this approach looks promising there are few issues here (as reported by authors themselves) such as -

- In optimizations problems such as these, which involve a large number of technical criteria, authors state that even minor deviations in true/normal forms of Bezier curve lead to major faults in meshing conditions.
- Even if the profiles that don't confer to theoretical meshing conditions are excluded from further generations of optimization process, profiles represented by simple splines seriously deviate from optimized solution.
- A complex consistency check must be performed after each iteration to ensure that all segments (discrete shape functions) are tangent after minor variations. This impedes the computation time and convergence of solution.

Unlike above mentioned points, analytically represented curves pose no problem with deriving or satisfying the theoretical meshing conditions. Also, in this approach, the objective of optimization focuses on maximizing or minimizing purely geometric features of rotor profiles such as sealing line, blow hole, inertia, etc. which might not necessarily reflect as it is in thermodynamic performance. Reason for this is that many a features of rotors which have serious influence on overall performance such as length, wrap angle and interlobe sealing line are 3-dimensional in nature and independent of the cross-sectional design of profile. Furthermore, the geometric improvements translate to thermodynamic improvements by acting through the operational and working parameters. Hence, this is an indirect approach which may not guarantee improved performance of generated profiles at least up to the same extent as anticipated in optimization. The use of genetic algorithm for profile shape optimization underutilizes the years of knowledge built in small incremental steps into modern efficient profiles. It is not a completely opaque problem but the designer at the least knows basic principles of profiling through years of trial and error with different shapes of profiles.

Hauser et al. (2008) addressed some of the challenges in previous attempts of using this approach by suggesting NURBS (Non-Rational Uniform Rational B-Spline) for representing the curves. Authors claimed advantages such as high quality of shape representation with relatively less information content as well as the complex consistency checks after each iteration could be skipped. Svígler (2010) has commented in his book on use of NURBS in screw rotor profiling - it is said, though spline curves are advantageous for curve formation or representation, they are very inconvenient for

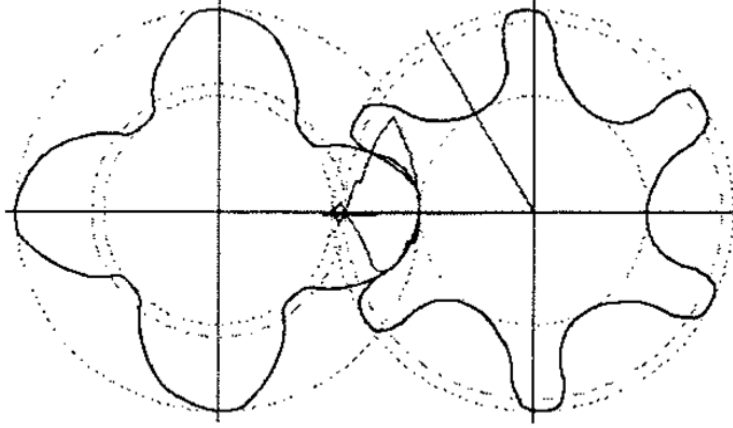


**Figure 2.10:** Optimized rotor profiles generated using bezier curves (Kauder et al., 2002)

calculating contact points of conjugate surfaces. This could pose some practical challenges in design such as calculating interference or clearance of rotors and ensuring good manufacturability. From the point of view of this development which aims at delivering an efficient and easy to manufacture rotor profile ready to be commercial in current industrial set-up, this promising approach may not be a feasible direction for it. Instead, an already in use and established profile such as N-Profile is preferable to build the study upon. However, some of the modern profiles use this approach of using splines and other numerical shape functions in their designs.

Another approach to optimizing the shape of profiles was demonstrated by Stosic et al. (2003b) who stuck to analytical representation of profile curves and optimized within the already known and tested N-profile to take advantage of all the features inherently built in its design through years of experience. The algorithm used for this optimization “Box-Complex method” searches for the optimized solution in the vicinity of the base profile based on thermodynamic performance of different variants. The representation of curves in N-profile offers a distinct advantage too. The general circle arc equation  $ax^p + by^q = 1$  enables to represent wide range of curves (all conic sections and lines) along with ability to parametrically tweaking them using  $a$ ,  $b$ ,  $p$  and  $q$ . Proof of this approach being highly feasible is found in the same article (Stosic et al., 2003b) where it has been reported that screw compressors for different operating conditions and applications were designed using this approach and tested too.

Coming to the more basic point of the challenge of choice of right curves for profile, almost all of the successful and patented profiles till date follow the tested path of analytically represented curves. In order to improve or incorporate other desirable features such as varying radius of curvature along the curve (which is not possible with circles as radius of curvature is fixed with its radius) for better distribution of contact stress or reducing blow hole area by sharpening tips at the end, inventions like Kim and Lee (2004) have introduced better representations of the common analytical curves such as hyperbolae in a parametric way so as to control flatness or roundness of the hyperbola. This provides advantage of already stated analytical representations as well as control over curve features.

Some of the other methods of generating screw rotor profiles from literature are worth mentioning. These methods didn't prove to be widely useful in industry or at producing practical rotor profiles. It includes profile generation from sealing line by Zaytsev and Ferreira (2005) which focused too much on a single feature shadowing complexity of screw rotors and interconnectedness of their features. Another recent work by Huang (2015) used deviation function method to optimize shapes of numerically represented profiles. This work is relatively recent to evaluate it impartially.

The deviation function method is based on conjugate pair design and generates new twin screw rotor profiles from generating curves derived by the deviation functions. The deviation functions used by Huang (2015) are composed of bezier curves. The theory of deviation functions is based on reshaping an original pitch curve by a function describing the amount of deviation between contact point on the conjugate pair and that on the corresponding pitch pair. This method has certain mathematical advantages such as non-circular pitch curves can be utilized without solving higher order non-linear equations. In this study by Huang (2015), a partially overlapped three-segment third order Bezier curve based deviation function is proposed to achieve geometrically superior profiles. Authors claim that the adoption of Bezier curves for deviation functions eliminates the complicated problem of having to select and define generating curves for a rotor profile. It is also claimed that this method helps discover a wider range of designs and optimal results.

However this study could be extended with more deviation functions. Use of B-splines or NURBS could provide more flexibility and advantage due to their popularity in CAD (Huang, 2015). Similar to the many very specific novel approaches to profile generation, this method heavily focuses on the simple aspect of geometry (leakage area). Further design consideration such as torque characteristics, thermodynamic efficiency of desired operating conditions, manufacturability, etc would definitely improve this approach. It still feels less intuitive than the lack generation or rotor generation approach to rotor profiling for externally twin screws meshing compressors. Though it is very intuitive for design of symmetric and identical type conjugate rotor such as those in lobe pump or gerotor pump.

The road to new generation of profiles lies in finding the better shape of rotors within constraints of performance, cost and reliability for given application. Distancing a little bit from literature on screw rotor profiles alone, looking in the wider frame of engineering and other disciplines, such a problem is generally termed as "shape optimization". It finds great attention in the fields of aerodynamics (Mäkinen et al., 1999) for designing better wings and in the field of thermo-fluids for designing better turbine blade shapes. Multidisciplinary problems and principles of shape optimization applied to these problems can be found as reported in Haslinger and Mäkinen (2003) which are very similar to approaches by Helpertz (2003). Though these methods look promising, the geometric complexity of a wing or blade and a screw rotor are entirely on different levels. Hence at current stage, such methods may look promising for rotor shape optimization on paper, but practically they very well might be infeasible.

Based on all the considerations and indications from literature review of different methods, there is a need for method that can handle analytical curves like those in conventional profiles while providing better control over curve features like that of recent approaches based on numerical shape functions. Such method lying on the middle-ground is found in the abstract science of topology which is not yet used in mechanical engineering applications. The concept is known as “Path Homotopy” (Armstrong, 2013) and it has the potential to cater most of the desired features needed for new profile development as understood and extracted from this literature review.

### 2.3 On the Manufacturability of Rotor Profiles

Manufacturability is an essential aspect of this research on profiling. The new profile primarily has to be more energy-efficient and if it could be more manufacturable as well, it would only be better. The energy efficiency of a profile can be directly evaluated in terms of numeric indicators such as profile displacement, leakage areas and thermodynamic performance in terms of either specific power or isentropic efficiency at specified operating conditions. Hence, any rotor profile can be objectively evaluated for its efficiency and compared with another profile on the basis of these quantitative indicators. A similar quantitative and complete evaluation of the manufacturability of rotor profiles is not available in literature. We find several works on various manufacturing aspects of rotor profiles and how different parameters can affect their overall manufacturability. But they are either qualitative approaches or they don't take into consideration all the necessary aspects of manufacturability. Manufacturability as a feature or a quality of rotors has an impact on compressors' performance, cost and reliability. Hence, there seems to be a scope for research and contribution into quantitative evaluation of any profile's manufacturability in order to be able to better incorporate it in the new profile development.

First a review of all the works on screw rotor profile manufacturability available in the open literature is presented. Fleming et al. (1994) presented for the first time a relationship between screw rotor profile cutting tool shapes and the the manufacturing costs associated with it. But this analysis was more qualitative and compared multiple tool shapes to establish which one would have more or less wear based on general indicators such as presence of sharp edges and steep angles of cutting. An actual extent of cost saving or manufacturability could not be determined in numbers but only subjectively.

Sauls (1998) evaluated for the first time, the effects of manufacturing variations on rotor pair clearances which affect compressor performance and reliability to a great extent. His observations were that different profiles react differently and to a varying extent to the same kind of manufacturing variations. Hence it was analytically proved that manufacturability of rotors does not only have a dimension of cost but performance and reliability too. In the follow up paper Sauls (2000), the manufacturing simulation methods developed in the previous work were used to compare two different profiles on the basis of the effect of manufacturing variations on each profile's rotor pair clearance

characteristics. This approach is somewhat quantitative in the sense that it evaluates average pairing clearance along the meshing line and compares it to minimum and maximum values to get a range of tolerance band consumed by certain rotor profile. Rotor profiles that consume minimum tolerance band upon manufacturing variations and showcase a good clearance distribution characteristics are obviously more desirable.

In a further extension of this work, Sauls (2002) presented a statistical approach to compare two profiles based on a similar premise as that of his previous works. By randomly introducing process parameter variations (based on machine capabilities) into his manufacturing simulation tool, a realistic data of 1000 pairs of virtual rotors was generated. Measuring these profiles by a numerical CMM (virtual coordinate measuring machine), number of acceptable and unacceptable pairs were evaluated. Since different profiles respond differently to manufacturing variations, a more robust profile from manufacturability point of view was supposed to have a lesser number of unacceptable pairs in this lot. Saul's approach to evaluating manufacturability has a quantitative aspect as it also covers performance and repeatability aspects of manufacturability as discussed. Still it could be improved on 2 fronts- first, it left out the effect of tool shapes, wear and their impact on cost of machining; and second, the manufacturing process parameters taken into consideration for this study are only three (tool-rotor center distance, tool setting angle and the tool axial position) among at least 5 others (lead, rotation, angular positions in other planes, tool dressing error, etc.).

Guo and Tang (2003a) included more of the process parameters in the Sauls (2002)'s manufacturing simulation with three parameters. In a follow up paper Guo and Tang (2003b), evaluation of screw rotor manufacturability using profile design data was presented. They discuss screw rotor manufacturability from three aspects- the required minimum tool profile radius, the range of valid setup conditions, and the severity ratio which is a measure of relative tool profile load distribution (first introduced by Sheth and Malkin (1990) in their work on helical groove machining). These aspects typically focus on the tool and evaluate manufacturability based on that alone.

Stosic (2006b) presented the tool wear aspect of screw rotor machining in detail. Screw rotors are helical and their cutting involves rotation and sliding motion at once. This has an effect of non-uniform wear across the tool profile for a given depth of feed. It used mathematical formulation to determine the non-uniform wear on the profile and compensate it by correcting tool profile pre-machining. This works is really important because it talks for the first time the impact of rotor geometry on its machining on account of the different lengths of cutting paths along the tool rotor meshing line. This work along with Stosic (2006a) entail an important aspect (tool wear) of the manufacturability of rotor profiles.

If one looks into the physics of rotor machining process, it is actually a contact of rotor and tool across a certain contact length at a certain feed which are different for each point on rotor profiles. But an important parameter that affects tool wear but missing from all the previous works on tool wear studies; is the relative speed between tool and rotor at the contact point during their engagement. Higher relative

speed at the contact point will lead to a higher wear rate of tool at that corresponding point. It is also evident that a portion of tool is more prone to wear if it is sharper (relatively low radius of curvature). Hence a complete model of tool wear associated with rotor profiles should incorporate radius of curvature, relative speed, contact path length and the depth of cut along each point of tool-rotor meshing line. This has been foreshadowed in Sheth and Malkin (1990) for helical groove machining but it has not been mathematically extended fully to screw rotor machining. This has been identified as a potential contribution in relation to this study.

Already existing models such as Stosic (2006b) which give a measure of relative tool wear across the profiles can be slightly modified to include the effects of contact path length, depth of cut, radius of curvature and relative speed. The term hence formulated could be used as a tool wear quantifying term. This term would serve as an indirect indicator of the costs associated with profile manufacturing since more tool wear will lead to more frequent dressings of tools which in turn increase not only the tooling cost but also the manufacturing cycle times closely linked with the costs of operation. But this approach still leaves out the impact of profile's manufacturability on performance and reliability for which Sauls (1998) calculated the proneness of profile clearances to manufacturing variations. This model could be either directly incorporated in this development as a check on good behavior of rotor pair clearances under manufacturing variations or be ignored since the clearance distributions imposed on profiles through rack itself enable quite sophisticated control on generated profile clearances. Hence, the potential impact of manufacturability of profile on its performance or reliability can be safely transferred and tackled in good clearance distribution design for the profile. This is again an advantage of using the principle of rack-generation for profile design.

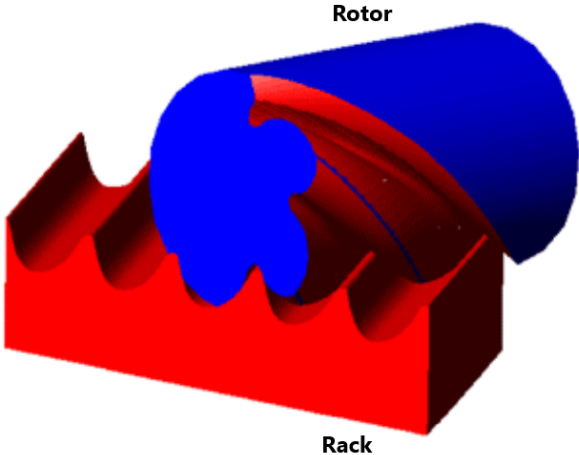


**Figure 2.11:** Illustration of the rack profile generating rotor virtually like a tool

Another argument against a heavy focus on manufacturability aspects of the new profiles being explored in this study is that the principle of rack-generation is a proxy way of generating profiles from tools. This is because a rack is virtually a tool of very

large radius that generates the given rotor profiles (Figure 2.11). Hence, in case of rack-generated profiles, the design flow is from a tool to rotor. This inherently makes the rack-generated profiles almost always manufacturable unlike some rotor generated profiles wherein a valid tool profile can not be physically guaranteed. Hence, as backed in the previous section on the review of methods, new efficient rotor profile development should be based on the principle of rack-generation for all its advantages. That makes the issue of manufacturability less worrisome for the new profiles.

## 2.4 Study of N-Rack Characteristics and its Curves

A comparative analysis to follow in the next chapter as well as the literature review presented in this chapter confirms that N-Profile is by far one of the best rotor profiles. There are several reasons for that, its foundation in rack generation, each constituent curve, its flexibility and optimization friendliness, etc. all of which make it a solid starting point for putting further efforts in improving rotor profiles. It is for this reason that the N-Profile rack also termed as ‘N-Rack’ is taken up as a frame for this new development.

In order to identify the scope of improvements in N-Rack, it is necessary to de-construct it curve by curve and understand each curve’s role in the overall profile’s efficiency. This could give more specific directions for the new profile development. Hence, its detailed review has been presented in this section.

Since the design of a general rack is composed of multiple analytical curves put side by side, there are more than one ways of cutting the entire rack profile along its arc length and representing each with an analytical curve. Each analytical curve section has certain constraints on it in order to maintain continuity and differentiability along the profile. Doing so, the final rack shape is generated which eventually generates conjugate main and gate rotor profiles. The choice of less or more number of sections on the analytically represented rack profiles depends on two factors-

1. The desired level of control over the shape of rack in its analytical form
2. The complexity in profile definition that comes with more number of profile sections and curves

The above two factors are seemingly competing. It is only desirable to have more control over profile shape for it gives more scope for shape optimization. But in analytically represented profiles, the continuity and differentiability is maintained by defining constraints on adjacent curve sections and their curve parameters. This demands for more complex mathematical derivations and definitions of profile curves and conditions. Hence, a good balance of an adequate level of control over the profile shape and the minimum possible complexity of definition must be met with the chosen number of curves on rack profile.

Typically the most well known profiles- SRM-A (Schibbye, 1970), SRM-D (Astberg, 1984), SIGMA (Bammert, 1982), Rinder (Rinder, 1987), Cyclon (Hough et al., 1987),

N (Stosic, 1997) are defined by anywhere between 5 to 8 curve sections on either the rotors or the rack. One example is presented here in Figure 2.12 of N-profile rack with 8 curve definitions. This structure of rack seems fairly balanced between number of curve sections and the control it gives over profile shapes. This exact rack outline is used in some of the later modern profiles with minor modifications such as those analyzed in the last section, Fu Sheng Profile (Lee et al., 2006) and Gardner Denver Profile (Cavatorta and Tomei, 2014).

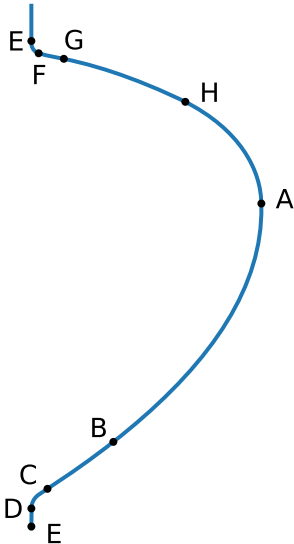


**Figure 2.12:** N-Rack with 7 curve sections on the rack profile

The curves on the rack profile are transformed on to the main and gate rotor lobes to generate respective profiles for rotors. Figure 2.13 shows this for the N-Rack. Table 2.1 lists the definitions of curves in N-Rack as the design flows from definition of rack to generation of rotors.

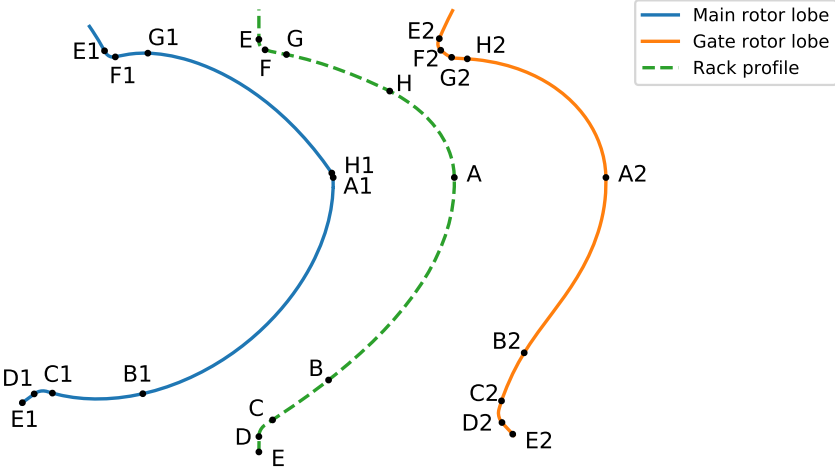


**Figure 2.13:** The conjugate main and gate rotor profile sections generated from the respective N-Rack profile sections

Curve	N-Rack	On Main Rotor (1)	On Gate Rotor (2)
D-E	Vertical straight line	Circular arc	Circular arc
E-F	Circular arc	Trochoid	Trochoid
F-G	Straight line	Involute	Involute
G-H	Cycloid	Trochoid	Circular arc
H-A	Cycloid	Circular arc	Trochoid
A-B	General arc*	Roulette <sup>†</sup>	Roulette <sup>†</sup>
B-C	Straight line	Involute	Involute
C-D	Circular arc	Trochoid	Trochoid

\*Parabolic, Elliptic or Hyperbolic arc, depending upon the arc exponents

<sup>†</sup>Roulette is a general form of trochoid where generator is not a circle

**Table 2.1:** The curves constituting N-Rack and the respective conjugate curves on main and gate rotors

Each pairs of conjugate curves has some unique characteristics which could be interesting from screw compressor's working principle point of view. These unique characteristics drive the choice of curves for a profile. For example, a choice of straight line on rack results in pair of involutes on the rotors. When a pair of involute curves mesh, they create a sealing line path that is a straight line. Straight line is a shortest path between any two points in space. From screw compressor's performance point of view, smaller sealing line length leads to smaller leakage path area hence better performance. Involute are also interesting from power/torque transmission point of view. Point is that the curve choices in profile design at appropriate positions is driven by such logics.

Each of the N-Rack curves is analyzed in following sections to understand such logics which are used to pin down scope of improvements for the new profile based on N-Rack. The already alluded homotopy approach will also be looked after for potential application in respective sections of the N-Rack.

### 2.4.1 Rack Section D-E

This section on rack generates male rotor root and and gate rotor tip face. In case of a straight vertical line at this section on rack, the respective main and gate portions coincide with the inner and outer circles of rotor respectively. The flat tip face of gate rotor (D2-E2) especially is a path of high pressure fluid leaking via radial gap between gate rotor teeth and the casing. The air oil mixture has certain viscosity and the fluid in this gap creates drag forces on rotating gate rotor. It is highly possible that the larger flat surface of the gate rotor leads to higher drag due to more contact area. Abdan et al. (2022) recently presented analytical means to accurately evaluate the drag losses in such gaps in screw machines.

It is hence desirable to try the inclined portion at D-E on rack to make main root and gate tip surface inclined and less engaging with casing in order to minimize drag. The foretold effect will be more significant in oil-flooded compressors. This inclined gate tip face may even act as sealing strip and avoid excessive heating due to engagement

of larger lobe tip area with casing. It can be visualized as presented in Figure 2.14.



**Figure 2.14:** The representation of flat and inclined gate tip face

The calculations presented by Abdan et al. (2022) predict that such a profile modification could give smaller drag power losses in oil injected machines especially running at high tip speeds. The introduced inclination will probably reduce the oil drag as predicted, but it is also likely to increase leakage. Hence, the two competing effects are at play. If the oil drag is relatively small, the effect of its reduction will be small, thus the overall effect of the leakage may be more important. However, if the oil drag is relatively high, its reduction may be more important than the leakage increase. The surest way to know this for certain compressor application is to test an inclined profile against a retrofitted regular profile.

#### 2.4.2 Rack Section D-C, E-F and A-H (Rotor Tips)

Main rotor lobe has one tip A1-H1 whereas gate rotor lobe has two tips E2-F2 and C2-D2. Conjugates of these curve sections on rack are A-H, E-F and C-D respectively. N-profile is a combined rotor-rack generated profile to be precise. The cycloidal section G-H-A on short side of rack is defined actually on rotors. Hence, the main lobe tip A1-H1 is defined as it is on main rotor. The gate rotor tips though are both defined on rack itself.

The interaction of main tip A1-H1 and gate tip E2-F2 is of importance from the point of view of the leakage area of a profile. These two influence the high pressure cusp blow hole area of a profile. In order to minimize the blow hole area, it is desirable to make these two sections on profile as sharp as possible. But sharper tip radii also influence the sealing line length to be longer. Hence it is a compromise between the two major leakage areas of the profile. Profiles like those by Tang (2007) have modified the gate tip to be narrower by using curves like ellipse directed such that semi major axis points outwards. In this way, gate tip that influences blow hole area gets to be narrower/sharper and reduce the overall leakage with relatively less impact on sealing line length. With homotopy approach in hand, some experimenting could be done with the main and gate rotor tips that influence blow hole area. Homotopies can be so written that the sharpness of chosen curves will be controlled precisely to affect the leakage areas in the most desired way.

The other gate rotor tip C2-D2 is more important from the sealing line length point of view. Changing its curvature affects the sealing line length and displacement area in various ways depending on the profile. The trend of this effect is not quite straightforward and linear. Each case needs to be evaluated and checked according to the profile. Still experiments can be done on this section of the profile too with a homotopy similar to the one to be used at leading edge gate tip.

The tips are specifically interesting from manufacturability point of view too. Being the sharpest regions on the profile, the cutting tools portions that cut profile tips wear out faster. Hence to achieve a good form of tips (especially the sharper ones), tools need relatively more frequent dressings and it adds up to tooling cost and cycle times. So the tip designs are closely linked to the manufacturability aspect of profiles and not only performance.

### 2.4.3 Rack Section A-B-C (Long Edge)

This section of rack constitutes one of the longest single continuous curves on the profile. It majorly affects the displacement area of profile and the sealing line length. These two parameters compete with each other in order to affect the profile efficiency. The profile efficiency is a purely geometric characteristic which is defined as a ratio of profile displacement/throughput area and the total leakage area. The larger displacement area is desirable to gain more flow per cycle as its influence on the compressor performance is positive. Whereas, sealing line length is a leakage path and it influences compressor performance in a negative way. So profile efficiency is a good metric to evaluate a profile entirely geometrically.

This section consists of two curves in N-rack, general arc A-B and a straight line B-C. For the sake of discussion and further evaluation, a version of N-Rack wherein the general arc defined as  $y = 0.5x^n$  (Hanjalic and Stosic, 1993) with a control parameter ‘ $n$ ’ is considered. The control parameter ‘ $n$ ’ associated with this curve influences the aforementioned competing profile parameters. Hence it is important to set it up rightly to achieve maximum profile efficiency.

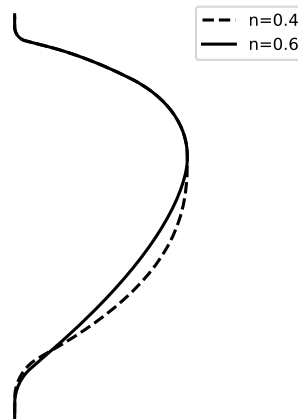


**Figure 2.15:** Depiction of flatness characteristic of the arc at section A-B w.r.t parameter ‘ $n$ ’

It is observed that the considered arc gets flatter in portion A-B of the rack as the control parameter ‘ $n$ ’ increases (see Figure 2.15). The A-B section was hence examined to see how the its flatness feature quantitatively affects the profile displacement area and leakage areas. The graphs are presented in Figures 2.16 and 2.17.

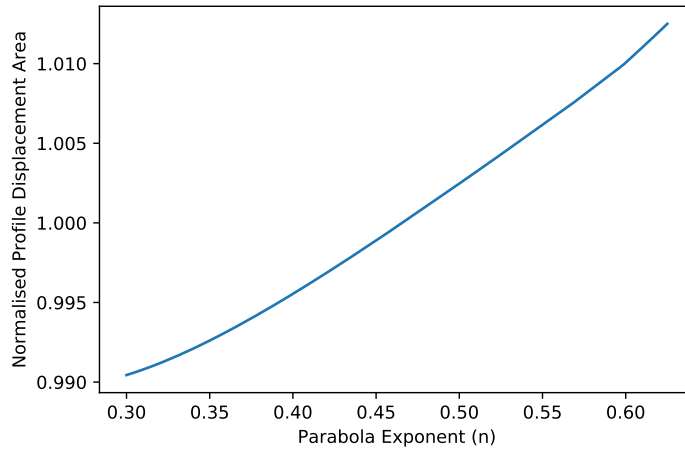


**Figure 2.16:** Influence of ‘ $n$ ’ on Displacement area

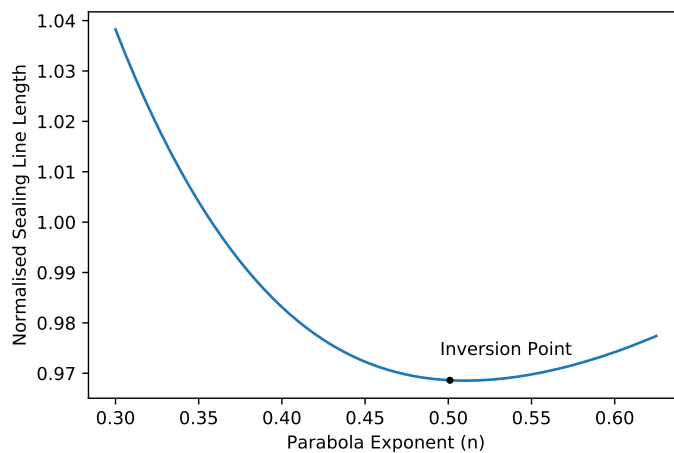


**Figure 2.17:** Influence of ‘ $n$ ’ on Sealing line length

It is observed that the displacement area increases steadily with ‘ $n$ ’ whereas the sealing line length first decreases and then increases from an inversion point. Hence, a flatter curve is desirable in this section of rack but not too flat where leakage areas rise again after the inversion point. The other major component of overall leakage area is the blow hole area. It is observed that it remains unaffected by this curve portion and is only affected by rotor tips as described in previous subsection.

Other curves in this section have been tried such as Ellipse by Lee et al. (2006) and Hyperbola by Cavatorta and Tomei (2014) and Kim and Lee (2004). The claims are that different features of curves such as ellipse or hyperbola may improve the ratio of displacement area and sealing line length. Hence, in order to achieve the best ratio of

these competing parameters, different curves with a more control on their features may give better results. Homotopy could be handy to set these up.

The straight line following the arc falls in the profile section which comes into play while driving one rotor with the other rotor. Straight lines on rack transform as involutes on rotors and these are desirable curves where power transmission is involved. There is an additional benefit of straight lines on rack w.r.t sealing line leakage paths. When involute sections of rotors mesh, the sealing line they produce is a straight line. Straight lines being the shortest paths between two points, involutes in a way generate the shortest sealing line while meshing. Hence for all its benefits, it is less interesting to change or experiment with any other curve here. Straight line is the best choice for this section.

#### **2.4.4 Rack Section F-G-H-A (Short Edge)**

This is a very critical portion of any profile as it directly affects one of the major leakage area called 'high pressure side blow-hole area'. Stosic (1997) elaborates on this matter at length as this very portion is one of the key feature of his invention. With examples of prior arts, it is established that in order to minimize the high pressure side blow-hole area, this portion (G-H-A) in almost all rotor generated profiles is produced by a conjugate action of both rotors which undercuts each other's high pressure side (the same portion of profile under discussion). In rack generated profiles, a proper curve on high pressure side of the rack that translates to undercuts on respective rotors is not found in literature before Stosic (1997). N-profile settles this problem by adopting a rotor-rack generated approach to define profile in this part of the rack. A portion of main rotor (G1-H1) undercuts the high pressure portion on rack (G-H) whereas a portion of female rotor (H2-A2) undercuts the rack portion (H-A). This continuous rack segment (G-H-A) is then used to generate complete main and gate rotor lobe short sides.

Since this is the most perfect form of the curve that can fit in this portion of profile, there is little to no scope of modification in rack portion G-H-A. This is evident in many later rack generated profiles after Stosic (1997), such as Lee et al. (2006) and Cavatorta and Tomei (2014) which fully retain this aspect of the rack profile but vary others to claim patents. Hence in the new rack generated profile, this section will remain unchanged.

The straight line G-F is again similar in characteristics to the straight line B-C on long side of the rack. It generates involutes on the rotors and they in turn generate the minimum sealing line length while meshing. This section of profile is also meant to provide tight sealing, which this curve seems to serve perfectly well. Though there are some later variants of N-profile that specifically eliminate this straight line G-F in order to further reduce the blow-hole area at high pressure side. This feature could be exploited by designing gate rotor lobes with larger addendums resulting in greater throughput area but limiting the blow-hole area to minimum values through this emission of straight line. Hence, only this section G-F out of the short edge of rack

(F-G-H-A) has some potential to be considered in the new profile development.

## 2.5 Review of Performance Calculations in Screw Compressors

Screw compressor performance is governed by the interactive effect of thermodynamic, fluid flow processes and the machine geometry. Thus their performance calculation or what is more generally known as 'simulation' can be reliably done only by the simultaneous consideration of all these three aspects. This may be achieved by mathematical modeling in 1-dimension.

A more rudimentary approach can be taken for performance calculation by neglecting the leakage effects and the friction losses in the gas. In the absence of any cooling flow and by neglecting heat losses through the compressor housing, the compression process proceeds approximately isentropically. This is an extremely simplified thermodynamic model for the calculation of the screw compressor performance. Some of the early literature such as Rinder (1979) recommends this in the absence of computer aided tools for more rigorous mathematical models. However, the more rigorous mathematical models are better at capturing the complexity of compression process in screw compressors as well as confer more closely to the actual experimental results.

Some of the known commercially available one-dimensional mathematical models for screw compressor performance calculation are SCORPATH, SCORG, KaSIM and PDSim. Mathematical models in more than one dimension are also possible. But for most applications, one dimensional model is sufficiently accurate. A 3-dimensional model is equivalent of a CFD simulation which is more complex and takes significantly more time for calculation than 1-D model.

The 1-D model is based primarily on the relationship of instantaneous volume of the working chamber (formed between the teeth of screw rotor pair) and the angle of rotation of the rotors. It is also known as the 'Volume-Angle' relationship, which is unique for a given rotor profile and geometry of a rotor pair. The principle of conservation of energy and mass along with the properties of the working fluid are applied to the 'Volume-Angle' relationship for working chamber to get "Pressure-Angle" and "Temperature-Angle" relationship. Based on the evaluated thermodynamic state of the working fluid at every instant throughout the cycle from suction to discharge, compressor's flow deliverable, various efficiencies (volumetric, isothermal, isentropic) as well as the shaft power can be evaluated.

Mathematical models such as SCORPATH, SCORG and KaSIM work according to the similar logic. Mathematical details of these models could be formed in Stosic et al. (2005) for SCORPATH, Ziviani et al. (2020) for PDSim, etc. The specification of these model differ based on some of the working assumptions they make in their respective models as well as some of the "real life" effects they choose or choose not to include in their models. Such effects include more complicated phenomena such as-

- oil-injection (in oil flooded screw compressors) and its mixing with the air to form

a two-phase mixture

- Heat transfer between gas and rotors
- Leakage of the working fluid through various leakage paths
- Compression of a mixture of gases (properties of mixture must be known)

This study specifically has been conducted with the use of mathematical modeling tool SCORPATH. It enables user to define a rotor profile and its geometry, based upon which a thermodynamic calculation routine can be run. Some of the assumptions in SCORPATH’s mathematical model for performance calculation are-

- The fluid flow in the model is assumed to be quasi one-dimensional.
- Kinetic energy changes of the working fluid within the chamber are negligible compared to internal energy changes.
- Gas or gas-liquid inflow to and outflow from the compressor parts is assumed to be isentropic.
- Leakage flow of the fluid through the clearances is assumed to be adiabatic.

This model, as specified earlier takes into consideration multiple “real-life” effects inside the working chamber which makes it a good tool for predicting compressor performance. It has been validated with experimental data over the years through multiple studies and has been improved as multiple industrial users have adopted it.

From the point of view of this study, wherein various rotor profile geometries are evaluated/compared using this tool, it is important to understand how the “geometry” and “thermodynamic” routines of this tool are connected. This knowledge will put the comparison of different profiles in SCORPATH in a better perspective.

When a rotor profile is imported or designed in SCORPATH, which is done in terms of a point-data (co-ordinates) of the rotor profile (main and gate lobes). Based on this data and clearance distribution, profile characteristics such as its tip sealing line length, interlobe sealing line length, blow-hole area, total displacement and clearance gaps are calculated in the “geometry” routine of the SCORPATH. This output of the “geometry” routine is given as an input to the “thermodynamics” routine. It works on these inputs along with the properties of the fluid being compressed according to the mathematical model previously described to generate compressor shaft power, work, free air delivered and temperatures at the discharge as outputs. Hence, the way these two routines communicate is through the values of profile characteristics calculated by the “geometry” routine based on the profile point data.

In this study whenever a profile is evaluated in SCORPATH, its point-data is either generated in SCORPATH or is imported from an external source (some routine separately written to generate specific profiles). Then the “geometry” routine in SCORPATH calculates the profile characteristics and based on those, the “thermodynamics” routine calculates the performance of the screw compressor with the imported profile

upon its rotors. During comparison of two or more profiles, one only has to ensure that the working conditions such as inlet/outlet pressures, temperatures of working fluid as well as injected fluid need to be same for a fair comparison across profiles. These inputs are required essentially for performance calculation.

## 2.6 Summary of the Literature Review

Upon the general review following the history of profiling along with the review of methods of rotor profiling that followed, the literature review on the manufacturability of profiles has been presented. It is concluded with a detailed review of N-Rack features while identifying scope for improvement in each of its constituent curves. A comprehensive review of performance calculations in screw compressors has also been presented. The literature review on the whole provides following directions for the new profile development-

- From the review of different mathematical formalisms to calculate screw rotor profiles (conjugate shapes and their mathematical representations), ‘envelope approach’ is the most befitting one.
- From the review of profile generation principles, ‘rack-generation’ turns out to be better than rotor-generation or sealing line generation. The reasons for which are multiple advantages it has to offer along with the simplicity in design procedure.
- In new profiles, analytical representation of curves has its advantages; whereas at the same time if curve features such as radii of curvature and its variation, roundness and flatness could be controllable parametrically, that will bring an additional leverage in curve choice.
- ‘Path homotopy’ could turn out to be promising for application in profiling based on the previous point. Especially for designing the low pressure side flank and high pressure side tips of the rotors.
- The choice of novel curves and methods for new profile development must take advantage of the years of expertise and empirical wisdom transfused in some of the best and time-tested profiles of contemporary times.
- Profile generation to minimize oil drag losses can lead to substantial improvements in the energy efficiency of the oil-injected screw compressors
- The criterion for search of optimized/better screw rotor profiles in any suitable algorithm must be the predicted/calculated isentropic efficiency with a check to reasonable manufacturability (which is difficult to measure quantitatively) of the produced geometry.
- The existing models of estimating non-uniform tool wear across the profiles can be modified to account for further factors such as radii of curvature and relative

speeds across tool/rotor profiles. The resulting quantitative wear indicator can be used to compare two or more profiles for their higher or lower manufacturability.

In the intellectual tradition of the art of screw rotor profiling; the undertaken research aims at contributing in a way briefly summarized in this chapter, which is built upon the comprehensive review of literature and methods to the best of author's knowledge.



# Chapter 3

## Methods and Approach

THIS chapter is aimed at explaining the specific methods, techniques and how they have been used in the development of a new rotor profile. Before discussing the methods and their application, it is important to put the objectives of this study in a right perspective. It also calls for a justification of why the certain methods have been used? And it is closely linked to the directions derived from the literature review. The new profile development has been mapped in three steps- conception, evaluation and validation. Next chapters of the thesis follow on the three distinct concepts proposed here and the methods briefly introduced which would be further developed in later chapters.

### Contents

3.1	Better Profiles, but how much? . . . . .	42
3.2	New Profile Development . . . . .	47
3.2.1	Conception . . . . .	47
3.2.1.1	Three Concepts for the New Profile . . . . .	47
3.2.1.2	The Concept of Homotopy . . . . .	48
3.2.2	Evaluation . . . . .	50
3.2.2.1	Methods to Evaluate Profile Geometry and Thermodynamic Performance . . . . .	50
3.2.2.2	Method to Evaluate Manufacturability (Stosic, 2006b) . . . . .	51
3.2.3	Validation . . . . .	56
3.3	Expected Contributions . . . . .	56

### 3.1 Better Profiles, but how much?

The primary goal of this study is to develop a new screw rotor profile with better energy efficiency. The scope of work also involves application of methods to qualify and quantify the developed new profiles on suitable metrics. An important task is to put the “better efficiency” in a right perspective before setting out to actually design a new profile. The literature review set out a detailed account of the history and methods of profiling. The evolution of profile design principles is hence well put in perspective but their impact is not. It is hence attempted here to scientifically evaluate the impact of profiles on the energy efficiency of screw compressors.

If one turns to literature for the accounts of improvements in energy efficiencies of screw compressors with the use of new profiles, there are three such reportings to be found. Stosic et al. (2000) presents a case of retrofitting old SRM-A profiled rotors in an oil flooded twin screw compressor with the N-profiled rotors and thereby improving the energy efficiency of the machine by 2.5%. The combined profile and geometry optimization with Kaeser’s new profile (Weih, 2019) is claimed to have improved upon the old SIGMA profile (Bammert, 1982) by up to 3%. Similarly, Fu Sheng’s rack generated profile (Lee et al., 2006) is claimed to have improved on their own old rotor generated profile (Lee, 1990) by 1.32% in terms of the energy efficiency (Wu and Fong, 2009). These are the cases in which fairly modern profiles have been compared with old profiles. Patil et al. (2022) presents a case for contribution of modern rotor profiles to energy efficiency of screw compressors. Its conclusion states that the screw compressor manufacturers already in possession of a good modern profile should expect improvements from any new profiles in the order of 1% at maximum.

The improvements in energy efficiency of compressors over a long period of time can not entirely be attributed to the profiles. For over time, not only profiles but also the manufacturing precision, assembly techniques and process control significantly improve to aid the performance. However, with the use of modern profile calculation software suite such as SCORPATH, the impact of profiles’ evolution over the time on a typical screw compressor’s energy efficiency can be calculated. For this, some of the seminal rotor profiles could be chosen and generated for a similar size of screw compressors. Evaluating them at similar operating conditions using the same software suite, impact of only the profile on energy efficiency could be known. Profiles starting from very symmetric to most modern ones could be selected for such evaluation. It will set up the objectives of this study in right perspective of how much improvements are reasonable to expect with the new profile development.

For this evaluation, one profile each from the four phases of evolution described in the literature review could be selected. Hence, a circular symmetric profile from first phase of simplistic profiles could be chosen. An asymmetric SRM-A profile could be chosen to represent the early asymmetric profiles of the second phase. On top of all, N-Profile could be selected to represent the most modern rotor profiles wherein all the known principles of a good rotor profile (such as rack generation and variable clearances) are incorporated. These profiles are designed for 4/6 lobe combination and

at a common center distance of 100 mm and same rotor addendum. This is to ensure a fair comparison of these profiles.

The reason for choosing these three particular profiles for comparison has been made clear. However, various rotor geometries could be selected with these profiles for calculation. The reason for selecting the 4/6 lobe combination is that it is one of the most commonly used lobe combination in screw compressors, made popular by SRM; especially for air application and moderate pressure ratios. Since SRM primarily and most commonly used only 4/6 lobe combination, no reference is available to rightly design a ‘SRM-A’ profile for any other lobe combination. For this reason, other two profiles in comparison- ‘symmetric’ and ‘N’ are also designed with a 4/6 lobe combination, even though they can be easily designed for any other lobe combination.

The center distance of 100 mm was roughly chosen because the screw compressor of this center-distance is usually of a moderate size. The power rating of such a compressor for air application falls somewhere between 30 kW to 75 kW. Such a screw compressor is neither “too small” nor “too big”. It is well known that smaller screw compressors are relatively less efficient and longer ones are relatively more efficient. To eliminate this additional variations with respect to size, a moderate size is selected for comparison of profiles. And for calculation, SCORPATH has been used.

The rest of the profile geometrical parameters such as wrap angle and L/D ratio are set to  $300^\circ$  and 1.65 respectively. They are known to be good design choices for the application in this study.

Refer Figures 3.1, 3.2 and 3.3 for the profiles chosen for evaluation. Refer Table 3.1 for the comparison of the geometric characteristics of these profiles. Refer Table 3.2 for the comparison of energy efficiencies of these profiles at common operating conditions (oil injected air application, ambient suction and 8.5 bar discharge).

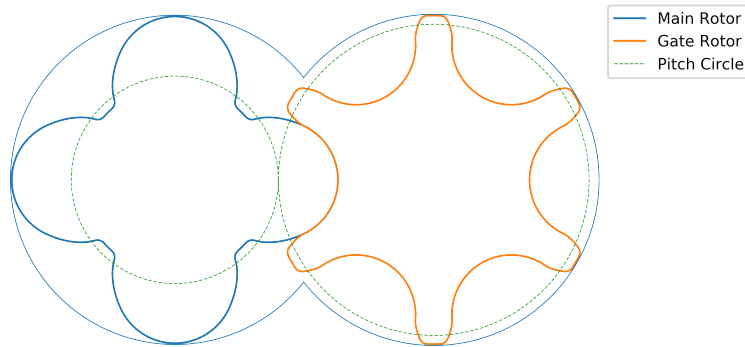


**Figure 3.1:** 4/6 Symmetric Circular Profile with center distance 100 mm

Profile Characteristic	Symmetric Profile	SRM-A Profile	N Profile
Total throughput area (mm <sup>2</sup> )	7541	7773	7835
Interlobe leakage area (mm <sup>2</sup> )	4.162	5.046	5.017
Blow hole area (mm <sup>2</sup> )	41.515	7.794	6.784

**Table 3.1:** Geometric profile characteristics for retrofitted Symmetric Profile, SRM-A and N-Profile

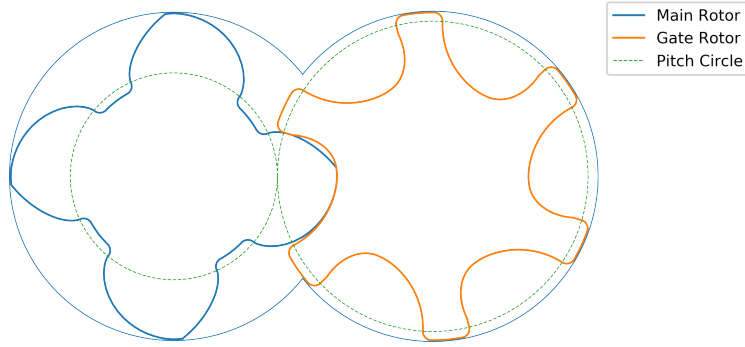


**Figure 3.2:** 4/6 SRM-A Profile with center distance 100 mm

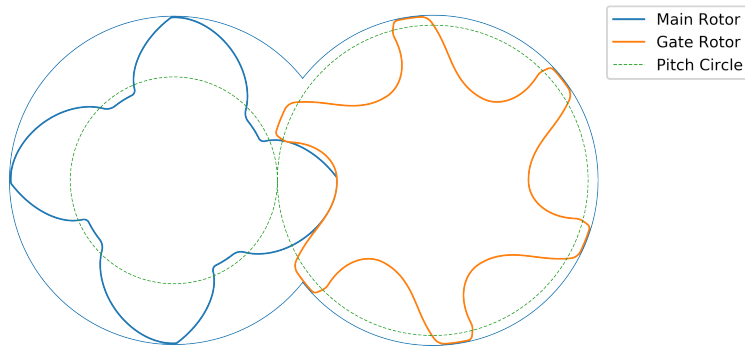


**Figure 3.3:** 4/6 N-Profile with center distance 100 mm

Adiabatic Efficiencies	Symmetric Profile	SRM-A Profile	N Profile
At male rotor tip speed of 10 m/s	53.8%	67.0%	70.6%
At male rotor tip speed of 20 m/s	71.5%	77.5%	79.1%
At male rotor tip speed of 30 m/s	74.3%	78.2%	79.0%
At male rotor tip speed of 40 m/s	74.4%	77.1%	77.6%

**Table 3.2:** Thermodynamic profile characteristics for retrofitted Symmetric Profile, SRM-A and N-Profile (oil injected air application, ambient suction and 8.5 bar discharge)

As evident from Table 3.1; the blow hole area is a major issue with symmetric profiles. Asymmetric profile SRM-A has almost 5 times smaller blow-hole area compared to symmetric circular profile. The sealing line length however increases by 20% , the overall effect is positive since the reduction in blow hole area is tremendous. The increase in throughput area or displacement is also evident from the symmetric profile to the SRM-A profile. Thermodynamically, improvements from symmetric profile to SRM-A range from 2.6% to 13.2% (Table 3.2) which is a huge leap. That is why, as already mentioned in the literature review, SRM-A played a major role in making screw compressor technology commercially viable for the first time.

The case of N-Profile improvements over SRM-A is interesting since it demonstrates clearly the benefits of rack-generation, better curves and optimized profiles. It can be observed from Table 3.1 that the N-Profile throughput area is almost 1% larger along with 15% smaller blow-hole area that too with a smaller sealing line length. The improvements in energy efficiency range from 1% to 3.6% (Table 3.2), which is

consistent with Stosic et al. (2000).

Continuing this analysis into modern rotor profiles that come after N-Profile (Stosic, 1997), it is observed that the % improvements in energy efficiency are further narrowed down. Since most of the modern rotor profiles have incorporated the principles of good rotor profiles in their designs over the time, their differences are now very small. Many patents tried to mimic the N-Profile by replacing only few curves but sticking to the philosophy of overall generation and principles embedded in it. Similar to the analysis with symmetric profile and SRM-A, modern profiles like Lee et al. (2006) patented for Fu Sheng, Cavatorta and Tomei (2014) patented for Gardner Denver and a further fine tuned version of N-Profile called N-Silent (Stosic, 2017) patented by City University could be retrofitted and compared.

Figure 3.4 and 3.5 are a representation of retrofitted modern profiles but this time with a 5/6 lobe combination and larger profile depth at approximately 100 mm of center distance. Hence these are not directly comparable to the analysis with symmetric and SRM-A profile but it is indicative to some extent. However this comparison is helpful to understand the scope of improvements in between the modern profile; which is more relevant to set the goals for development of a new and better profile.

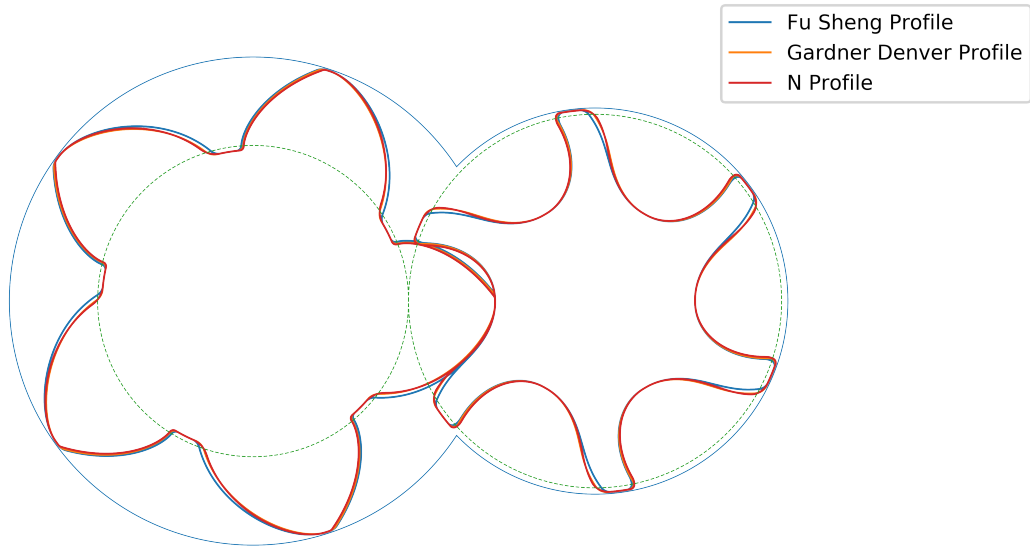


**Figure 3.4:** Retrofitted Profiles- Fu Sheng, Gardner Denver and N with 5/6 lobe combination and  $\sim 100$  mm center distance

Table 3.3 is presented with a comparison of the modern retrofitted profiles based on their geometric characteristics such as displacement and leakage areas. It is clear from the data that the differences are small yet result of minute detailing in the profiles. Which for the most part is the scope of modern profiling. In terms of the energy efficiency, again calculated at the same working conditions, the N-Profile is better than the other two. The range of difference however is now between 0.29% to 0.35% (Table 3.4).

This points to a conclusion that with the application of already known principles of rotor profiling, the further improvements in efficiency are only going to come in the

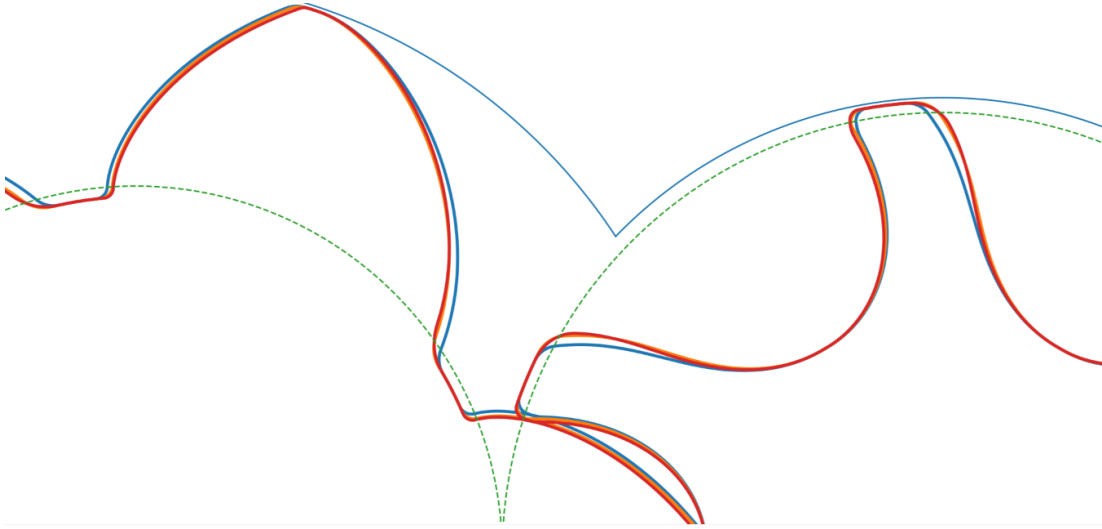


**Figure 3.5:** Zoomed in view of the profiles in Figure 3.4

Profile Characteristic	Fu Sheng	Gardner Denver	N Profile
Total throughput area (mm <sup>2</sup> )	8507	8621	8627
Interlobe leakage area (mm <sup>2</sup> )	4.693	4.873	4.863
Blow hole area (mm <sup>2</sup> )	1.852	1.191	1.380

**Table 3.3:** Geometric profile characteristics for retrofitted Fu Sheng Profile, Gardner Denver Profile and N-Profile

Adiabatic Efficiencies	Fu Sheng	Gardner Denver	N Profile
At male rotor tip speed of 10 m/s	72.56%	72.88%	72.91%
At male rotor tip speed of 20 m/s	79.30%	79.57%	79.62%
At male rotor tip speed of 30 m/s	80.28%	80.53%	80.59%
At male rotor tip speed of 40 m/s	79.76%	79.99%	80.05%

**Table 3.4:** Thermodynamic profile characteristics for retrofitted Fu Sheng Profile, Gardner Denver Profile and N-Profile (oil injected air application, ambient suction and 8.5 bar discharge)

order of 0.5%. The trend in Figure 3.6, plotted based on the maximum improvements in each of the comparison made in this chapter’s analysis, makes it easy to visualize this fact. This calls for either an innovation in profile generation or better understanding of the physics of compression to further improve the profiles. If this is achieved in this development; then the improvement between 1 to 1.5% can be expected.

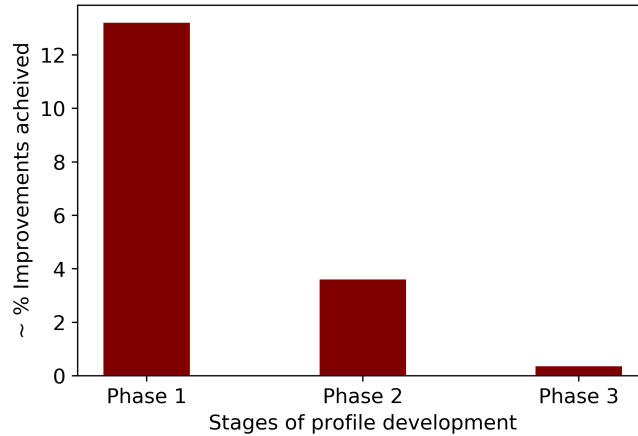


**Figure 3.6:** Profile development over the years Vs. improvements in energy efficiency

This is also due to an important fact about efficiencies of machines that could help put the goals of this study in a right perspective. It gets more and more difficult over the years to make machines more efficient since the battle after a point is not with the efficiency but with inefficiencies. Hence, the anticipated improvement having the order of magnitude of 1% is not to be seen as a 1% improvement over the existing 80% adiabatic efficiency; but rather a 5% reduction in the remaining 20% inefficiency of the screw compressors in general.

## 3.2 New Profile Development

Three stages of the new profile development are presented in this section. It is based on the conclusions of literature review, the comparative analysis of profiles and the study of N-Rack characteristics. It is more aimed at technique and methods that are adopted in this study.

### 3.2.1 Conception

#### 3.2.1.1 Three Concepts for the New Profile

The concepts for the new profile are drawn from the study of N-Rack characteristics and the literature review. To summarize, these concepts are on top of the N-Rack design and they include-

1. Application of path homotopy to improve selection of the general arc on long edge of the rack

2. Application of path homotopy to control rotor tip features more in the favor of minimum blow-hole areas without impacting sealing line length and manufacturability too much
3. Profile generation to minimize drag power loss

The full extent of the conceptualization would realize with actual profiles generated with these ideas. In order to design profiles inspired by these ideas, the N-Rack calculation module available in commercial software SCORPATH (Stosic, 1993) is used as a base. Its source code is modified according to the need of the concept and new profiles are generated.

The first two concepts are linked to path homotopy. Its application in profiling and improvements achieved are presented in Chapter 4. It is a core contribution of this study in terms of how this method has been successfully adopted to profiling and it is shown to substantially improve profiles. The third concept of profile generation to minimize oil drag losses has been presented in Chapter 5 which includes validating this concept experimentally. The manufacturability aspect of profiling which is a key element of second concept about using homotopy to design tips of the rotors, first requires a quantification of this rather subjective term to evaluate the impact of design on it. Such a quantification is proposed and used to evaluate manufacturability of new profiles in chapter 6.

Path homotopy is at the core of the new profile generation. Hence is explained in next subsection. Following this introduction, next chapter builds upon it to generate new and more efficient profiles using this idea.

### 3.2.1.2 The Concept of Homotopy

In topology, homotopy (Armstrong, 2013) is a concept related to ‘paths’ which in the language of topologists, is defined as a continuous function on a closed unit interval  $[0,1]$  in a topological space. A ‘homotopy of paths’ is a notion of continuously deforming a path while keeping its endpoints fixed. Topologists usually talk in terms of spaces, manifolds and higher dimensions but essentially speaking from application point of view, this simple yet elegant concept of homotopy is what allows a parametric deformation of any two continuous functions (or curves for profile designer’s interest) between fixed endpoints. And the form of ‘path homotopy’ which will be used herein is its most simplistic form in 2-D space where continuous functions are two dimensional analytical curves representing rotor profile shapes.

Mathematically speaking, homotopy between two curves  $Curve_1$  and  $Curve_2$  having fixed common endpoints is written as-

$$\mathcal{H} = (q)(Curve_2) + (1 - q)(Curve_1) \quad (3.1)$$

where ‘ $q \in [0, 1]$ ’ is the homotopy parameter or the deformation parameter. The  $Curve_1$  is set as the initial state of homotopy and  $Curve_2$  is set as the final state of the deforming homotopy. When  $q = 0$ ,  $\mathcal{H} = Curve_1$ ; and when  $q = 1$ ,  $\mathcal{H} = Curve_2$ . The

homotopy parameter ‘ $q$ ’ continually deforms the  $Curve_1$  into the  $Curve_2$  by taking all intermediate shapes as  $q$  goes smoothly from the closed interval 0 to 1 (three such instances depicted as  $q = 0.2$ ,  $q = 0.5$  and  $q = 0.8$  in Figure 3.7).

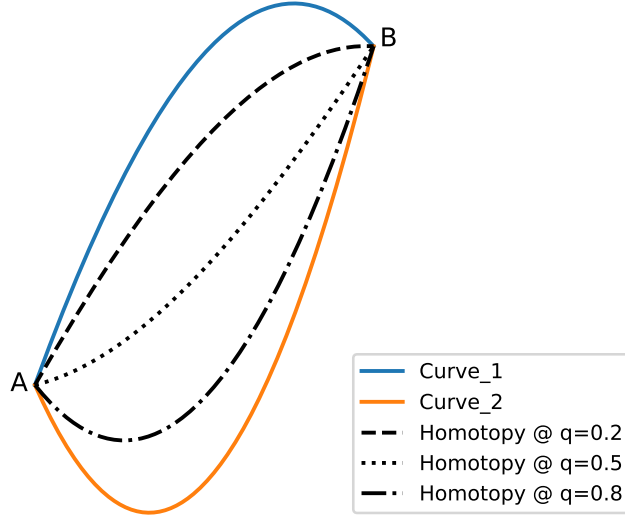


**Figure 3.7:** Demonstration of the homotopic deformations across any two curves defined in between fixed endpoints

In order to demonstrate a formulation of homotopic curve out of two known analytical curves,  $Curve_1$  could be assumed to be a circle and  $Curve_2$  as an ellipse. The parametric equations for these curves (assumed to be centered at origin) could be written as-

$$\begin{aligned} x_1 &= r \cos(t) \\ y_1 &= r \sin(t) \end{aligned} \quad (3.2)$$

where  $r$  is the radius of circle and  $t$  is the curve parameter. And,

$$\begin{aligned} x_2 &= a \cos(t) \\ y_2 &= b \sin(t) \end{aligned} \quad (3.3)$$

where  $a$  and  $b$  are semi-major and semi-minor axes of the ellipse,  $t$  being the curve parameter.

The homotopic curve that continually deforms in between these two curves is constructed as-

$$\begin{aligned} \mathcal{H}_x &= q(x_2) + (1 - q)(x_1) \\ \mathcal{H}_y &= q(y_2) + (1 - q)(y_1) \end{aligned} \quad (3.4)$$

where  $q$  is the homotopy deformation parameter and  $x_1$ ,  $x_2$ ,  $y_1$  and  $y_2$  are as defined in Equations 3.2 and 3.3. It is presented in Figure 3.8, how this parametric homotopy in Equation 3.4 deforms in between the circle and the ellipse.

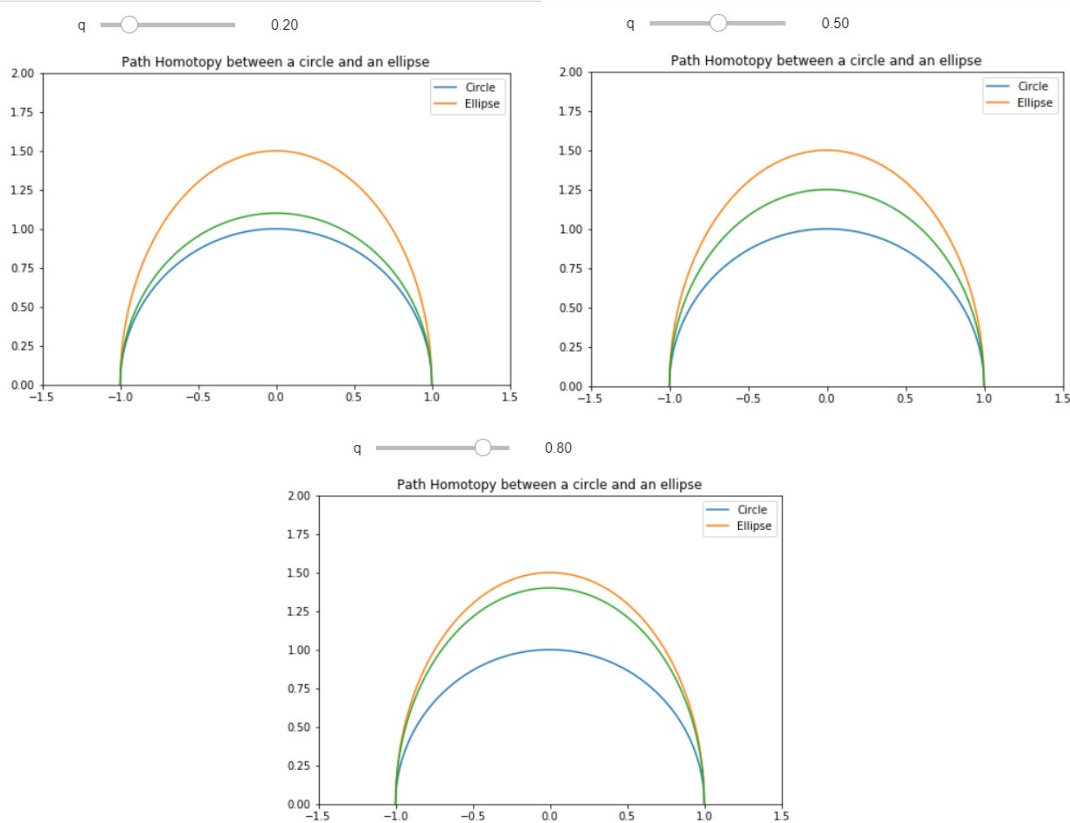


**Figure 3.8:** Homotopic deformations between a circle and an ellipse

## 3.2.2 Evaluation

### 3.2.2.1 Methods to Evaluate Profile Geometry and Thermodynamic Performance

The generated profiles need to be evaluated both geometrically and thermodynamically in order to compare them with state of the art rotor profiles and judge their improvements. Again, software packages SCORPATH and SCORG are well equipped to calculate geometric characteristics such as displacement area and various leakage paths for a new profile. The thermodynamic simulation of the compression process is also possible with these tools which is used to compare energy efficiency of new profiles with state of the art profiles.

However, the thermodynamic simulation requires one to set working and operating conditions for a certain profile before comparison. A certain profile's improvement is sensitive to the point of evaluation (operating conditions) too. The point of evaluation was set in the interest of the industry sponsor of this research project. However this does not limit the scope of results and the body of knowledge generated hereby. Oil-injected air application with ambient suction at standard conditions and discharge at around 8-10 bar pressure is the most common evaluation range from thermodynamic point of view for the new profiles presented in the course of this thesis.

In order to compare the energy efficiency of two profiles, they could be compared based on either the specific power or the adiabatic efficiency. For a given screw com-

pressor profile, geometry and working conditions, the specific power is defined as the shaft power consumed for delivery of an unit volume of the compressed gas at its suction conditions. It is a measure of energy efficiency since more amount of compressed gas is desired at minimum expenditure of the power. Lower specific power is indicative of better energy efficiency.

Adiabatic efficiency is the ratio of a compressor's shaft power (actual work consumed for compression) to the isentropic power of compression between the set suction and discharge pressures. It indicates how far is a certain compression process from the almost ideal compression without the irreversible heat and mechanical losses to the surroundings. Higher adiabatic efficiency for certain profile at set conditions is indicative of its higher energy efficiency.

At certain occasions, it is also interesting to look at the volumetric efficiency of the compressor with the designed profile and chosen clearances. It gives insights into the efficiency of profile to limit internal leakages which would indicate smaller leakage paths relative to the throughput volume. It all translates to better energy efficiency too.

The trickiest of all profile evaluation parameters is its manufacturability. It has been discussed in literature review too. And new profiles specially the ones wherein homotopy is expected to improve performance by modifying tip designs totally hang on to the ability to quantify manufacturability of profile. Otherwise, it will be impossible to judge if modifications by homotopy are even beneficial or not? One such method from literature (Stosic, 2006b) has been presented here which does it by calculating tool wear for profiles. This method will later be modified to incorporate effects of relative speed between tool and rotor in chapter 6. However, following subsection lays out how it is done in Stosic (2006b) and the discussions in chapter on manufacturability are built upon this method.

### 3.2.2.2 Method to Evaluate Manufacturability (Stosic, 2006b)

The form milling process of a screw rotor is presented in Figure 3.9 (Stosic, 2006b) where it can be seen that the tool is a wheel like body with its cutters having their own profile. The axis of cutting tool is inclined at an angle of  $\Sigma$  and is parallelly placed at a distance of  $C$  with respect to the rotor axis. The grinding cutter wheel is similar to the milling cutter except that its entire body is made of material such as silicon carbide or aluminium oxide. It is given the shape of desired tool profile (like that of inserts on milling cutting tool) by dressing it with dresser wheels made of even harder material.

Figure 3.9 also helps to visualize the rotor ( $X - Y - Z$ ,  $X_h - Y_h - Z_h$ ) and tool ( $X_t - Y_t - Z_t$ ) coordinate systems which are useful for calculating the rotor and tool profiles from one another. In addition to these transformations, it is also useful for calculating relative speed between tool and rotor along their contact line.

Given a rotor profile which has coordinates  $x$  and  $y$  along with known slopes  $\frac{\partial y}{\partial x}$  at each point in the transverse plane (which is plane perpendicular to the rotor axis) and setup conditions such as value of  $\Sigma$ ,  $C$  and lead of the rotor ( $2\pi p$ ), a unique tool

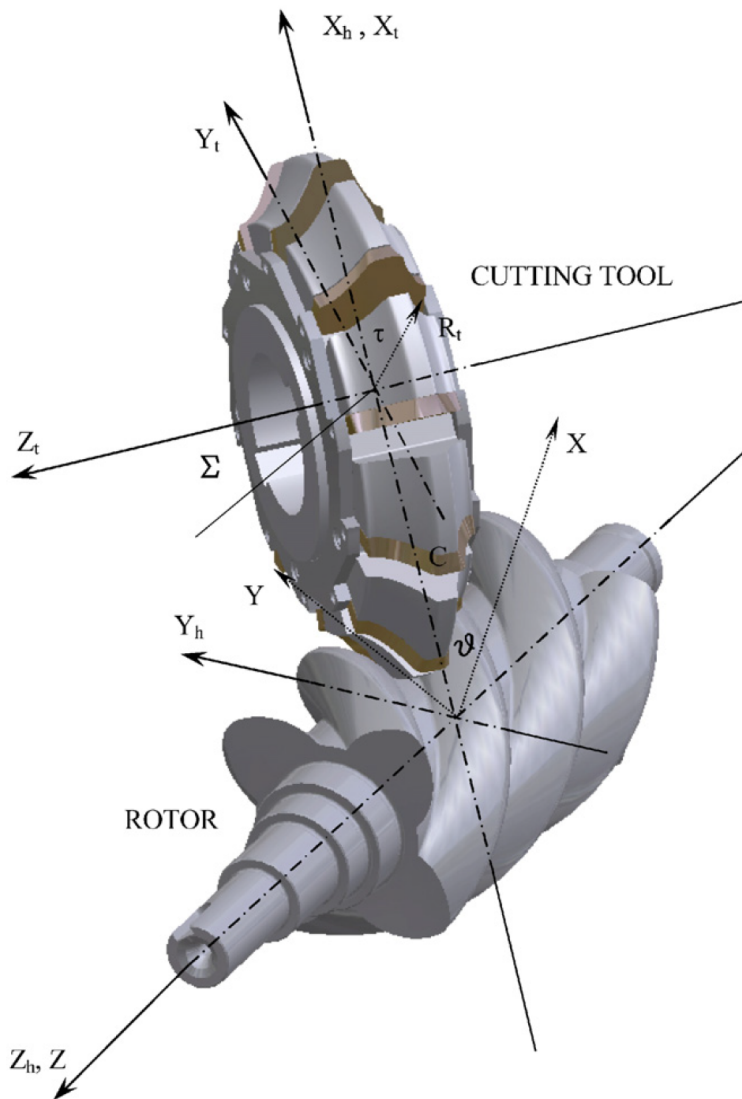


**Figure 3.9:** The rotor and tool coordinate system and orientation (Stosic, 2006b)

profile for the cutting tool can be obtained by solving following Equations 3.5, 3.6 and 3.7 simultaneously.

$$\begin{aligned}x_h &= x \cos(\theta) - y \sin(\theta) \\y_h &= x \sin(\theta) + y \cos(\theta) \\z_h &= p\theta\end{aligned}\tag{3.5}$$

$$(C - x_h + p \cot(\Sigma)) \left( x_h + y_h \frac{\partial y_h}{\partial x_h} \right) + p \left( z_h \frac{\partial y_h}{\partial x_h} - C \cot(\Sigma) \right) = 0\tag{3.6}$$

$$\begin{aligned}x_t &= x_h - C \\y_t &= y_h \cos(\Sigma) - z_h \sin(\Sigma) \\z_t &= z_h \cos(\Sigma) + y_h \sin(\Sigma)\end{aligned}\tag{3.7}$$

The tool profile is best represented in the  $X_t - Z_t$  plane as cylindrical coordinates  $R_t$  and  $Z_t$ , where  $R_t = \sqrt{x_t^2 + y_t^2}$ . The main rotor lobe of benchmark profile (split between points of largest diameters) and a tool profile calculated for the same (in terms of  $R_t$  and  $Z_t$ ) using aforementioned procedure are presented in Figure 3.10.

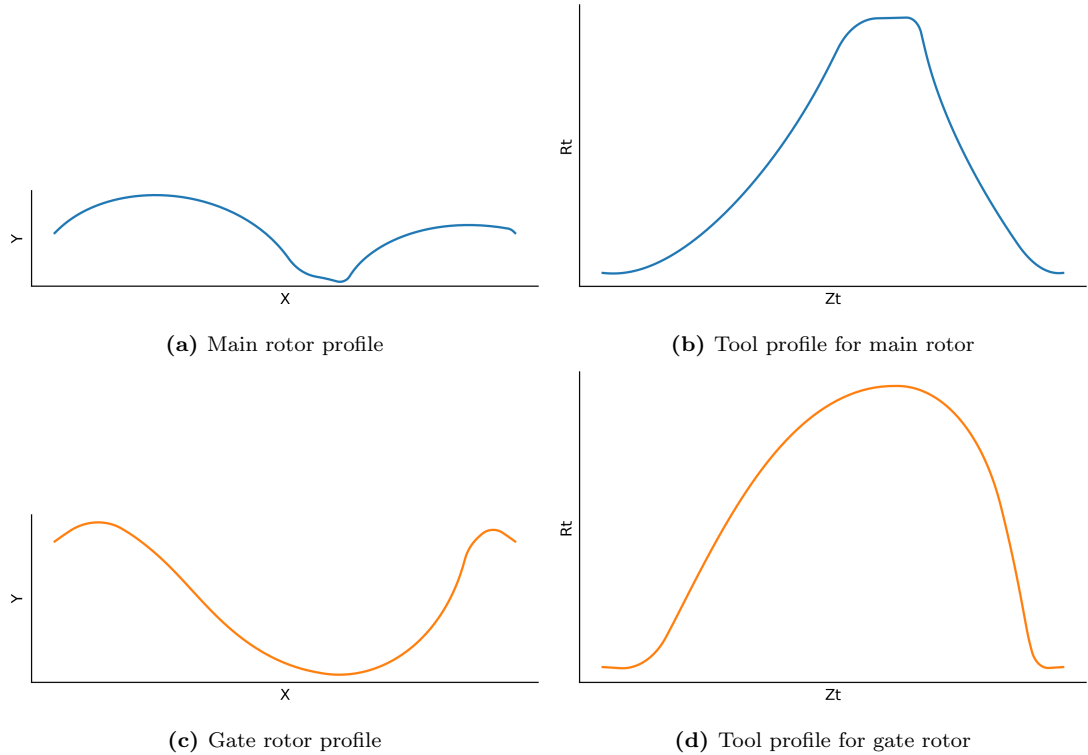


**Figure 3.10:** Rotor and tool Profiles for the benchmark N-Profile

As per Stosic (2006b)'s geometric approach to quantifying tool wear, a specific stock of metal (thickness  $\delta$ ) could be assumed to be on the theoretical profile. Using the rotor-to-tool transformation given hereby, tool profiles can be calculated for the theoretical rotor profile as well as the rotor profile created with a stock of material.

This is essentially a simulation of tool wheel instances before and after cutting a metal layer of thickness  $\delta$  from the rotor blank. The change in the two tool profile coordinates are representative of tool's movement during the cutting process. Hence it can be interpreted as a relative measure of tool wear. The differences in tool profile coordinates can be plotted along with the rotor or the tool profile to visualize which portions of the profile endure maximum wear.

Since the tool-rotor interaction occurs in a direction normal to the rotor helicoidal surface, it is more logical to add the stock of metal  $\delta$  in the same direction, normal to the rotor helicoid surface. Based on the known rotor coordinates in transverse plane  $(x, y)$ , the new coordinates  $\delta$  distance away normal to the helicoidal surface of rotors  $(x_{hn}, y_{hn}, z_{hn})$  are given as in Equation 3.8.

$$\begin{aligned}x_{hn} &= x + p \frac{\delta}{D} \frac{dy}{d\phi} \\y_{hn} &= y - p \frac{\delta}{D} \frac{dx}{d\phi} \\z_{hn} &= \frac{\delta}{D} \left( x \frac{dx}{d\phi} + y \frac{dy}{d\phi} \right)\end{aligned}\tag{3.8}$$

where  $\phi$  is a profile parameter and  $D$  is given as in Equation 3.9

$$D = \sqrt{p^2 \left( \frac{dx}{d\phi} \right)^2 + p^2 \left( \frac{dy}{d\phi} \right)^2 + \left( x \frac{dx}{d\phi} + y \frac{dy}{d\phi} \right)^2}\tag{3.9}$$

Readers interested in the details of these normal and transverse transformations on profile coordinates may look at Tang and Fleming (1994).

Since the rotor-to-tool transformation is based on rotor profile coordinates in the transverse plane, the  $x_{hn}, y_{hn}, z_{hn}$  are needed to be transformed in the transverse plane  $(x_n, y_n)$  using Equation 3.10. Thereafter, a tool profile can be calculated for rotor profile  $x_n, y_n$  following Equations 3.5, 3.6 and 3.7.

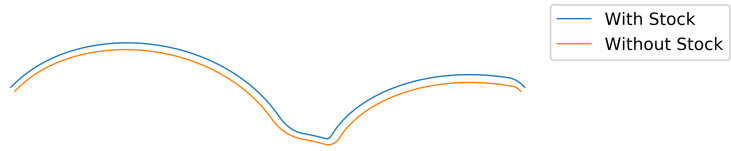
$$\begin{aligned}x_n &= x_{hn} \cos \left( \frac{z_{hn}}{p} \right) + y_{hn} \sin \left( \frac{z_{hn}}{p} \right) \\x_n &= -x_{hn} \sin \left( \frac{z_{hn}}{p} \right) + y_{hn} \cos \left( \frac{z_{hn}}{p} \right)\end{aligned}\tag{3.10}$$

The rotor profiles  $x, y$  and  $x_n, y_n$  along with their respective tool profiles are presented in Figure 3.11 superimposed. As per Stosic (2006b), the relative tool wear ( $TW_{rel}$ ) can be given as the distance between each point on with and without stock profiles formulated as either Equation 3.11 or 3.12.

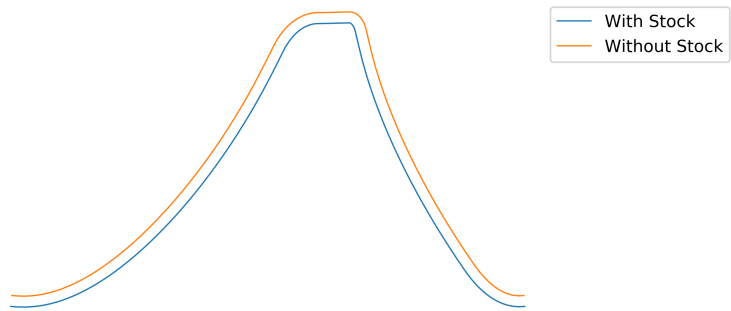
$$TW_{rel} = \sqrt{(x_n - x)^2 + (y_n - y)^2}\tag{3.11}$$

$$TW_{rel} = \sqrt{(R_{tn} - R_t)^2 + (Z_{tn} - Z_t)^2}\tag{3.12}$$

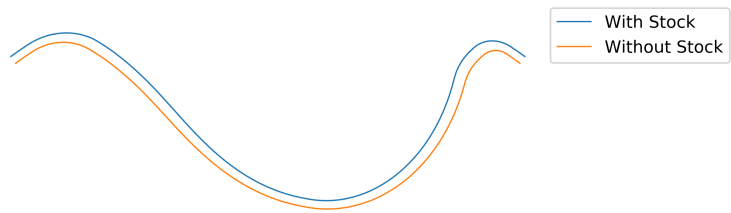
However, in this model, it is assumed that the relative speed between the rotor and tool will equally affect the with and without stock profiles. Hence, the relative tool



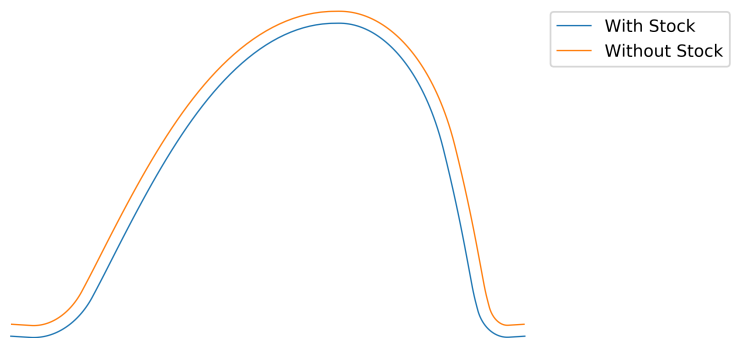
(a) Comparison of main rotor profiles



(b) Comparison of tool profiles for main rotor



(c) Comparison of main rotor profiles



(d) Comparison of tool profiles for gate rotor

**Figure 3.11:** Rotor and tool profiles with and without stock metal ( $\delta$  enlarged to 1 mm for visualization)

wear term is solely based on coordinate differences. But the hypothesis of this study is that a higher relative speed at certain region of profile will incur higher wear in spite of the same coordinate difference. Hence, by incorporating this effect into the current model, a modified tool wear indicator can be used to quantify manufacturability more accurately. This is developed and used in chapter 6.

### 3.2.3 Validation

In order to validate the calculations and predictions done for some of the new profiles, testing on actual rotors and compressors need to be carried out. Especially the profile with modification of rotor top lands in order to reduce the drag power losses needs strong validation and testing to figure out how best to exactly incline the top land and how much. This is partly because the software tools used for evaluation of new profiles are not very well equipped in predicting profile's impact on the drag power loss. This is still a regime where deeper understanding of the phenomenon is developing and hence experimental validation is a must.

The best way to validate profile changes and their effects in an experiment is to retrofit the new profiles over an already known rotor profile. For this purpose, a compressor of medium size, flow and power was chosen from the sponsor's range of products. Its existing N-profile of 4/5 lobe combination and 141 mm male rotor size was benchmarked for retrofitting of the new profiles. The size and power rating of the chosen machine is an essential element of the design of such experiment. Since these new profiles need to be manufactured, relatively smaller rotors (<100 mm diameter) are more challenging from the point of view of achieving the close form tolerances. They also have smaller rated flows and powers which make their flow and power measurement errors relatively larger. Hence a fairly large machine running in the range of 20 to 40 m/s tip speeds is chosen for experiments, since effects of oil drag are particularly dominant at larger tip speeds making them more easily detectable.

For manufacturing of the rotors having new rotor profiles, the rotor manufacturing machine from Samputensili at the sponsor's facility has been used.

## 3.3 Expected Contributions

Following the road-map to new profile development through this research, the expected contributions from this study are-

1. Adopting path homotopy for rotor profiling
2. Profile generation that minimizes drag losses in oil-injected screw compressors to improve their energy efficiency
3. Quantifying manufacturability of rotor profiles by modifying existing models that quantify it using tool wear (Stosic, 2006a)

4. Proposing a new profile system based on aforementioned contributions which would have 1-2% higher energy efficiency and good manufacturability compared to the state of the art benchmark N-Profile



# Chapter 4

## Path Homotopy

PATH homotopy as an idea from topology is explored in this chapter for its application in rotor profiling. With a brief introduction on how to adopt path homotopy in rotor profiling, later sections are based on various profiles generated by incorporation of homotopic curves in the N-Rack. The new profiles are evaluated based on various parameters such as profile efficiency, adiabatic efficiency and volumetric efficiency as elaborated in the last chapter. It is concluded with mention of specific homotopic curves which if incorporated in N-Rack could give 0.5-1% advantage in the energy efficiency.

### Contents

4.1	Homotopy in Rotor Profiling . . . . .	60
4.2	Rack Generated Homotopy Profiles . . . . .	64
4.2.1	Homotopic curves on long edge of the rack . . . . .	65
4.2.2	Homotopic curves on tips of the rack . . . . .	73
4.3	Summary of Homotopic Curves for the New Profile . . . . .	81

## 4.1 Homotopy in Rotor Profiling

As concluded in and from the literature review, the analytical representation of profile curves has definitive advantages. However, it was also pointed out that it needs to be accompanied with considerable control over curve features in order to explore wide range of shapes to design a better profile. In order to achieve this goal, the current method of using general arc equation in N-Rack is rather effective. It covers all the most commonly used curves in profiling such as lines, circles, conic sections and even few more with its choice of a set of 4 parameters ( $a, b, p, q$ ) in general arc equation-

$$ax^p + by^q = 1 \quad (4.1)$$

Using this equation and 4 parameters, all the essential curves on N-rack can be represented and desired sections such as the round side of rack can be manipulated parametrically to search for the most efficient curve.

Almost all of the successful and patented profiles till date follow the tested path of analytically represented curves to define the profiles. In order to improve or incorporate other desirable features such as varying radius of curvature along the curve (which is not possible with circles as radius of curvature is fixed with its radius) for better distribution of contact stress or reducing blow hole area by sharpening tips at the end, inventions like Kim and Lee (2004) have introduced better representations of the common analytical curves such as hyperbolae in a parametric way so as to control flatness or roundness of such curves. It is similar to general arc approach. This provides advantage of already stated analytical representations as well as control over curve features.

Based on all the considerations, one thing is clear- there is a need to find a method that can handle analytical curves like those in conventional profiles while providing better control over curve features. ‘Path homotopy’ as proposed in the previous section is fit for the purpose. It is not yet used in mechanical engineering applications or in any known shape optimization problem. Only one known application of this idea in engineering is found in computer graphics by Dym et al. (2015). However, rotor profiling can benefit from it.

In rotor profiling, such homotopic constructions could be used in place of certain profile sections. One such example is demonstrated using the ‘Demonstrator profile’ (Stosic et al., 2005) in Figure 4.1. It is a rotor generated profile entirely made of circles defined primarily on main rotor. The main rotor lobe section marked as ‘A1-B1’ in Figure 4.1 is also a circular arc with a radius  $r$  and a center at  $(x_0, y_0)$  which can be defined as-

$$y = \sqrt{r^2 - (x - x_0)^2} + y_0 \quad (4.2)$$

This curve ‘A1-B1’ can be replaced by a homotopy that deforms according to a paired curve in homotopy construction. If the other curve is chosen to be a straight line

between points  $A1 = (x_1, y_1)$  and  $B1 = (x_2, y_2)$ -

$$y = \left( \frac{y_2 - y_1}{x_2 - x_1} \right) (x - x_1) + y_1 \quad (4.3)$$

The homotopy hinged on points  $A1$  and  $B1$  is constructed using Equations 4.2 and 4.3 as -

$$\mathcal{H} = (q) \left( \left( \frac{y_2 - y_1}{x_2 - x_1} \right) (x - x_1) + y_1 \right) + (1 - q) \left( \sqrt{r^2 - (x - x_0)^2} + y_0 \right) \quad (4.4)$$

Equation 4.4 also serves an example for constructing a homotopy in an explicit form as opposed to the parametric form demonstrated in the previous section.

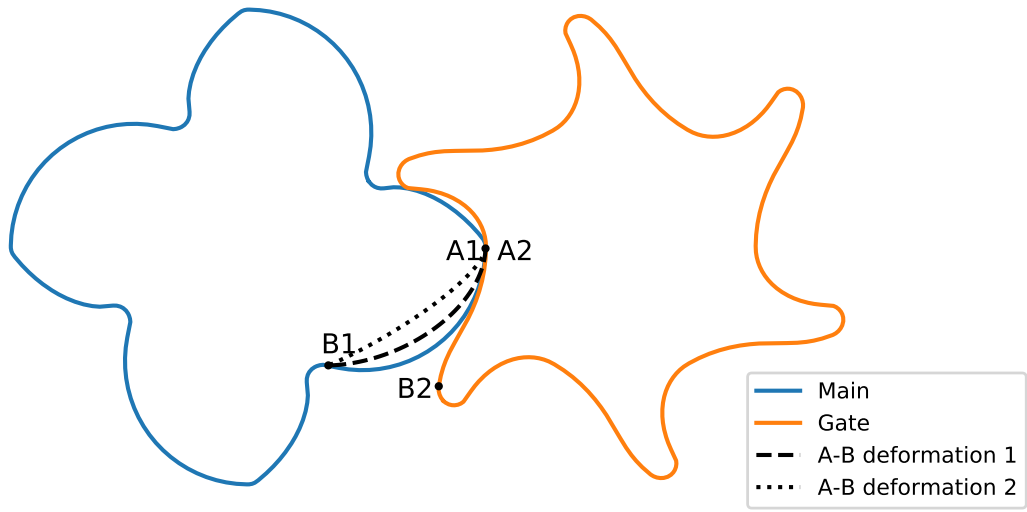


**Figure 4.1:** Example of the application of homotopy in a typical rotor profile (Patil et al., 2021)

The homotopy parameter  $q$  can be changed continuously to deform the circular arc into a straight line. Two such instances of deformations are presented in Figure 4.1. These deformed states of the profile section  $A1-B1$  still have an analytical representation. The generation of the corresponding curve  $A2-B2$  on gate rotor can be followed from solving the conjugacy condition derived using Euler's envelope theory as presented in Stosic and Hanjalic (1997). Alternatively, the homotopy on main rotor can be transformed onto a rack and the respective rack profile can then be transformed to the corresponding section on gate rotor.

In profiling there are more elements to follow than only representation of the curve. Especially the first order continuity of the profiles; or in other words the tangency of adjacent curved at the nodes. This is fairly easy to handle if the homotopic curve is placed between two curves at either side. Its tangency condition can be then predetermined by treating it like any other analytical curve and constraints on the adjacent curves could be derived in such a way that first order continuity is maintained even if the curve deforms. This gets more complicated if two homotopies are placed side by side on the profile. As the homotopy parameter varies and morphs each of them, they

need to maintain the continuity and differentiability at the node. In order to be able to do so, following mathematical derivation helps. It gives a condition that must be met while constructing these two homotopies for them to remain continuous and differentiable throughout. This mathematical basis is essential in order to use homotopy approach in its full potential over entire rack for optimizing separate portions and their shapes. Hence it is presented here.

Construction of one homotopy requires two curves. Hence let the first homotopy  $\mathcal{H}_1$  in the rack be constructed between curves  $\mathcal{C}_1$  and  $\mathcal{C}_2$  defined within points  $a$  and  $b$ . Whereas the second adjacent homotopy  $\mathcal{H}_2$  be constructed between curves  $\mathcal{C}_3$  and  $\mathcal{C}_4$  defined within  $c$  and  $d$ . Since the curves are adjacent, points  $d$  and  $b$  will be identical ( $b=d$ ). See Figure 4.2 for details-

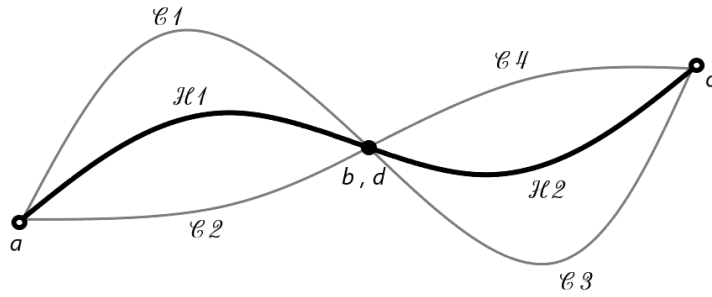


**Figure 4.2:** Two adjacent Homotopies  $\mathcal{H}_1$  and  $\mathcal{H}_2$  constructed within points  $a$ - $b$  and  $c$ - $d$  respectively with curves as depicted.

From Figure 4.2, mathematically the homotopies are -

$$\mathcal{H}_1 = q \mathcal{C}_1 + (1 - q) \mathcal{C}_2 \quad (4.5)$$

$$\mathcal{H}_2 = q \mathcal{C}_3 + (1 - q) \mathcal{C}_4 \quad (4.6)$$

For the homotopies to be continuous at connection  $b$  or  $d$  throughout the morphing, following condition must to be satisfied-

$$b = d \quad (4.7)$$

Then by the very definition of homotopy, which is continuous morphing between two curves with fixed end points,  $\mathcal{H}_1$  and  $\mathcal{H}_2$  will remain continuous throughout  $q : 0 \rightarrow 1$ . Now one only needs to ensure the differentiability at the junction. Individual homotopies by themselves are differentiable at their endpoints which makes them differentiable on their own. It is a necessary condition, but not sufficient. The sufficient condition for node is that the (first) derivatives of individual homotopies are equal at the node (points  $b$  and  $d$ ). Since they are one and the same point, the first derivatives

left and right of that point must be equal.

Following the constituent curves  $\mathcal{C}_1$ ,  $\mathcal{C}_2$ ,  $\mathcal{C}_3$  and  $\mathcal{C}_4$  to be individually differentiable at their respective end points  $a$ ,  $b$ ,  $c$  and  $d$ , slope of the homotopies at junction will be

$$\mathcal{H}'_1 \Big|_b = q \mathcal{C}'_1 \Big|_b + (1 - q) \mathcal{C}'_2 \Big|_b \quad (4.8)$$

$$\mathcal{H}'_2 \Big|_d = q \mathcal{C}'_3 \Big|_d + (1 - q) \mathcal{C}'_4 \Big|_d \quad (4.9)$$

For the junction to be differentiable for any value of homotopy parameter  $q$ , Equations 4.8 and 4.9 must be equal, i.e., first derivatives left and right of the node must be equal;  $\mathcal{H}'_1 \Big|_b = \mathcal{H}'_2 \Big|_d$  -

$$q \mathcal{C}'_1 \Big|_b + (1 - q) \mathcal{C}'_2 \Big|_b = q \mathcal{C}'_3 \Big|_d + (1 - q) \mathcal{C}'_4 \Big|_d \quad (4.10)$$

Rearranging the expression in Equation 4.10 -

$$q \left( \mathcal{C}'_1 \Big|_b - \mathcal{C}'_2 \Big|_b - \mathcal{C}'_3 \Big|_d + \mathcal{C}'_4 \Big|_d \right) + \left( \mathcal{C}'_2 \Big|_b - \mathcal{C}'_4 \Big|_d \right) = 0 \quad (4.11)$$

Since the the curves  $\mathcal{C}_1$ ,  $\mathcal{C}_2$ ,  $\mathcal{C}_3$  and  $\mathcal{C}_4$  are fixed, their slopes at end points will be constants. Hence for the expression in Equation 4.11 to be zero for any value of homotopy parameter  $q$ , the coefficient of  $q$  as well as the additional term in brackets has to be zero simultaneously. Mathematically, this can be written as-

$$\left( \mathcal{C}'_2 \Big|_b - \mathcal{C}'_4 \Big|_d \right) = 0 \quad (4.12)$$

$$\left( \mathcal{C}'_1 \Big|_b - \mathcal{C}'_2 \Big|_b - \mathcal{C}'_3 \Big|_d + \mathcal{C}'_4 \Big|_d \right) = 0 \quad (4.13)$$

Equation 4.12 implies that slopes of  $\mathcal{C}_2$  and  $\mathcal{C}_4$  at the junction must be equal.

$$\mathcal{C}'_2 \Big|_b = \mathcal{C}'_4 \Big|_d \quad (4.14)$$

Whereas Equation 4.13 along with Equation 4.12 implies that the slopes of  $\mathcal{C}_1$  and  $\mathcal{C}_3$  at the junction must be equal.

$$\mathcal{C}'_1 \Big|_b = \mathcal{C}'_3 \Big|_d \quad (4.15)$$

Equations 4.14 and 4.15 together set the conditions for ensuring differentiability at the junction of two homotopies. It implies that if the designer ensures that the respective initial ( $q = 0$ ) and final ( $q = 1$ ) curves that define two continuous homotopies have equal slopes, their junction will be differentiable throughout the morphing ( $0 < q < 1$ ).

This proof is immensely useful for constructing further profiles based on homotopy. One just needs to ensure that the respective curves one uses to construct two different homotopies (just like the line and circle used in the demonstrated profile) should have equal slopes. If it is so, as proved in this section, all the subsequent morphs will be

tangent too at the connecting point.

With all the mathematical background required for application of homotopy in rotor profiling derived in this section, the next section focuses on the design of novel profiles based on this approach. As a conclusion, following are the key points why this novel approach could prove useful in rotor profiling-

- It brings definitiveness to the search space of probable curves with determination of initial and final curves beforehand. These could be chosen based on already known best shapes in certain portions of the rack and/or rotor profiles. Then the designer can optimize around those shapes using the homotopic deformations.
- This method is so general that one can write homotopy between any two arbitrary analytical curves without any restriction to certain form or family of curves. (It is perfectly usable along with the general arcs of N-Rack).
- The method also provides provision to choose our initial and final states of the curves in such a way that the curve features such as radii of curvature at certain points could be controlled more efficiently.
- Designer gets the advantage of analytical representation (avoiding intrinsic problems in numerical shape function approaches) while gaining a wider search space (avoiding the constraint of strictly analytical approach).
- The method is general enough to be seamlessly used in any type of profile design be it rotor generated, rack generated or a rotor-rack generated. Homotopies can be defined either on rotors or rack and transformed suitably using appropriate meshing conditions.

In next section, the method explained here is applied to modify N-Rack. The portions of rack identified by the study of N-Rack characteristics presented in the last chapter are targeted for experimenting with different homotopic curves.

## 4.2 Rack Generated Homotopy Profiles

Homotopic curves induced N-Racks could be referred to as H-Rack profiles. While experimenting with the homotopic curves on N-Rack, the analysis of N-Rack presented in the last chapter could be used as a guide. Two key portions, the long edge of rack and the high pressure side tip of the rack had the most potential from new profile development point of view. Different homotopic curves constructed out of pairs of commonly known analytical curves have been tried at this portion to generate new profiles. As elaborated in the methods and approach chapter, a 141 mm N-Profile is used as a benchmark during this study. Hence the new experimental profiles will be compared against this profile to measure their improvements.

### 4.2.1 Homotopic curves on long edge of the rack

To refer to N-Rack, see Figure 4.3 wherein section  $A - B - C$  represents the long edge of rack. From the study of N-Rack curves and their characteristics,  $B - C$  is a straight line and is known to be already a good choice of curve at this position which need not be changed. However there is scope of improvement in finding a curve at  $A - B$  that may give better efficiency. In the benchmark profile, the general arc at  $A - B$  is set to the following curve-

$$\begin{aligned} x &= x_o + r_1 \cos(\phi) \\ y &= y_o + \frac{y_b}{(x_b - x_a)^n} (x_a - x)^n \end{aligned} \quad (4.16)$$

where,  $\phi$  is a profile parameter and  $n$  is equal to 0.5 making it a parabola. The proposal is to replace this parabola by a more general construct of homotopy which can incorporate any pair of analytical curves at  $A - B$ . Thereafter, various settings of homotopy deformation parameter  $q$  could be tried to search for an instance where the profile's efficiency comes out better than the benchmark N-Profile.

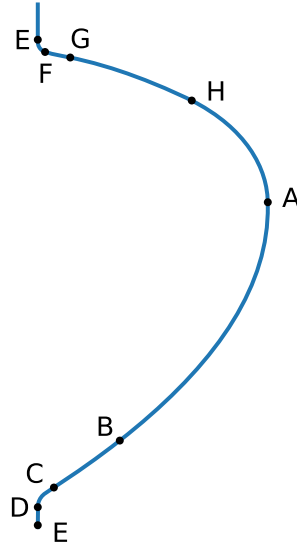


**Figure 4.3:** N-Rack profile for reference

Experiments for  $A - B$  could be set up with homotopies between pairs of the most commonly known analytical curves or general arcs such as conic sections including circle, line, ellipse, parabola and hyperbola along with cycloids which are not representable as general arc. This will keep the complexity of approach within check while allowing exploration of a wide enough types of shapes with the help of homotopic deformations. However, even with the choice of pair of curves settled, there is another challenge to address. That is, for given pair of curves for constructing the homotopy between two points on rack ( $A - B$ ), to find a combination of individual curve parameters and the homotopy deformation parameter that will give the maximum the adiabatic efficiency.

Usually for defining a conic section fully, one or two curve parameters are required

as input. Hence for the types of homotopies under discussion, 3 to 4 inputs are required to be searched through for their best possible combination. While doing so, rest of the rack profile is kept unchanged. To get a perspective on the scale of time required for a typical brute force search through 4 independent parameters (3 curve parameters and 1 homotopy deformation parameter), let's do a simple calculation. SCORPATH typically takes 1 second from the time of making a change in inputs to running all calculations and saving the results in a file. The actual time for calculations is quicker than 1 second but interaction with files takes time. Hence, for practical reasons a speed of 1 second per iteration on a standard PC during the search. The range and number of points to search for each independent parameter (4 here) determine the total number of iterations. For example, the range of homotopy deformation parameter is by definition 0 to 1. One may want to search over 10 intermediate values of homotopy parameter that makes the list - [0, 0.1, 0.2,..., 1]. Similarly, if for the other curve parameters, one wishes to have 20 search points each, the total number of iterations for the complete brute search become  $20 * 20 * 20 * 10 = 80000$ . And at the speed of 1 second per iteration, the total time for this one run will be 80000 seconds which is approximately a full day (~22 hours). Hence, this approach was found to be inefficient and not practical especially when the aim is to experiment with multiple homotopy curves and over a diverse range.

An alternative, a more intelligent algorithm is required. It has to be quick and a simple multivariate optimization algorithm which enables it to converge its search more rapidly and convincingly. Framework for rotor profile optimization such as box-complex method by Stosic et al. (2003b) is readily available in SCORPATH. Hence it could be used effectively for these search experiments. It is a quick and proven framework.

In addition to this framework, one way to do this is through brute force search trying out all possible combinations of curve parameters and homotopy parameter. But unlike doing all calculations like SCORPATH, proxy and computationally less expensive properties of the profiles can be evaluated which are more or less correlated to the energy efficiency of the profile. The results can then be sorted according to these characteristics and checked for their validity one by one (if the profiles have any reversals). The best profiles hence picked from the data can then be compared with the benchmark profile and a relative improvement can be claimed by running all calculations in SCORPATH only for few such cases.

The evaluation criteria could be geometrical profile parameters such as displacement and sealing line length which are very quickly calculable from the profile coordinates. Blow-hole is not affected by the curve at  $A - B$  hence it need not be evaluated. Hence their ratio is a close enough approximation of profile efficiency, which is a ratio of displacement area and total leakage area. Since other leakage areas than sealing line are essentially unchanged, the ratio of displacement and sealing line length is a good enough objective function. Higher displacement and lower sealing line length would usually give better performance but it is not always the case. Since geometric parameters do not always affect the thermodynamics in the same way. It is affected by other setup

conditions such as oil quantity in the system and clearances which hugely affect the impact of various geometric parameters on the thermodynamics of compression. Hence, a thermodynamic evaluation at the end is unavoidable to see improvements in a typical new profile. Proxy evaluation is simply to narrow down the possible combinations of curve parameters that make better profiles and boost the speed of the experiments with H-Rack.

Figure 4.4 is a algorithm that follows the process entailed here. It is quick enough to finish experiment with homotopic curve (a pair of two conic sections) in about an hour. Which is followed by thermodynamic evaluation of top 1% profiles sorted by this algorithm in SCORPATH and their comparison with benchmark N-Profile. The logic is rather self-explanatory from the flow chart. Basically, profiles displacement ( $D$ ) and sealing line leakage areas ( $A$ ) are calculated over each and every combination of the input parameters (only those required for defining homotopy at  $A - B$ ) and valid profiles are filtered through code and sorted according to the objective function. The top ' $n$ ' profiles (up to 1%) from this sorted list are then checked for minimum and maximum values of each curve parameter since these are the ranges in which the valid and more efficient profiles are most likely to fall. Then these revised input ranges are refined for closer spacing and search is run again. The refine and search loop stops when the difference between the current and previous maximum of proxy objective function  $O$  (ratio of displacement to leakage area) falls below a certain small limit given by  $\delta$ .

Multiple combinations of the common curves were used to form homotopies and they were experimented with using this framework. The target curve was as determined, the section  $A - B$  on N-Rack. Starting with common curves- line, circle, ellipse, parabola, hyperbola and cycloid- choosing a pair at a time, homotopies ( $\mathcal{H}(Curve_1, Curve_2)$ ) were constructed and put in section  $A - B$  of the N-Rack (Table 4.1).

The seven homotopies in Table 4.1 were put through the algorithm in Figure 4.4 to find the combinations of curve and homotopy parameters that would maximize displacement and minimize the sealing line length. The benchmark for comparison is off course KPCL 141 mm N-Rack profile. So, all other profile parameters such as center distance, addendums and tip radii on the N-Rack were kept unchanged. The new retrofitted H-Rack generated homotopy profiles fine tuned by this algorithm in comparison to the standard benchmark profile are presented in Table 4.2. The comparison is based on the proxy objective function which is ratio of profile displacement to the sealing line leakage area. It is a purely geometric comparison.

The optimization variables in the algorithm are particularly the curve parameters such as semi-major axis ('a'), semi-minor axis ('b'), slope of the line ('m'), y-intercept ('c') and the homotopic deformation parameter ('q') which completely define the homotopic curve.

Since they are all based on the same principle of fine-tuning, the best of them, with  $\mathcal{H}(Hyperbola, Parabola)$  can be taken for evaluation based on thermodynamics. For that, as elaborated in the last chapter on methods and approach, volumetric and adiabatic efficiencies could be compared. In this evaluation, the working conditions

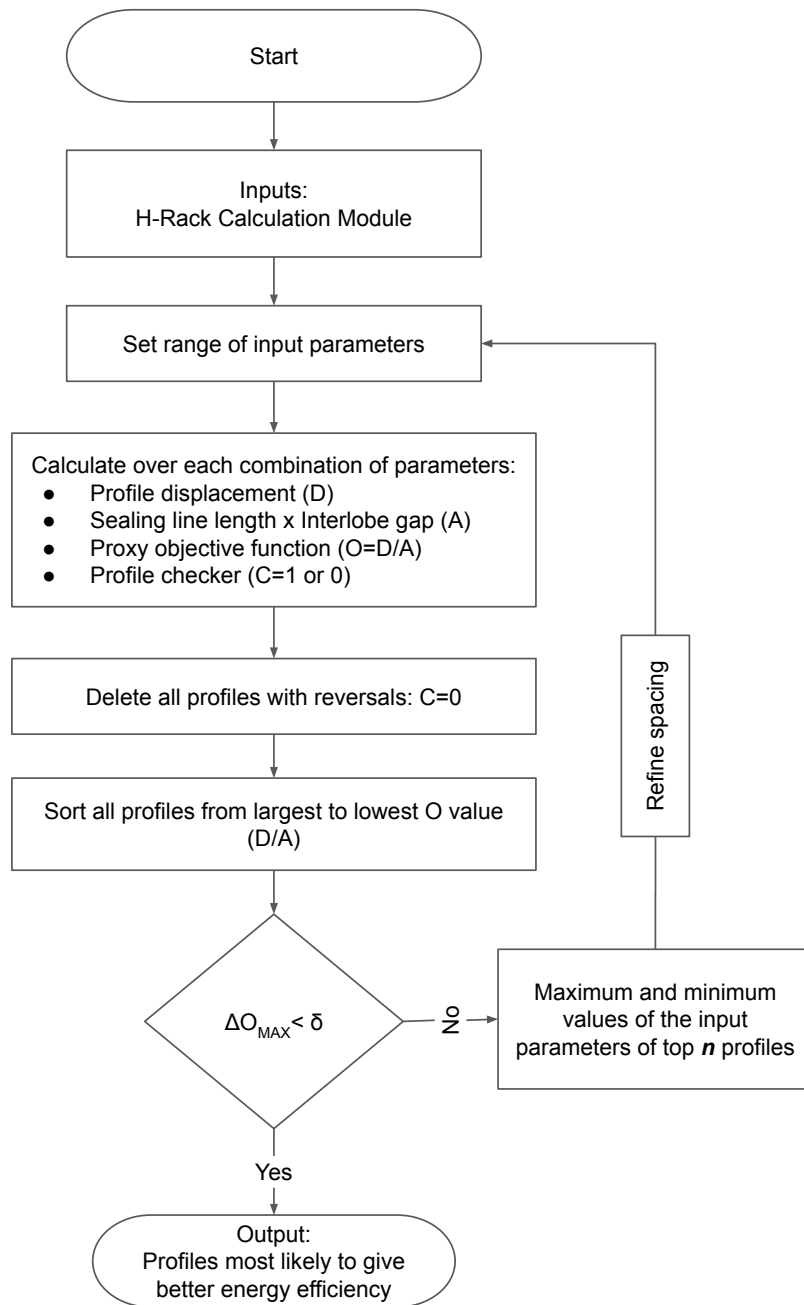


**Figure 4.4:** Algorithm for finding good combinations of curve parameters for homotopies tested in H-Rack at  $A - B$

Homotopy at $A - B$ in N-Rack	Parametric equations of the curves used to construct the homotopy
$\mathcal{H}(\text{Ellipse}, \text{Line})$	$x_1 = a \cos(\phi) ; y_1 = b \sin(\phi) \&$ $x_2 = x ; y_2 = mx + c$
$\mathcal{H}(\text{Hyperbola}, \text{Line})$	$x_1 = a \cosh(\phi) ; y_1 = b \sinh(\phi) \&$ $x_2 = x ; y_2 = mx + c$
$\mathcal{H}(\text{Parabola}, \text{Line})$	$x_1 = a\phi^2 ; y_1 = 2a\phi \&$ $x_2 = x ; y_2 = mx + c$
$\mathcal{H}(\text{Cycloid}, \text{Line})$	$x_1 = a(\phi - \sin(\phi)) ; y_1 = -a(1 - \cos(\phi)) \&$ $x_2 = x ; y_2 = mx + c$
$\mathcal{H}(\text{Ellipse}, \text{Hyperbola})$	$x_1 = a \cos(\phi) ; y_1 = b \sin(\phi) \&$ $x_2 = a \cosh(\phi) ; y_2 = b \sinh(\phi)$
$\mathcal{H}(\text{Ellipse}, \text{Parabola})$	$x_1 = a \cos(\phi) ; y_1 = b \sin(\phi) \&$ $x_2 = a\phi^2 ; y_2 = 2a\phi$
$\mathcal{H}(\text{Hyperbola}, \text{Parabola})$	$x_1 = a \cosh(\phi) ; y_1 = b \sinh(\phi) \&$ $x_2 = a\phi^2 ; y_2 = 2a\phi$

$\phi$  is a curve parameter while  $a, b, c$  &  $m$  are curve inputs that fully define them

**Table 4.1:** Homotopic curves experimented in section  $A - B$  of the N-Rack

Homotopy at $A - B$ in N-Rack	% increase in geometric evaluation parameter
$\mathcal{H}(\text{Ellipse}, \text{Line})$	1.42%
$\mathcal{H}(\text{Hyperbola}, \text{Line})$	1.10%
$\mathcal{H}(\text{Parabola}, \text{Line})$	1.12%
$\mathcal{H}(\text{Cycloid}, \text{Line})$	0.90%
$\mathcal{H}(\text{Ellipse}, \text{Hyperbola})$	1.27%
$\mathcal{H}(\text{Ellipse}, \text{Parabola})$	1.27%
$\mathcal{H}(\text{Hyperbola}, \text{Parabola})$	1.74%

**Table 4.2:** Percentage improvements in the H-Rack profiles based on geometric evaluation parameter- ratio of displacement to sealing line leakage area w.r.t benchmark N-Rack

were set again as elaborated in the last chapter- oil injected air application, ambient suction and 8.5 bar discharge with typical clearances and oil injection parameters for such a machine. This profile as overlapped with the benchmark N-Profile is shown in Figure 4.5. The comparison of the H-Rack profile having  $\mathcal{H}(Hyperbola, Parabola)$  at  $A - B$  in N-Rack with the benchmark profile is presented in Table 4.3.

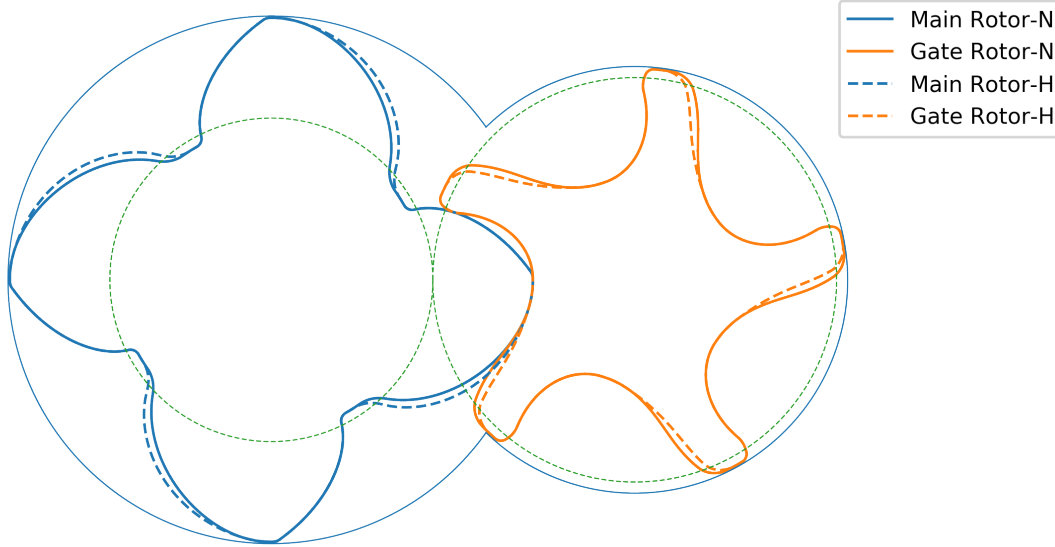


**Figure 4.5:** H-Rack profile with  $\mathcal{H}(Hyperbola, Parabola)$  at  $A - B$  section in N-Rack

% Improvement in H-Rack	Volumetric efficiency	Adiabatic efficiency
At male rotor tip speed of 20 m/s	0.5%	0.2%
At male rotor tip speed of 25 m/s	0.4%	0.2%
At male rotor tip speed of 30 m/s	0.3%	0.1%
At male rotor tip speed of 35 m/s	0.2%	0.1%

**Table 4.3:** % improvements in H-Rack in Figure 4.5 w.r.t benchmark N-Profile

So, the improvement in volumetric efficiencies is between 0.2% to 0.5%. The homotopy between hyperbola and parabola reduces the interlobe sealing line w.r.t benchmark profile by almost 2.5%. But it also happens to reduce the displacement by  $\sim 0.7\%$  and hence an overall improvement of 1.74% in the ratio of displacement to sealing line is observed to begin with. These two effects, reduction of displacement and reduction of sealing line affect the thermodynamics of compression in different ways depending on the operational clearances and oil in the system too. The lower displacement profile (one with homotopy in this case) can be as better as 1.5% than the higher displacement (N-Profile) if the interlobe clearance is very large and oil flow insufficient. Namely, the longer interlobe sealing line of the higher displacement rotor has smaller influence if the interlobe clearance is low. In the SCORPATH calculation setup however, the clearances were setup as in contemporary machines which happen to be rather small ( $\sim 30-40$  micron). The effect of smaller interlobe clearances is further diminished if there is more oil in the system which seals these gaps.

As a result, if the profile in Figure 4.5 is subjected to even lower clearance and more quantity of oil than that in usual setup, just to demonstrate its effect; the H-Rack profile loses its advantage significantly. See Table 4.4.

% Improvement in H-Rack	Volumetric efficiency	Adiabatic efficiency
At male rotor tip speed of 20 m/s	0.1%	-0.1%
At male rotor tip speed of 25 m/s	0.0%	0.0%
At male rotor tip speed of 30 m/s	0.0%	-0.1%
At male rotor tip speed of 35 m/s	0.1%	-0.1%

**Table 4.4:** % improvements in H-Rack in Figure 4.5 w.r.t benchmark N-Profile when more oil is present in the machine and clearances are even smaller

The vice versa effect can also be demonstrated wherein the new profile is starved of oil and clearances are larger. In this case, the H-Rack profile turns out to be better than N-Rack by up to 0.5-0.9% (Table 4.5). Based on the trend of these results w.r.t the speed of compressor, another important conclusion can be drawn. The fine improvements in profile achieved using homotopy are less influential if the compressor is run at high speeds. To best utilize these improvements, compressor must be designed to run slowly <30 m/s tip speed and oil over-flooding should also be avoided as it is shown to be counterproductive to the energy efficiency on account of profile's design itself. Also, this profile is less demanding of smaller operational interlobe clearance than N-Profile. Even if interlobe clearance was set larger for reasons such as improving reliability, performance of homotopy profile in Figure 4.5 will degrade lesser than that of N-Profile. It is an important conclusion of the results in Table 4.5.

% Improvement in H-Rack	Volumetric efficiency	Adiabatic efficiency
At male rotor tip speed of 20 m/s	0.9%	0.6%
At male rotor tip speed of 25 m/s	0.8%	0.5%
At male rotor tip speed of 30 m/s	0.7%	0.4%
At male rotor tip speed of 35 m/s	0.5%	0.4%

**Table 4.5:** % improvements in H-Rack in Figure 4.5 w.r.t benchmark N-Profile when less oil is present in the machine and clearances are larger

This is also a good demonstration why optimization of rotor profiles based on purely geometric criteria are not that effective. The geometry affects energy efficiency by acting through the operational and working conditions whose effect can be precisely caught by only one way- a good thermodynamic simulation model.

However, one of the observations in these experiments with different homotopies was that the specific homotopy between a hyperbola and a parabola with homotopy parameter 0.8 shows up frequently in profiles having smaller sealing line lengths. Profiles with this particular homotopy tend to have a smaller sealing line length than profiles with either hyperbola or parabola individually placed at the same location. This effect was further investigated and this time with a small modification in the algorithm to solely see the effect of profile modification on sealing line. The sorting of profiles was not done

according to the proxy objective function, but rather as per the sealing line. Then only the profiles having displacements equal and larger than that of benchmark N-Profile were filtered out. This eliminates the impact of displacement and since the benchmark profile has a parabola in the same place as there is homotopy, a fair comparison can be made.

With this method, an H-Rack profile was obtained with  $\mathcal{H}(Hyperbola, Parabola)$  and  $q = 0.8$  which has the same displacement as that of benchmark profile but the sealing line is 0.9% shorter (Figure 4.6). Other leakage areas such as blow hole are anyway same for these profiles. Hence here a straight thermodynamic advantage of up to 0.5-1% can be expected without a large influence of oil or clearances as in previous case. This is also to further demonstrate that profile design is closely linked with choice of operational conditions of the compressor.

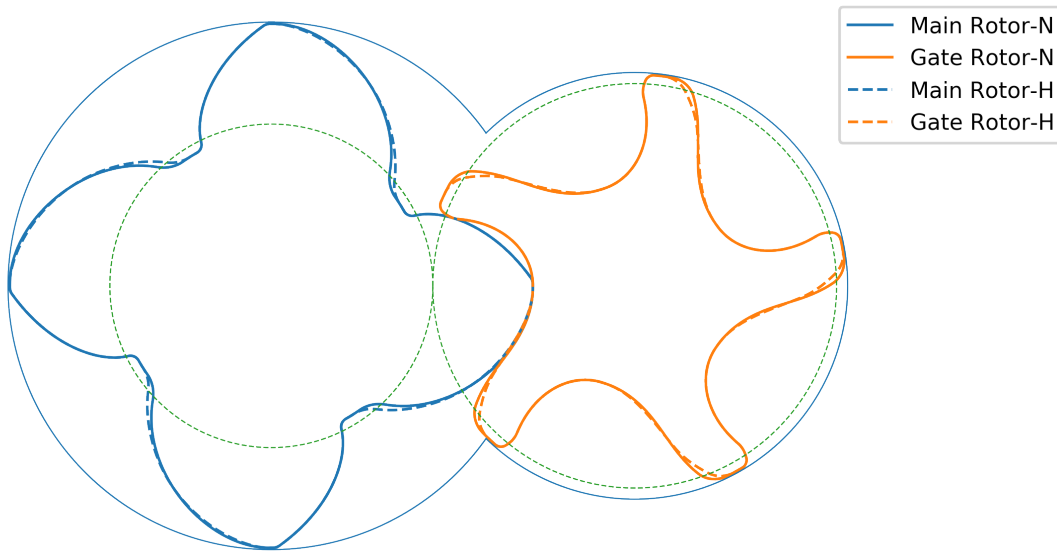


**Figure 4.6:** H-Rack profile with  $\mathcal{H}(Hyperbola, Parabola)$  and  $q = 0.8$  having same displacement as N-Rack but 0.9% shorter sealing line length

The thermodynamic evaluation of this profile again at same conditions as that presented in previous cases confirms superiority of this homotopic curve which is a blend of parabola and a hyperbola in 80-20 proportion. As it can be observed in Table 4.6; this profile (Figure 4.6) is less prone to changes in oil quantity and clearances as opposed to the one in Figure 4.5 since it traded displacement in exchange of shorter sealing line length. This profile manages to do so purely by the homotopic curve characteristics without compromising on displacement.

Average % improvement in H-Rack	Volumetric efficiency	Adiabatic efficiency
With nominal oil quantity & clearances	0.5%	0.4%
With more oil & reduced clearances	0.4%	0.4%
With less oil & increased clearances	0.5%	0.5%

**Table 4.6:** % improvements in H-Rack in Figure 4.6 w.r.t benchmark N-Profile

This type of profile shape could also be achieved in N-Rack by adjusting its long

edge general arc exponents along with the long edge tip radius ( $B - C$  in Figure 4.3). However, the advantage of this specific homotopic curve is not only in its shorter sealing line length but also in its flexibility and degree of movements at this section of rack which make it easy to set up a rack profile with shortest sealing line length. More on this aspect in the next section.

#### 4.2.2 Homotopic curves on tips of the rack

From the analysis of N-Rack curves, the other section than the long edge of rack which had potential for improvement was the high pressure side rack tip. This portion of rack affects the blow-hole area which is a major leakage area that affects the performance to a significant degree. As much as the last section was focused on sealing line length and displacement; this section focuses on blow-hole area and sealing line length.

The blow-hole area is bound by the high pressure side casing cusp and male and female rotor tips generated by entire N-Rack high pressure side  $E - F - G - H - A$ . Blow-hole is generally inversely correlated to sealing line length since any attempt to reduce it stretches the topmost point on sealing line further near the cusp and resulting in lengthening of the sealing line. The easiest and most straightforward way to reduce blow-hole in N-Rack is to reduce the main rotor tip radius (which generates rack section  $H - A$ ) and the radius of circular arc  $E - F$  on the rack. The effect of only reducing the radius of  $E - F$  by 1 mm in comparison with the benchmark N-Profile which has this radius set to 2.5 mm, is presented in Figure 4.7.

From the view in Figure 4.7, it can be crudely interpreted how outward leaning of the gate rotor tip could result in reduction of the blowhole area. The blowhole areas and sealing line lengths of the two profiles in Figure 4.7 are presented in Table 4.7. It is evident that the reduction in blowhole by 34% is accompanied by an increase in sealing line length by 4.9%.

Profile Characteristic	N-Rack with $E - F$ 2.5 mm	N-Rack with $E - F$ 1.5 mm
Total throughput area (mm <sup>2</sup> )	9598	9626
Interlobe leakage area (mm <sup>2</sup> )	5.179	5.434
Blow hole area (mm <sup>2</sup> )	6.304	4.174

**Table 4.7:** Comparison of geometric profile characteristics for N-Profiles generated from N-Racks with tip  $E - F$  radii 2.5 mm and 1.5 mm

Thermodynamically, calculations indicate that the effect of the trade-off in Table 4.7 is highly dependent on the value of interlobe clearance in the compressor. If it is large, the effect of reducing the sealing line will be more influential than the reduction of the blow hole. However, for the conditions set in this study, the value of interlobe clearance is rather small between 30 to 40 micron. Refer Table 4.8 for the performance comparison of these two profiles. The reduction of blow hole at the cost of sealing line turns out to be favorable for the energy efficiency of the benchmark profile at 30 micron interlobe clearance.



**Figure 4.7:** N-Profiles generated by N-Racks with tip radii for  $E - F$  as 2.5 mm and 1.5 mm

% Improvement in N-Rack (1.5 mm @ $E - F$ )	Volumetric efficiency	Adiabatic efficiency
At male rotor tip speed of 20 m/s	-0.26%	0.55%
At male rotor tip speed of 25 m/s	-0.24%	0.44%
At male rotor tip speed of 30 m/s	-0.22%	0.37%
At male rotor tip speed of 35 m/s	-0.20%	0.31%
At male rotor tip speed of 40 m/s	-0.18%	0.28%

**Table 4.8:** % improvements in thermodynamic efficiencies of N-Profile with sharper tip (1.5 mm) at  $E - F$  on rack in comparison to the benchmark profile (2.5 mm)

It might seem that the easiest way to improve upon the benchmark profile is through reduction of the tip radii on high pressure side of the N-Rack. But reduction of the tip radii comes with some practical constraints. First of them is in manufacturing and inspection of such rotors. Achieving tight form tolerances for sharp tips is challenging and also expensive. Second constraint is more from functional point of view- sharp tips wear faster as rotors mesh during the operation. The worn rotor tips on high pressure side of rotors may lead to poor sealing and more leakages as the compressor ages.

Also, the reduction in volumetric efficiency in Table 4.8 should be noted. As seen in the previous section; the effect of trade-offs such as this in profiling are subject to operating conditions of the machine. Reduction of blow-hole area at the cost of sealing line length works well at the operating conditions set here. But, at very high tip speed and/or high pressure ratios assuming less quantity of oil to seal the interlobe sealing gaps, the effect of increased sealing line length may outweigh the effect of reduction in the blow-hole area. Hence, there is a scope for finding ways to reduce the blow-hole area with as low as possible increase in the sealing line length.

One variant of the N-Rack does this by omitting the straight line curve  $F - G$  (see Figure 4.3). In this case, the circular arc  $E - F$  directly connects with  $G - H$  at  $G$ . What this does to gate rotor tip is rather ingenious; it pushes the gate rotor tip slightly outwards leading to reduction of the blow-hole with minimal impact of the sealing line length. The retrofit versions of N-Profiles generated with and without the line  $F - G$  on N-Rack are presented in Figure 4.8.

The ingenuity of this modification is evident from Table 4.9, which compares the sealing line length and blow-hole area for the two profiles in Figure 4.8. Unlike the profiles compared in Table 4.7 with only reduction of  $E - F$ 's radius, here the 32% reduction in blow-hole area is met with only 1.8% increase in the interlobe leakage area. Effect of this is reflected in the energy efficiency too. The performance of profiles from Figure 4.8 is presented in Table 4.10.

Profile Characteristic	N-Rack with $F - G$ (Benchmark profile)	N-Rack without $F - G$
Total throughput area (mm <sup>2</sup> )	9598	9640
Interlobe leakage area (mm <sup>2</sup> )	5.179	5.271
Blow hole area (mm <sup>2</sup> )	6.304	4.260

**Table 4.9:** Comparison of geometric characteristics of the profiles generated with and without the line  $F - G$  in N-Rack

This feature of omission of the curve  $F - G$  from N-Rack could be very effectively used in the new profile design. In addition to that, the idea of homotopy is also capable of working with the aforementioned features that affect blow-hole and especially the practical constraints on sharp rotor tips. Homotopic deformations are capable of fine and local adjustments of curve features such as its sharpness (similar to demonstration in Figure 3.8). A simple homotopy constructed with a circular arc and a straight line or more generally an ellipse and a straight line suits perfectly well for use at the rack

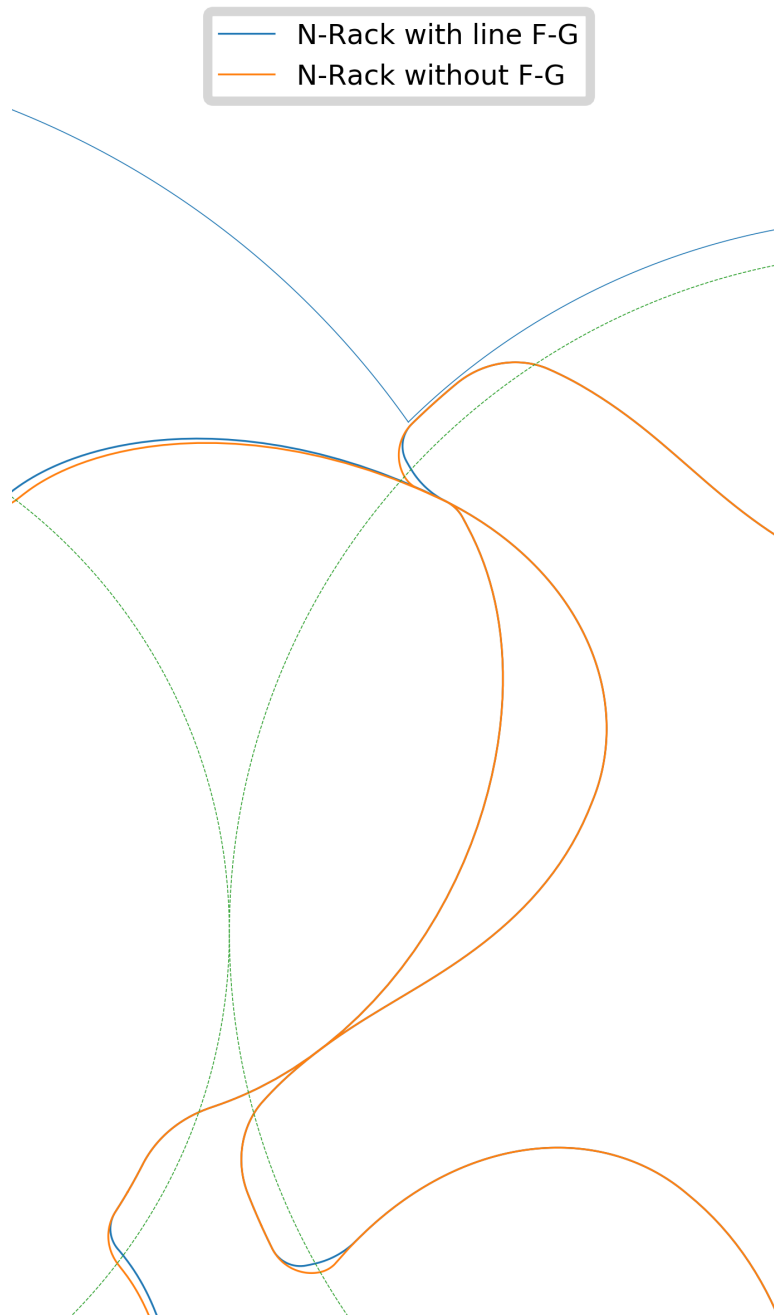


**Figure 4.8:** N-Profile generated by omitting line  $F - G$  in N-Rack retrofitted over the benchmark N-Profile with  $F - G$

% Improvement in N-Rack (with omission of $F - G$ )	Volumetric efficiency	Adiabatic efficiency
At male rotor tip speed of 20 m/s	0.09%	0.76%
At male rotor tip speed of 25 m/s	0.07%	0.61%
At male rotor tip speed of 30 m/s	0.05%	0.51%
At male rotor tip speed of 35 m/s	0.04%	0.43%
At male rotor tip speed of 40 m/s	0.03%	0.39%

**Table 4.10:** % improvements in thermodynamic efficiencies of N-Profile generated without  $F - G$  on rack in comparison to the benchmark profile (with  $F - G$ )

tips.

For finding out the most suitable homotopy at the rack tip, again similar variables as those required for fully defining the individual curves (semi-major and semi-minor axes) along with homotopic deformation parameter ('q') need to be searched or optimized. Since a circle is a special case of an ellipse which happens to be an instance of the homotopy at  $q = 1$ , such a construction can simply mimic the regular N-Rack and with some fine tuning of the homotopy parameters, tip features can be controlled. An example of such a fine control possible with a homotopy at tip is demonstrated in Figure 4.9 wherein tip of the benchmark profile is sharpened and flattened without affecting any adjacent curve.

Such a capability can be used along with the sharp tip profiles in Figure 4.7 to mitigate the effect of very sharp tips on manufacturing, inspection or wear by flattening them using homotopy. That lets the designer keep the benefits of smaller blowhole and improved performance that come with sharper tip without having to worry about the practical constraints. Such a profile with  $E - F$  curve radius on N-Rack set to 1.5 mm to 2.5 mm in benchmark profile but flattened at the same time using homotopy is plotted in Figure 4.10. One can observe that though the tip is leaning outward as in Figure 4.7 giving advantage of smaller blow-hole, it is not as sharp as fully circular tip with 1.5 mm radius.

Refer Figure 4.11 for comparison, where the profile in Figure 4.7 with  $E - F$  radius 1.5 mm is plotted along with the profile in Figure 4.10 whose tip is flattened using homotopy. The radius of curvature on the tip after flattening is enlarged up to 2.5 mm which is equal to the tip radius is benchmark profile. The geometric and thermodynamic evaluation of this H-Rack profile with homotopy at tip in comparison to the benchmark N-Rack profile is given in Tables 4.11 and 4.12 respectively.

Profile Characteristic	N-Rack (Benchmark profile)	N-Rack with $\mathcal{H}(Ellipse, Line)$ @ $E - F$
Total throughput area (mm <sup>2</sup> )	9598	9626
Interlobe leakage area (mm <sup>2</sup> )	5.179	5.361
Blow hole area (mm <sup>2</sup> )	6.304	4.360

**Table 4.11:** Comparison of geometric profile characteristics for N-Rack with homotopy  $\mathcal{H}(Ellipse, Line)$  at  $E - F$  and the benchmark profile with circle at  $E - F$

% Improvement in N-Rack (with $\mathcal{H}(Ellipse, Line)$ ) @ $E - F$	Volumetric efficiency	Adiabatic efficiency
At male rotor tip speed of 20 m/s	-0.12%	0.56%
At male rotor tip speed of 25 m/s	-0.11%	0.45%
At male rotor tip speed of 30 m/s	-0.11%	0.37%
At male rotor tip speed of 35 m/s	-0.10%	0.32%
At male rotor tip speed of 40 m/s	-0.09%	0.29%

**Table 4.12:** % improvements in thermodynamic efficiencies of N-Profile generated with homotopy  $\mathcal{H}(Ellipse, Line)$  at  $E - F$  on rack in comparison to the benchmark profile (with circle at  $E - F$ )

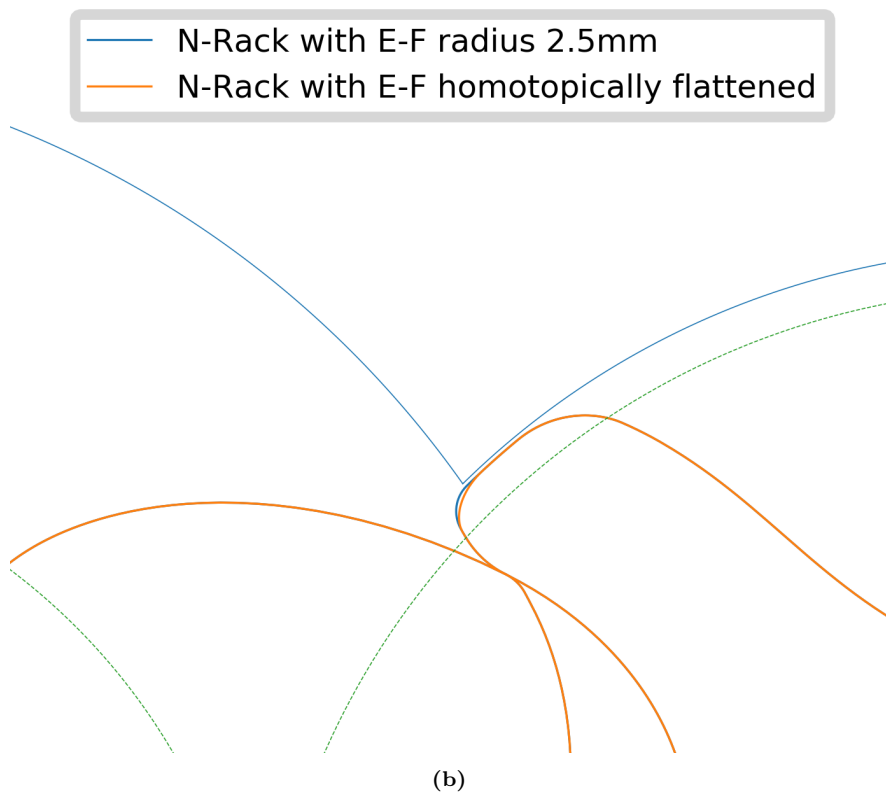
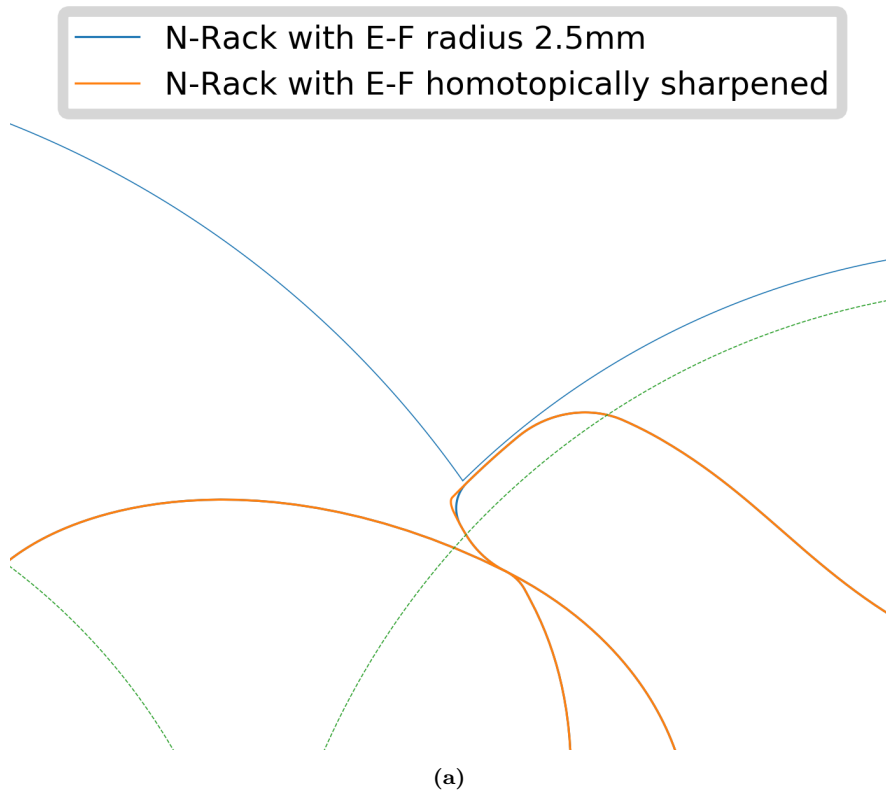


**Figure 4.9:** The application of homotopy constructed with an ellipse and a line to flatten(b) or sharpen(a) the gate rotor tips



**Figure 4.10:** Profile generated with  $\mathcal{H}(\text{Ellipse}, \text{Line})$  at  $E - F$  retrofitted with the benchmark N-profile which has a circle of radius 2.5 mm at  $E - F$



**Figure 4.11:** Profile generated with  $\mathcal{H}(\text{Ellipse}, \text{Line})$  at  $E - F$  retrofitted with benchmark N-profile if it had 1 mm smaller radius at  $E - F$

The comparison shows that such an application of homotopy in profile tip designs can improve the energy efficiency without compromising on the manufacturability. Not only homotopy but the omission of line  $F - G$  in the rack can also improve the energy efficiency of rotor profiles. This is in fact much simpler and straightforward than homotopy. With either technique or a combination of both, improvements in tips that affect blowhole can bring about 0.3 to 0.7% improvements in overall energy efficiency of the new profile. This is independent and in addition to the 0.5% improvement achieved through homotopy at the long edge of the rack.

### 4.3 Summary of Homotopic Curves for the New Profile

As a summary of the last section, two homotopic curves are found which could give an advantage of up to  $\sim 0.5\%$  each in terms of energy efficiency if incorporated in the N-Rack. Along with that, the omission of line  $F - G$  in N-Rack is found to give up to 0.7% gain in energy efficiency single-handedly.

The homotopic curve on the long edge of rack at  $A - B$  is constructed with a hyperbola and a parabola. It is presented in Figure 4.12, this particular homotopy plotted along with its generating curves. As observed during multiple calculations with this curve, homotopic deformation parameter  $q = 0.8$  seems to give better results in general.

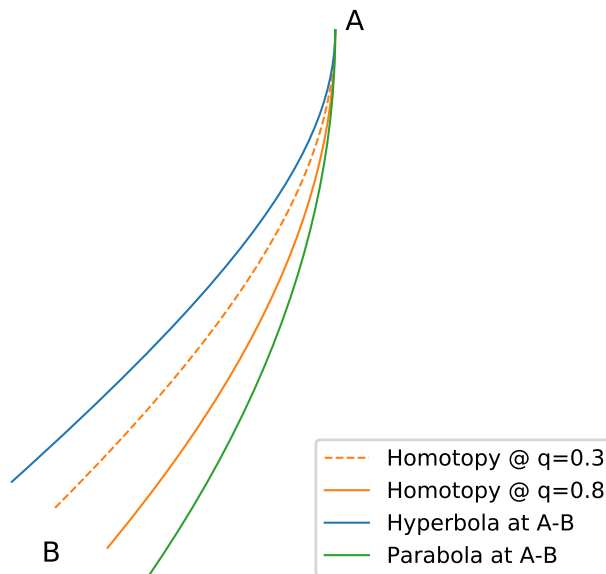


**Figure 4.12:** Homotopic curve constructed with a hyperbola and a parabola proposed for the long edge of the new profile rack

The homotopic curve on the high pressure side tip of the rack at  $E - F$  is constructed with an ellipse and a line. It is presented in Figure 4.13, this particular homotopy plotted along with its generating curves. It helps visualize the flattening effect that can be applied to the tips. Though it is defined as an ellipse, to avoid the complexity, designer can choose to define a regular circular arc by setting eccentricity of this elliptical arc

to 1. The control on flatness is still intact with that choice.

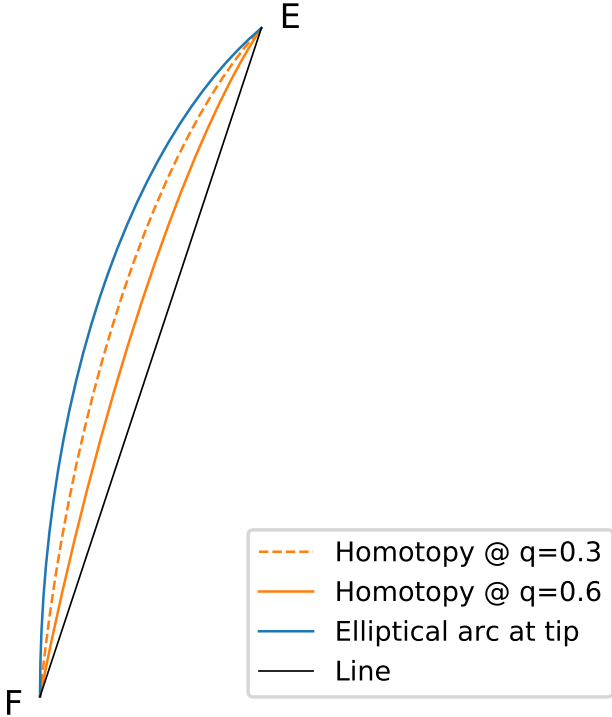


**Figure 4.13:** Homotopic curve constructed with an ellipse and a line proposed for the high pressure side tip of the new profile rack

One of the drawbacks of the homotopic curves is that they required one additional parameter  $q$  to fully define their shape. With two homotopic curves proposed for inclusion in the N-Rack, the new H-Rack would have two additional input parameters. Number of input parameters are directly proportional to efforts in optimization. But they also offer an additional degree of control over the curves which has been shown to benefit the profiles.

## Chapter 5

# Experiments with Further Profile Modifications

THIS chapter proposes further profile improvements which could reduce oil drag losses in the oil flooded screw machines. This is accompanied by a profile which is hypothesized to have higher drag losses but optimization algorithm based on thermodynamic criteria (better adiabatic efficiency) predicts it to be better than the benchmark profile. Since these profiles modifications involve an element of oil drag which is difficult to model in existing prediction tools, these profiles have been tested to confirm their improvement. They also reveal fine relationship and trade-offs between profile characteristics such as displacement and sealing line w.r.t. the overall performance. The chapter is concluded with detailed results and discussion of the experiments on these new profiles.

### Contents

5.1	Profile Generation to Minimize Oil Drag Loss . . . . .	84
5.2	Profiles Generated with Wide Gate Rotor Lobes . . . . .	88
5.3	Profile Generated by Combining Features of K-BETA1 and K-BETA2 . . . . .	91
5.4	Experimental Setup to Test K-BETA Profiles . . . . .	93
5.5	Results and Discussion . . . . .	94
5.5.1	Comparison of N and K-BETA1 Results . . . . .	95
5.5.2	Comparison of N and K-BETA2 Results . . . . .	96
5.5.3	Comparison of N and K-BETA3 Results . . . . .	97
5.5.4	Accuracy and Uncertainty Analysis . . . . .	98
5.6	Summary . . . . .	99

## 5.1 Profile Generation to Minimize Oil Drag Loss

In the study of N-Rack profile and its curves in the chapter on methods, it was identified that the gate rotor top land could potentially be adjusted to reduce the oil drag losses in the machine. Since this study is focused on improving the rotor profiles for oil flooded type screw compressor specifically; oil drag losses account for up to  $\sim 10\%$  of the total shaft power. If profile modifications could lead to reduction of drag losses, it can substantially improve the overall energy efficiency of the machine.

The phenomenon of drag in oil injected screw compressors has been extensively investigated by Abdan et al. (2022) and similarly so for screw expanders by Gräßer and Brümmer (2017). From these studies, it was understood that the drag losses in axial and radial clearance gaps are the major contributors to the total drag power loss. Whereas the drag loss in interlobe clearance does not contribute much to the total drag power loss. The oil drag loss depends on clearance gap, the leakage path length, the properties of fluid (oil in this case), the relative speed of shearing surfaces and the pressure difference on either side of the gap. Out of these parameters, from profile point of view, the sliding area where oil film is formed and sheared could be influenced. And this could help reduce drag losses especially visibly in machines running at high tip speeds. In order to offer economical sizes of screw compressors for various applications and flow requirements, running them at higher tip speeds is inevitable and at times a wise decision from commercial point of view.

The radial leakage path of the gate rotors can be adjusted by designing a narrow lobe, application of a variable clearance distribution, adding a sealing strip or by inclining an already wide lobe at the top. Such adjustments could create opportunities to minimize the drag losses. Gate rotor's sliding area along the radial leakage path in benchmark N-Profile (Figure 5.1) is represented in Figure 5.2.

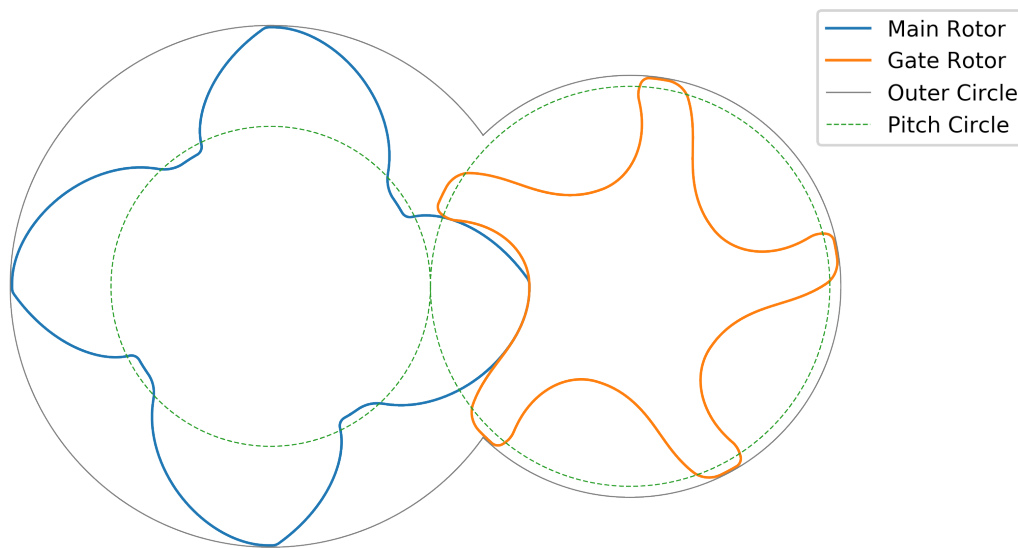


**Figure 5.1:** 141 mm benchmark N-profile used as a reference for profile modifications and comparisons

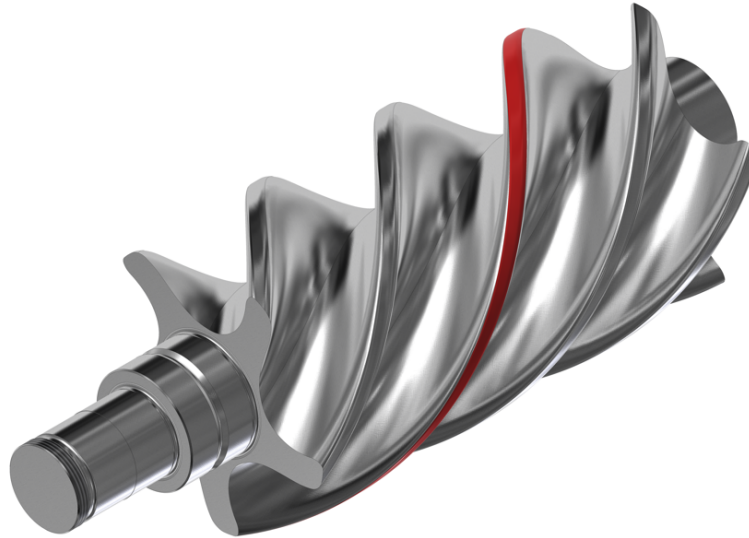


**Figure 5.2:** 141 mm benchmark N-profile gate rotor top land area of minimum clearance (marked red) that slides along rotor casing to create oil drag power loss

As it is noticed, the benchmark profile’s gate rotor top land follows the outer casing contour (also called outer circle) to maintain a constant minimum radial gap all across the sliding area (see Figure 5.1). However if the radial gap is progressively increased, while keeping it minimum only across a thin line, the effective sliding area is substantially reduced. The profile modification in cross section looks like as shown in Figure 5.3. The reduced sliding area on gate rotor top land is demonstrated in Figure 5.4. It can be compared with the benchmark profile in Figure 5.2. For the purpose of referring to this profile, it will be called ‘K-BETA1’.

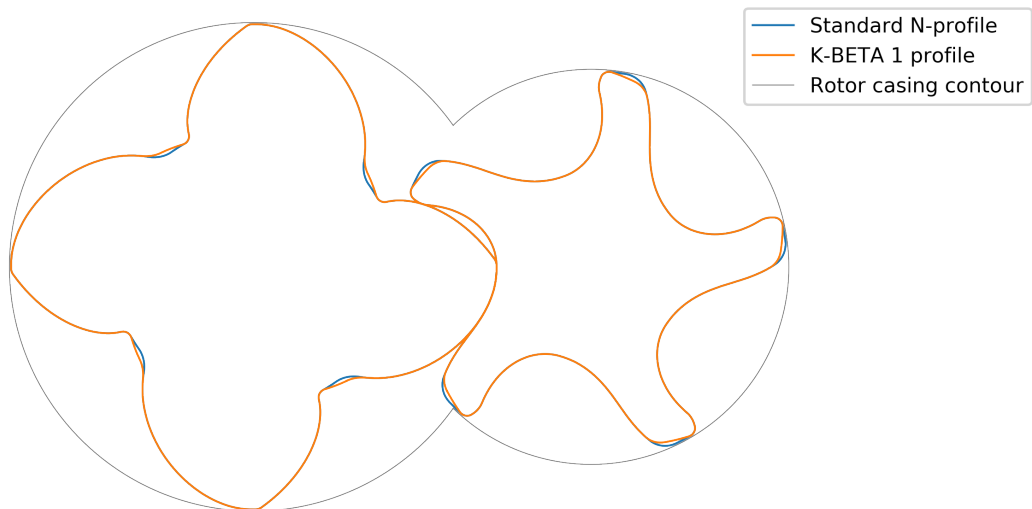


**Figure 5.3:** The modified N-Profile with an inclined gate rotor top land (K-BETA1), plotted along with the benchmark 141 mm N-Profile

This desired effect of tip design in K-BETA1 could also be easily achieved by imposing a large and varying clearance distribution on the top land of gate rotor. Herein, the radial clearance along the tip will be minimum across a small region and will increase

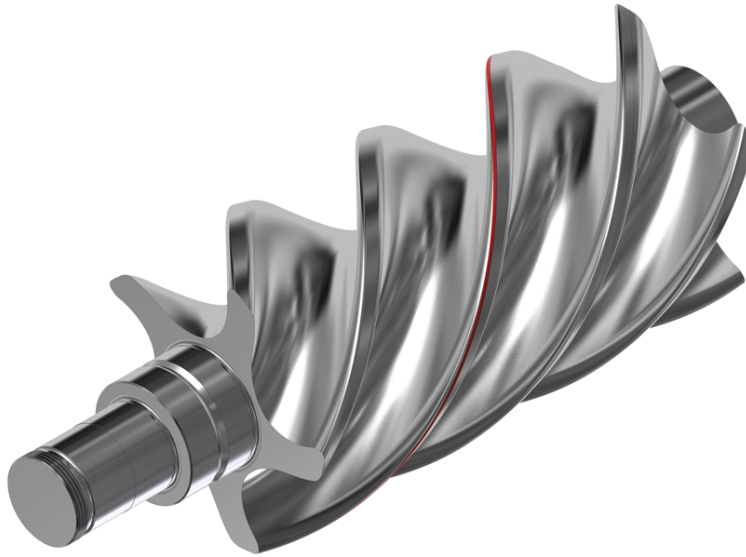


**Figure 5.4:** 141 mm BETA-1 profile (Figure 5.3) reduced gate rotor top land area of minimum clearance (marked red) that slides along the rotor casing

thereafter. Such a design applied on benchmark N-Profile (Figure 5.1) is presented in Figure 5.5 wherein clearance distribution on gate rotor top land is varied such that minimum clearance would be only across a small region thereafter a step is formed increasing the radial clearance substantially. However this way of adjusting tip results in sharp corners at the start and end of the step on gate rotor top land as well as main rotor root land.

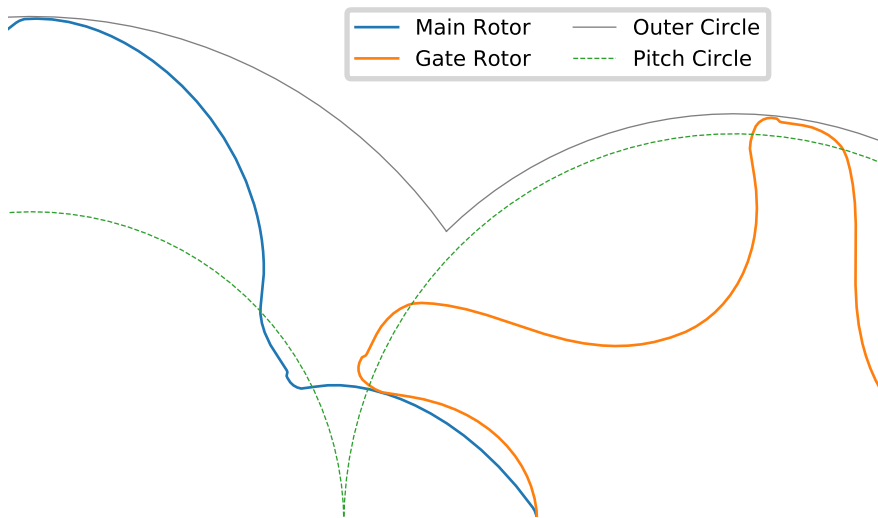


**Figure 5.5:** Minimizing rotor casing - gate rotor top land sliding area by imposing variable clearance distribution on a regular profile

However, the K-BETA1 profile in Figure 5.3 was generated by inclining the N-Rack vertical lines at either ends by few degrees. The comparison of rack profiles generating the benchmark N-Profile and K-BETA1 profile is given in Figure 5.6 where the inclination to the end vertical straight line of N-profile is clearly visible. This change reflects in the reduction of sliding area as presented in Figure 5.4 which is

reduced by at least a factor of five. This way of adjusting tip leads to more gradual change of profile hence it was preferred for prototyping such rotors. This change results in inclination of not only the gate rotor top land but also the main rotor root land due to conjugacy of both rotor shapes. The change reflected on the main rotor root land does not significantly influence the oil drag but it still has some effect on the leakage flow on account of the interlobe sealing line path it generates along with its conjugate curve on gate rotor top land.

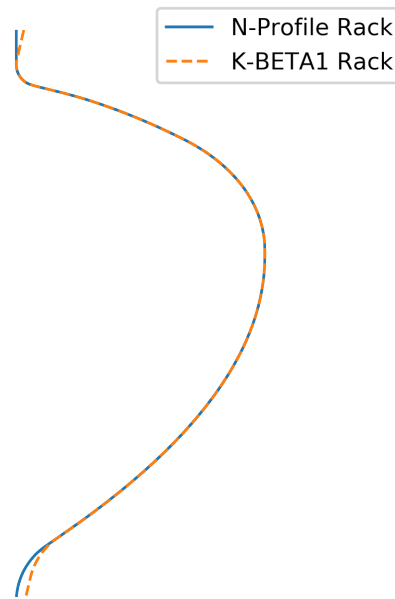


**Figure 5.6:** N-Profile rack and K-BETA1 rack comparison

The model developed by Abdan et al. (2022) could be used for evaluating the effect of such profile adjustments on flow output and power consumption of the compressor. It was predicted that the K-BETA1 could have up to 1% lower shaft power on account of saving in drag power loss especially at higher tip speeds  $>30$  m/s. The sliding area under discussion does not only create shear in oil film leading to drag loss but the oil film trapped here also acts as sealing against leaking air across two adjacent chambers on account of their pressure difference. Hence, reducing this area could very well have a negative impact on the flow output due to these leakages. However, this phenomenon too is complicated to model and predict beforehand. Hence it further substantiates the need for experimentally verifying these profiles.

The rotors with K-BETA1 profile were manufactured at sponsor KPCL's facilities for testing alongside the benchmark N-profile to validate if this change actually leads to reduction in drag power loss as per predictions. Figure 5.7 is the actual photograph of 141 mm K-BETA1 profiled rotors manufactured at KPCL.



**Figure 5.7:** The 141 mm K-BETA1 rotors manufactured at KPCL for testing

## 5.2 Profiles Generated with Wide Gate Rotor Lobes

The homotopy curves for improving profiles were searched by an algorithm (Figure 4.4) which used a proxy objective function based purely on evaluation of geometric characteristics of the profile. As discussed in the same chapter, though this approach is faster, it is not robust because the influence of geometry on energy efficiency is heavily influenced by the operating parameters. Hence, improvements in the proxy objective function based purely on geometric characteristics did not reflect to the same extent into improvements in energy efficiency.

This calls for optimization with the energy efficiency, calculated by complete thermodynamic simulation at set operating conditions, as the objective function for the algorithm. This is indeed advocated already in works such as Stosic et al. (2003b). If the benchmark N-Profile itself is put through an optimization framework wherein the objective is set to higher adiabatic efficiency without any other constraints such as torque characteristics, the results are always a profile with very thick gate rotor lobes.

Also, the box complex algorithm for optimization is far quicker than the one presented previously for the search of homotopic curves. It was used on the benchmark profile to find profiles with an objective of higher adiabatic efficiency and no constraint on gate rotor torque values (which usually limits the thickness of gate rotor lobes). The result was a profile presented in Figure 5.8. SCORPATH predicts it to have up to 1% higher adiabatic efficiency than the benchmark profile. It has far wider gate rotor lobes than than the benchmark profile which also results in unusually large and negative gate rotor torque.

Technically, the reasons for better energy efficiency of such profiles are their higher displacements and lower clearances in such machines. Such profiles also have higher profile efficiency (ratio of total throughput area to the total leakage area) especially at lower values of interlobe and radial clearances. The thicker gate rotor lobes lead to higher overall displacement of the rotor pair (approximately 5% in presented case) but also increase the sealing line length by 15%. The increase in displacement area and various leakage areas affect the adiabatic efficiency at specified pressures and operating

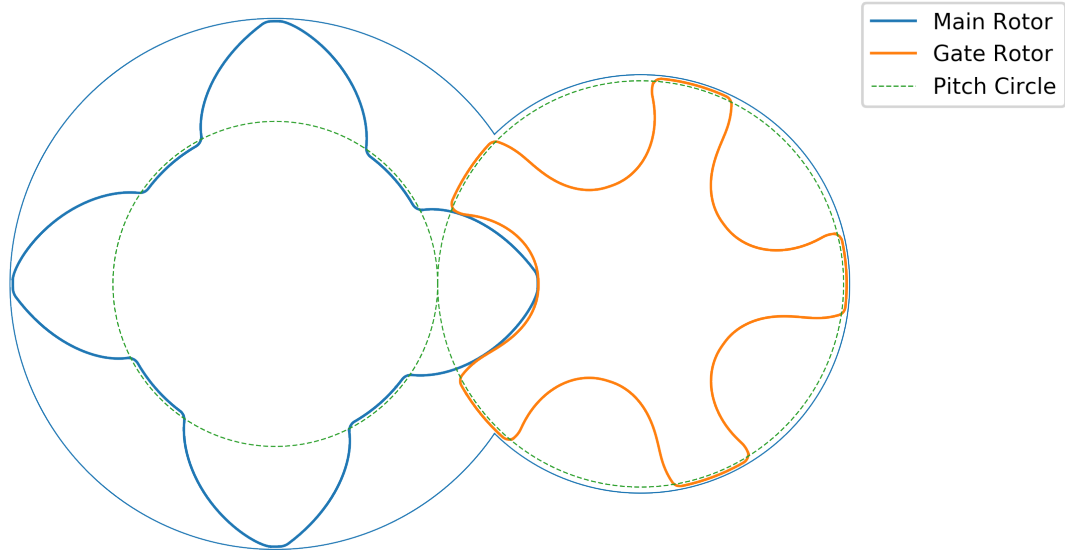


**Figure 5.8:** N-Profile optimized by box complex algorithm (Stosic et al., 2003b) for maximum adiabatic efficiency

speeds differently.

As the SCORPATH solves for the adiabatic efficiency, the negative effect of increase in sealing line leakage area on specific power is slightly belittled on account of the low interlobe clearance (30-40 micron) compared to the positive effect of increase in displacement for this particular case. However, if the clearances are large, the effect of the increased displacement will be higher than for the small clearances. Certainly, this is moderated by the increase in sealing line length. The operating conditions and assumptions/considerations of the thermodynamic solver, all influence this result. All in all, prediction come out to be 0.5-1% improvement in adiabatic efficiency for wide gate rotor lobe profiles than the benchmark N-profile.

The increased gate rotor top land area in such profiles would also lead to high oil drag power loss. Using Abdan et al. (2022)'s model, the increase in drag losses was calculated. Those were pointing at overall reduced energy efficiency on account of relatively larger impact of drag than the positive impact of higher displacement in such profiles even at lower clearances. Hence, to validate the new profile adjustments as well as the drag loss prediction model, a wide gate rotor version of the benchmark 141 mm N-Profile was designed (Figure 5.9) based on the profile in Figure 5.8. It is referred to as 'K-BETA2'. It would have same blow hole area and same rotor diameters but twice the gate rotor top land area of minimum radial clearance compared to the benchmark profile (Figure 5.10).

To validate K-BETA2 profile, it was also manufactured at KPCL and tested along with the benchmark N-Profile. See Figure 5.11 for the actual rotor pair with K-BETA2 profile.

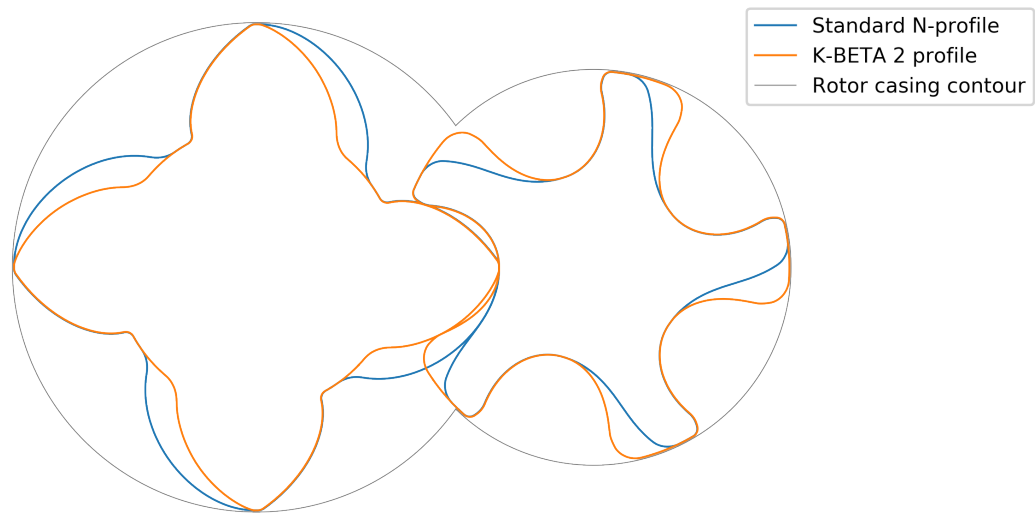


**Figure 5.9:** The modified N-Profile with wide gate rotor lobes (K-BETA1), plotted along with the benchmark 141 mm N-Profile

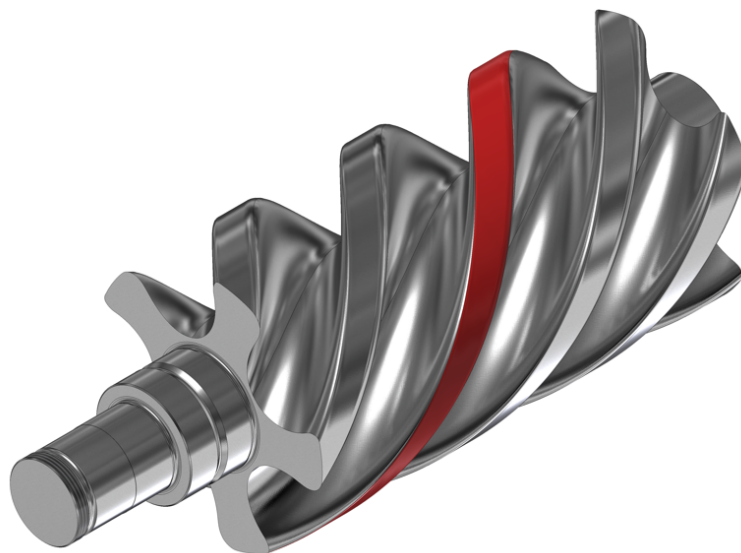


**Figure 5.10:** 141 mm K-BETA2 larger gate rotor top land area of minimum clearance (marked red) that slides along the rotor casing



**Figure 5.11:** The 141 mm K-BETA2 rotors manufactured at KPCL for testing

### **5.3 Profile Generated by Combining Features of K-BETA1 and K-BETA2**

The K-BETA1 was conceptualized from drag power loss calculations and K-BETA2 was conceptualized from optimization with strictly thermodynamic criteria. There could be a third new profile proposition which relies on both these concepts. It would be referred as ‘K-BETA3’.

In K-BETA2, calculations predict a slight gain in energy efficiency due to relatively larger increase in displacement compared to the increase in leakage. However calculations based on Abdan et al. (2022) predict that K-BETA2 design would also lead to significantly higher drag power loss. There could be a way to further validate the drag loss prediction model and to retain the advantage imparted by wide gate rotor lobe profiles without losing it in high drag loss due to increased shearing area. The idea is to combine K-BETA1 and K-BETA2 features into one profile; to incline the top land of wide gate rotor lobe profile so that its effective gate rotor top land sliding area reduces while the advantage of higher displacement also remains intact. K-BETA3 profile retrofitted on the benchmark N-profile is presented in Figure 5.12.

K-BETA3 was generated from K-BETA2 similar to how K-BETA1 was generated from N. The vertical lines at the ends of K-BETA2 rack were inclined by few degrees. The racks that generate K-BETA2 and K-BETA3 profiles are presented in Figure 5.13, overlapped. However, unlike N and K-BETA1, in order to accommodate inclination feasibly along with a wide gate rotor in K-BETA3, the pressure angle on long edge side of the rack had to be adjusted too. This creates an effect of long edge of the K-BETA3 rack slightly diverging K-BETA2. However, the effect of this change on the width of the gate rotor lobe as well as sealing line length is kept minimal.

K-BETA3 rotors were also manufactured at KPCL and tested along with the benchmark N-Profile and other K-BETA rotors. Figure 5.14 is a photograph of K-BETA3 gate rotor manufactured at KPCL.

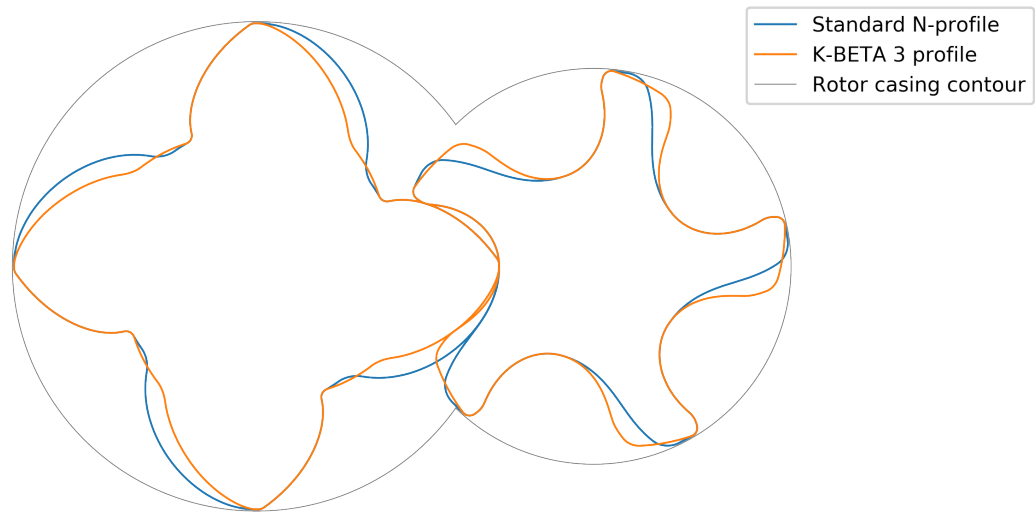


**Figure 5.12:** The modified N-Profile with wide gate rotor lobes having inclined top land (K-BETA3), plotted along with the benchmark 141 mm N-Profile

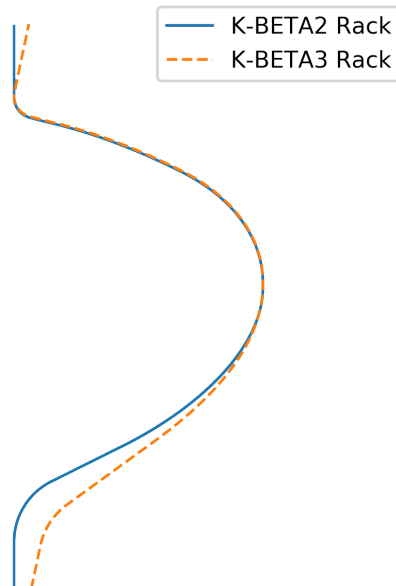


**Figure 5.13:** K-BETA2 and K-BETA3 rack comparison



**Figure 5.14:** The K-BETA3 gate rotor manufactured at KPCL for testing

## 5.4 Experimental Setup to Test K-BETA Profiles

An oil-flooded, twin-screw, air compressor packaged unit with a drive electric motor of 55 x 1.2 kW rating was used for the experimentation. This is shown in Figure 5.15. This is a main rotor drive compressor driven by an electric motor with a speed increasing gear pair in between.



**Figure 5.15:** A Kirloskar 55 kW oil-flooded, twin-screw, air compressor package used for testing K-BETA profiles

The benchmark 141 mm N-Profile rotors along with the retrofitted K-BETA1, K-BETA2 and K-BETA3 rotors were tested in the same rotor casing and compressor package one after the other without change of any component. The assembly clearances were also maintained the same for all rotor pairs to minimize the role of different

clearances on performance of the rotor pairs. The order of error in setting these clearances during the assembly procedure was at max 10 micron. Special care was taken to achieve such tight control over clearances. The nominal values of axial, radial and interlobe clearances were 60, 40 and 40 micron respectively for all rotor pairs.

Tip speed of 141 mm rotors in a 55kW machine is about 38 m/s. At this tip speed, the drag losses are expected to be higher. Abdan et al. (2022) also confirms that the contribution of the oil drag loss significantly increases with the increase in tip speed. So the experiments were carried out at relatively higher tip speeds to amplify the effects caused by drag in oil. Hence any saving in drag loss due to variation such as that in the K-BETA1 or K-BETA3 profiles would be measurable/detectable.

The rotors were assembled in the same bare compressor housing, one after the other, in the order of N (put first for benchmarking) followed by K-BETA1, K-BETA2 and K-BETA3. They were operated at a package discharge pressure of 7 bar(gauge), which translates to approximately 8.5 pressure ratio across the rotors. An electric motor drove the compressor through a gearbox with the main rotor rotating at a constant tip speed of 37.3 m/s (5044 RPM). The gate rotor side provided a single-point oil injection in the bare compressor housing. The oil with a density of 860 kg/m<sup>3</sup> and operating viscosity of around 9 cSt was used. Oil in the system is driven by the discharge pressure in air-oil receiver tank. Since all the three profiles were tested and compared at the same discharge pressures and the oil injection hole on the rotor casing remained same for all the profiles; the oil flow rate to the compressor would be similar across all three experiments. Hence it was not explicitly measured or controlled.

The volume flow rate is measured using a differential manometer at the discharge end of the compressor package and is normalized at the suction conditions. An energy meter with a current transformer (225/5A) of 0.2 class accuracy was used to measure the total compressor package power. With this accuracy of the current transformer, the power measurement accuracy is +/- 0.35% at the operating conditions specified above.

## 5.5 Results and Discussion

This section presents the experimental results for each K-BETA profile variant performance with respect to the benchmark N-Profile. The experiment is setup as explained in the previous section. To minimize the influence of ambient and transient conditions, each data point measurements were taken at different times of the day and on multiple days while keeping the machine running for extended periods of time to let the measurable values reach steady state before measuring them. Each profile was tested to capture 5 to 8 such reliable data points.

The presented data in this section is normalized and averaged. The normalization of test data points has been done at Pune conditions (the location of tests) of atmospheric pressure of 0.983 bar and ambient temperature of 25°C. And the test data has been averaged for concise presentation. Each average is across 3 to 6 reliable data points captured for each profile.

The results are also discussed at length along with a detailed comparison of these profiles' geometric characteristics and their probable influence on the results.

### 5.5.1 Comparison of N and K-BETA1 Results

The comparison between benchmark profile and K-BETA1 is presented in Table 5.1 which is to highlight how much difference the inclination of gate rotor top land can make on the performance. As highlighted previously, apart from this change, rest of the profile is exactly similar (see Figure 5.3). The modification was expected to reduce the shaft power consumption for a similar flow. A 0.8% reduction in shaft power for K-BETA1 rotors compared to N-rotors is exactly as anticipated from calculations based on work of Abdan et al. (2022).

@ Pressure ratio-8.5, Speed-5044 RPM	N-Profile	K-BETA1	% Difference w.r.t. N
Free air delivered [m <sup>3</sup> /min]	8.745	8.821	0.9%
Compressor shaft power [kW]	55.33	54.89	-0.8%
Specific power [kW/m <sup>3</sup> /min]	6.328	6.222	-1.7%
Volumetric efficiency [%]	85.11	85.81	0.8%

**Table 5.1:** Comparison of the experimental results of 141 mm benchmark N-Profile with the new K-BETA1 profile

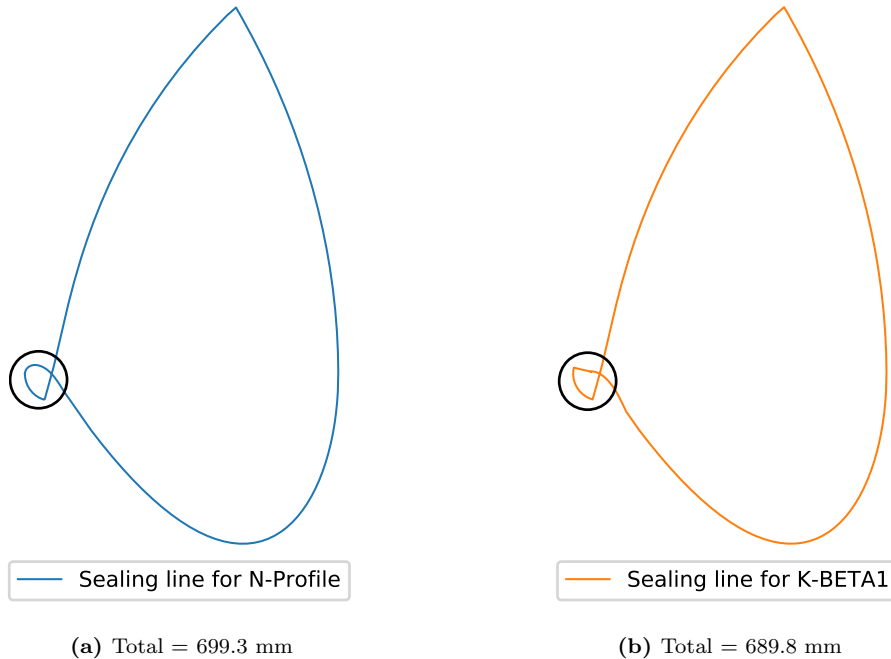


**Figure 5.16:** The interlobe sealing lines of N and K-BETA1 profiles projected on the plane perpendicular to the rotor axes; marked portion indicates region of sealing line generated by the gate rotor top land

But the slight increase in flow and volumetric efficiency was not anticipated at first. Assuming it to be error in measurements, the tests were repeated with different pairs of

rotors and reassembly of compressor. But the slight improvement in flow was evident. A much closer look at the K-BETA1 profile revealed some clues for explanation. Figure 5.16 is a plot of the sealing lines for N and K-BETA1 profiles in a view where they are projected on profile transverse planes. The difference could be spotted where a small circular portion on the sealing line for N-profile is replaced by a straight line in K-BETA1 profile's sealing line. Since a straight line between two points is shorter than a circular arc, sealing line length is slightly reduced due to this modification.

In numeric terms, the sealing line length for K-BETA1 is 1.4% smaller than N-Profile which makes around 10 mm difference across the total length of the rotors. Hence the profile modification in K-BETA1 made for reducing drag losses, positively affects purely geometric profile characteristics too. This results in improvement of volumetric efficiency and flow delivered by K-BETA1.

However these results of improvement in K-BETA1 are taken at very high tip speed and it is indicative of the effect an inclined tip could have on the drag power losses. The effect will very well be diminished at lower tip speeds and an improvement of the same order as observed in this experiment can not be expected across all tip speeds.

### 5.5.2 Comparison of N and K-BETA2 Results

It is presented in Table 5.2, the comparison between benchmark profile and K-BETA2 which was predicted by the optimization algorithm to have better specific power on account of its large displacement. However, the effect of drag on such profiles was also of interest. Due to its higher theoretical displacement, the anticipated increase in flow with respect to N-Profile was in the range of 4.5%. In testing, the flow increased by 4% but the shaft power increased by 11.2% which was anticipated to increase by only 3.5%.

@ Pressure ratio-8.5, Speed-5044 RPM	N-Profile	K-BETA2	% Difference w.r.t. N
Free air delivered [m <sup>3</sup> /min]	8.745	9.095	4.0%
Compressor shaft power [kW]	55.33	61.52	11.2%
Specific power [kW/m <sup>3</sup> /min]	6.328	6.765	6.9%
Volumetric efficiency [%]	85.11	84.53	-0.7%

**Table 5.2:** Comparison of the experimental results of 141 mm benchmark N-Profile with the new K-BETA2 profile

The higher than anticipated shaft power increase can be explained by the increase in drag power loss occurring due to increased radial oil shearing area over K-BETA2 rotors compared to N rotors. This is a reverse effect to that of K-BETA1 profile where reduction in the shearing area led to reduction in drag power loss.

The more than anticipated increase in power was accompanied by a rattling noise in the machine while testing. The noise indicates a bad gate rotor torque characteristic of the profile which was anticipated in the design stage itself. The gate rotor torque for K-BETA2 profile was calculated to be ten times higher than that of gate rotor torque

for N-profile at tested conditions.

Another reason for the higher than anticipated power could be that the discharge port is the same for all the profiles. Since the bearing housing is kept same in all cases and only the rotors are swapped, the discharge port is designed and manufactured for the N Profile. The ports of K-BETA1 and N are similar without any major differences. However, due to thicker gate rotor lobes in K-BETA2, its theoretical discharge port profile would be different than that for the N rotors. It could contribute to the higher power compared to N profile. This was one of the experimental limitations wherein different bearing housings for different rotors were not produced.

The higher theoretical displacement in K-BETA2 was also accompanied by a longer sealing line length too. The combined effect of increased displacement and sealing line length on the flow could be evaluated by volumetric efficiency of K-BETA2 rotors w.r.t. N rotors. At the tested conditions, K-BETA2 rotors have 0.7% lower volumetric efficiency than N rotors indicating the modification in profile might be in fact disadvantageous from the internal leakage point of view.

### 5.5.3 Comparison of N and K-BETA3 Results

It is presented in Table 5.3, the comparison between benchmark profile and K-BETA3 which is a combination of the two features in K-BETA1 and K-BETA2. It showed lower shaft power compared to K-BETA2 profile as anticipated on account of the reduction of oil drag loss in its radial clearance gap due to inclination of the gate rotor top land. This provides further strength to the hypothesis that inclination of gate rotor top lands in a normal profile leads to reduction in oil drag losses.

@ Pressure ratio-8.5, Speed-5044 RPM	N-Profile	K-BETA3	% Difference w.r.t. N
Free air delivered [m <sup>3</sup> /min]	8.745	9.157	4.7%
Compressor shaft power [kW]	55.33	59.25	7.1%
Specific power [kW/m <sup>3</sup> /min]	6.328	6.471	2.3%
Volumetric efficiency [%]	85.11	84.95	-0.2%

**Table 5.3:** Comparison of the experimental results of 141 mm benchmark N-Profile with the new K-BETA3 profile

Still the reduction in oil drag losses due to the inclination feature was not enough to get K-BETA3 on par with N-Profile. The higher flow due to higher theoretical displacement of this profile was intact in K-BETA3 just like K-BETA2 between 4 to 5%. But the shaft power is observed to be significantly higher (7.1%) than N-Profile. This indicates that the tip inclination contributed to reduce the drag power loss in radial gap by 4.1% (which is difference in shaft powers of K-BETA2 and K-BETA3). But the additional power arising due to either bad gate rotor torque characteristics or the experimental limitation of using the same discharge port is not being compensated for. This additional uncompensated component of power is what makes the K-BETA3 profile's specific power consumption up to 2-3% higher than the N-Profile.

The volumetric efficiency of K-BETA3 rotors however comes close to N rotors (within 0.2%). This is almost 0.5% improvement from K-BETA2 to K-BETA3 which is just an inclined tip version of the previous. This re-confirms the role of inclination in improving the volumetric efficiency of normal flat gate rotor top land profiles which comes through a slight reduction in sealing line leakage length. See Figure 5.17 which compares sealing lines for K-BETA2 and K-BETA3 similar to the comparison in Figure 5.16. K-BETA3 has 7 mm shorter interlobe sealing line length than K-BETA2 on account of the inclination. This difference should have been more than or at least equal to 10 mm difference between K-BETA1 and N. However, due to the change in long edge side pressure angle, K-BETA3 had a slightly thinner gate rotor lobe than K-BETA2 (see Figure 5.13) which would have effectively increased the sealing line length, but only slightly.

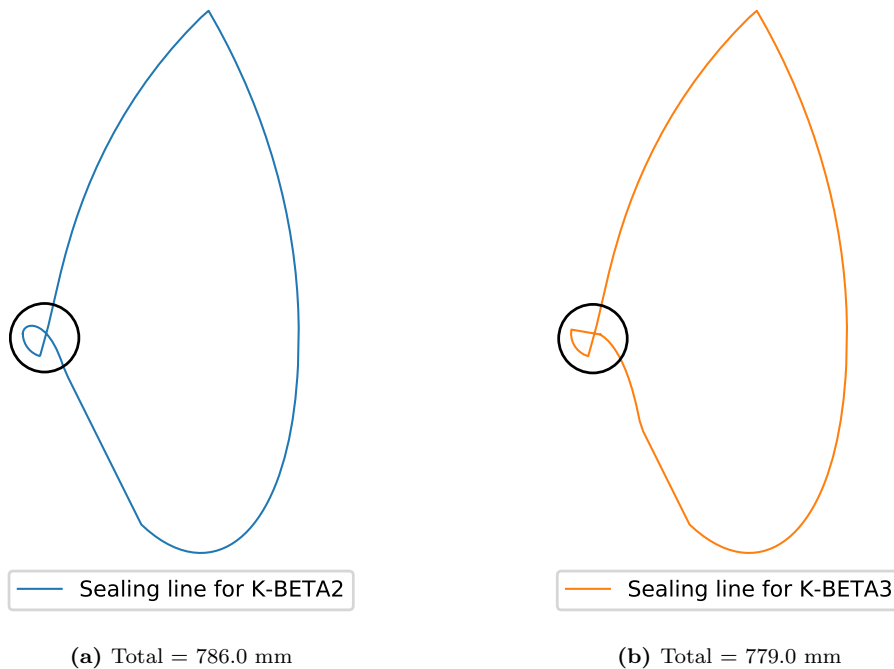


**Figure 5.17:** The interlobe sealing lines of K-BETA2 and K-BETA3 profiles projected on the plane perpendicular to the rotor axes; marked portion indicates region of sealing line generated by the gate rotor top land

#### 5.5.4 Accuracy and Uncertainty Analysis

The accuracy of the speed, pressure and, temperature sensors used during the experimental measurement is presented in the following Table 5.4 (Abdan et al., 2023). During the experimental measurements, different sets of readings were recorded for the same operating condition. For ‘N’, ‘K-BETA1’, ‘K-BETA2’ and ‘K-BETA3’, three, five, four and five sets of readings were recorded, respectively. An uncertainty analysis for each instrument reading is carried to understand the expected variation in the measurements (EDUBCA, 2022).

From the uncertainty analysis it is observed that the uncertainty in the pressure

Parameter	Instrument	Specification
Compressor speed	Digital tachometer, NCTM-1000, Metravi	Test range: 2 to 99999 RPM Accuracy: $\pm 0.05\% \pm 1$ digit
Temperature	RTD Pt-100, SIMPLEX Tempens Instrument (I) Pvt. Ltd.	Three-wire, DIN-43760, Class A Temperature range 30°C to 350°C Accuracy: $\pm 0.15^\circ$ at 0°C
Pressure	Pressure transmitter, MBS3000-2211-1 Danfoss	Two-wire, 4-20 mA Pressure range: 0 to 16 bar, Accuracy: $\pm 0.5\%$ FSD

**Table 5.4:** Accuracy of the instruments used in the experiments

measurement is up to 0.03%, in the temperature measurement is up to 0.27%, in the manometer reading is up to 0.54% and in the speed measurement is up to 0.08%. The resultant effect on the suction volume flow rate variation when calculated is up to  $\pm 0.36\%$ . An energy metre with a current transformer (225/5A) of 0.2 class accuracy was used for the measurement of the total compressor package power. The accuracy of the power measurement was  $\pm 0.35\%$ . The comparison results presented hereby are well outside the measurement uncertainty for the measured parameters such as flow and power.

## 5.6 Summary

Results of experiments on these new profile concepts based on oil drag and optimization results could be summarized in following three points-

- The inclination of gate rotor top land in any profile employed in a oil injected screw machine would lead to reduction of the oil drag power loss occurring in the radial gap between gate rotor tip and rotor casing. It also leads to improvement of volumetric efficiency by 0.5 to 1% (which is subject to vary for different pressures and speeds than those tested during these experiments).
- The screw rotor profiles with thicker gate rotor lobes have higher displacements but it also leads to higher gate rotor torque, longer sealing line length and a larger radial oil film shearing area. Thickening of gate rotor lobes in order to gain energy efficiency only works up to a point; thereafter too much thickening of gate rotor leads to very high drag power loss, lower volumetric efficiency and bad gate rotor torque characteristics.
- Profile designs for higher energy efficiency of machines can be inspired from more accurate modeling of the physics of internal processes such as leakage flows, drag losses and torque characteristics. A promising way ahead for improvement of existing state of the art rotor profiles is through better understanding of the finer and more complicated phenomenon inside the compression chamber. The improvement of the thermodynamic simulation capabilities of existing models which

incorporate these understandings can help trigger profile modifications which lead to better efficiency of screw machines.

# Chapter 6

## Manufacturability

**M**ANUFACTURABILITY of the profiles discussed in last two chapters is evaluated in this chapter. The literature on manufacturability has been reviewed in the second chapter. Based on that, the methods to evaluate manufacturability will be applied, with some modifications, to the profiles under discussion. It also backs up some of the claims made in fifth chapter regarding role of homotopy in improving profiles for energy efficiency without compromising too much on their manufacturability. The proposed model to quantify manufacturability of profiles based on Stosic (2006b) with additions to account for the role of relative speed between the tool and the rotor on tool wear can be viewed as a contribution of this study.

### Contents

6.1	Quantifying Manufacturability . . . . .	102
6.2	Modifying Relative Tool Wear Model with Considerations to Relative Speed between Tool and Rotor . . . . .	104
6.3	Manufacturability of Developed Profiles . . . . .	107
6.3.1	Comparison of H-Rack Profiles and N-Profile . . . . .	108
6.3.2	Comparison of K-BETA Profiles and N-Profile . . . . .	110
6.4	Summary . . . . .	111

## 6.1 Quantifying Manufacturability

A vast majority of screw rotors are manufactured by form milling and grinding process (Figure 3.9). Hence this study sticks to this machining process for discussion on manufacturability. Hobbing is also preferred fairly recently for smaller rotors and mass production but it is not included in the scope of this study. However the principles presented here may be applied to other machining processes to derive similar models but based on different mathematical theory suitable for that specific machining process.

Few basics about the form milling and grinding machining process are that a given rotor profile has a unique tool based on the setup conditions which include three parameters- tool-rotor center distance, tool inclination angle and the lead of the rotor. The transformations from a rotor to tool or tool to rotor are based on Euler's envelope theory similar to the rack to rotor or rotor to rotor transformations. The details of these can be found in Stosic (1998). The tool profiles are replicated on milling cutters and grinding wheels. After few passes of machining at certain depth of cut at a time and certain feed rate decided by the operator and machine itself, the tools wear out. Hence they require regrinding after certain number of passes. In a way, the tool wear characteristics govern how frequently a tool needs regrinding. It is also partly governed by how tight a tolerance is desired on the rotor profile form. Since a tighter requirement on form requires more frequent regrinding of tool to minimize variations in rotor profile due to the worn tool profile.

Manufacturability of rotor profiles is difficult to quantify. The term holds multiple aspects of rotor machining, the most basic being feasibility of machining a rotor profile followed by how easy it is to machine a rotor profile within reasonable tolerances and also the costs of machining which are related to cycle times of the process. Answers to some of these aspects can be only qualitative such as the feasibility of machining could only be either yes or no. However more manufacturable profiles may have wide range of feasible machining settings than the less manufacturable ones. Similarly, the questions such as how easy it is to machine a rotor profile within reasonable tolerances may be answered qualitatively based on operator's experience but it can also be quantified in some indirect measure such as tool wear or the profile's sensitivity to variations in machining process parameters.

Three different approaches to quantitatively measuring manufacturability of rotor profiles are found in literature. Guo and Tang (2003b) approached screw rotor manufacturability from three aspects- the range of valid tool setup conditions, the minimum radius on tool profile, and the severity ratio which is a measure of relative tool profile cutting load distribution (first introduced by Sheth and Malkin (1990) in their work on helical groove machining). Sauls (2002) presented a statistical approach to compare manufacturability of profiles by randomly introducing process parameter variations (based on machine capabilities) into his manufacturing simulation tool and comparing the number of profiles in a large sample that get rejected due to these variations. Since different profiles respond differently to manufacturing variations, a more robust profile from manufacturability point of view was supposed to have a lesser number of unac-

ceptable pairs in the sample. Stosic (2006b) approached the problem geometrically and quantified the relative tool wear for given profiles which can be used to compare manufacturability of two different profiles. Practical effects such as non uniform wear at profile portions that have high curvatures are captured in this approach and is relatively straightforward to calculate using tool-rotor and rotor-tool transformations. It is also an experimentally validated approach which has been used to achieve uniform wear of tool profile.

All three approaches are capable of being used for quantification of manufacturability but the choice is based on what is the purpose of such evaluation. If the purpose is to modify an existing rotor profile for better suitability to mass production through lower sensitivity to process parameters, statistical approach of Sauls (2002) is preferable. If the goal is to purely judge a profile based on how machining process friendly it is, such as how wide a setup conditions it allows or does it have very sharp radii which require careful and frequent regrinding, Guo and Tang (2003b)'s approach is more suitable. However if the goal is to simply compare two or more profiles on a relative term if they are more or less manufacturable than each other, geometric approach by Stosic (2006b) is more direct, simpler and hence preferable.

Since rack generated profiles are almost always guaranteed to have a valid tool setup condition, looking at manufacturability for the profiles presented hereby from valid tool setup conditions is not necessary. Also, the modern rotor machining machines are robust enough to induce minimum process parameter variations and achieve consistent form tolerances between 10-20 micron in a series production. This is good enough for most modern applications. Hence, looking at new profiles developed in this study (which had primary goal of improving energy efficiency) from the point of view of process parameters and mass production is not helpful either. However, a fair comparison of new profiles with benchmark profile in terms of the relative effects of proposed profile modifications on manufacturability are interesting to look at.

From this point of view, comparing profiles based on their severity ratios (Guo and Tang, 2003b) or relative tool wear (Stosic, 2006b) could be helpful. The later approach is adopted in this study because of its simplicity and direct availability for evaluation in the framework of software tools already being used (such as SCORPATH). On a more fundamental level, both approaches are equivalent since both measure the tool wear in terms of the depth of cut and relative penetration of tool at different locations on the profile.

But one important aspect of cutting process which is the relative speed of tool and rotor along the tool-rotor contact line is not included in either of these approaches. However it can be easily blended in Stosic (2006b)'s approach and a modified relative tool wear which also incorporates effect of tool-rotor relative speed can be used to quantify manufacturability of new profiles w.r.t the benchmark profile. Next sections follow exactly on this line of thought.

## 6.2 Modifying Relative Tool Wear Model with Considerations to Relative Speed between Tool and Rotor

As presented in Chapter 3, Stosic (2006b)'s model of relative tool wear can be used to compare manufacturability of various profiles. However, in this model, it is assumed that the relative speed between the rotor and tool will equally affect the with and without stock profiles. Hence, the relative tool wear term is solely based on coordinate differences. It has been attempted to modify the relative tool wear term to more accurately incorporate effect of other rotor-tool interactions in quantifying the manufacturability.

The hypothesis of this study is that a higher relative speed at certain region of profile will incur higher wear in spite of the same coordinate difference. And this dependence is assumed to be directly proportional to the relative speed. Following this, the relative tool wear ( $TW_{rel}$ ) (Chapter 3) at each point can be modified by multiplying it with a normalized relative speed term at that point.

The relative speed between rotor and tool along their contact line is derived in the following pages. The motion of tool with respect to the rotor is basically a rolling and sliding motion along its helicoidal surface. The tool as well as rotor have a certain angular rotational speed along their respective axes  $Z_t$  and  $Z$ . These shall be inputs to the calculation. They can be called  $\omega_t$  and  $\omega_r$ . A general arrangement of tool and rotor while cutting is already presented in the Figure 3.9.

The  $\Sigma$  is an angle between tool and rotor axes, also known as tool setting angle. Angle  $\theta$  is the rotor rotation angle around its own axis, whereas  $\tau$  will be the equivalent rotation of the tool-wheel around its own axis. The  $X_t - Y_t - Z_t$  and  $X - Y - Z$  are tool and rotor local coordinate systems respectively.  $X_h - Y_h - Z_h$  is the rotor helicoidal coordinate system.

The rotor-tool pair meshes and the cutting action is performed. The contact points are along a meshing line derived using Euler's Envelope Theory as demonstrated in (Stosic et al., 2005) and also in the third chapter. For each point on the rotor profile, a contact point in helicoidal coordinate system is obtained where a point coincides on tool as well as the rotor helicoidal surface. At each such point, the tool-wheel has a rolling and sliding motion with respect to the rotor. Hence a relative velocity between tool and rotor can be obtained at each of the cutting point.

The coordinate system  $X - Y - Z$  can be chosen for the evaluation of relative velocity. If the angular velocity of tool-wheel around its own axis  $Z_t$  is  $\omega_t$  and the angular velocity of the rotor-workpiece around its own axis  $Z$  is  $\omega_r$ , the relative velocity at a particular contact point along the meshing line is given by Equation 6.1.

$$\vec{V}_{rel} = \vec{V}_t - \vec{V}_r \quad (6.1)$$

where  $V_t$  and  $V_r$  are the instantaneous velocities of tool and rotor respectively at the contact point.

The  $\vec{V}_r$  has two components of motion in the actual manufacturing process, the

rotor rotates around its own axis with angular velocity  $\omega_r$  and it also moves axially (to create a helical motion w.r.t tool wheel) with a speed equal to the pitch ( $p$ ) times angular velocity ( $\omega_r$ ). Hence  $V_r$  can be expressed as in Equation 6.2

$$\vec{V}_r = \vec{\omega}_r \times \vec{R}_r + p \omega_r \cdot \hat{k} \quad (6.2)$$

where  $\vec{R}_r$  is the position vector of contact point in common coordinate system  $X-Y-Z$  and  $\vec{\omega}_r$  is oriented along the  $Z$  axis ( $\hat{k}$  is a unit vector along  $Z$  axis). The coordinates of the point in this coordinate system are directly represented as helicoidal surface coordinates of the profile which are rotation of the profile point by the angle calculated from meshing condition.

$$\vec{R}_r = \begin{bmatrix} x_h \\ y_h \\ z_h \end{bmatrix}; \vec{\omega}_r = \begin{bmatrix} 0 \\ 0 \\ \omega_r \end{bmatrix} \quad (6.3)$$

The  $\vec{V}_t$  has only one motion that is rotation about its own axis  $Z_t$  at an angular velocity  $\omega_t$ . But the axis of tool is inclined at an angle  $\Sigma$  w.r.t the rotor axis or the global coordinate system axis  $Z$ . Hence the velocity  $\vec{V}_t$  is given as in Equation 6.4

$$\vec{V}_t = \vec{\omega}_t \times \vec{R}_t \quad (6.4)$$

where  $\vec{R}_t$  is the position vector of the contact point and  $\vec{\omega}_t$  is the tool-wheel angular velocity vector in the common coordinate system  $X-Y-Z$ . The tool coordinate system  $X_t-Y_t-Z_t$  is offset from the  $X_h-Y_h-Z_h$  system by the tool rotor center distance  $C$  along the  $X_t, X_h$  axis. The inclination  $\Sigma$  is also along the same axis. Hence,  $R_t$  is transformed as in Equation 6.5.

$$\vec{R}_t = \begin{bmatrix} x_h - C \\ y_h \\ z_h \end{bmatrix}; \vec{\omega}_t = \begin{bmatrix} 0 \\ -\omega_t \sin(\Sigma) \\ \omega_t \cos(\Sigma) \end{bmatrix} \quad (6.5)$$

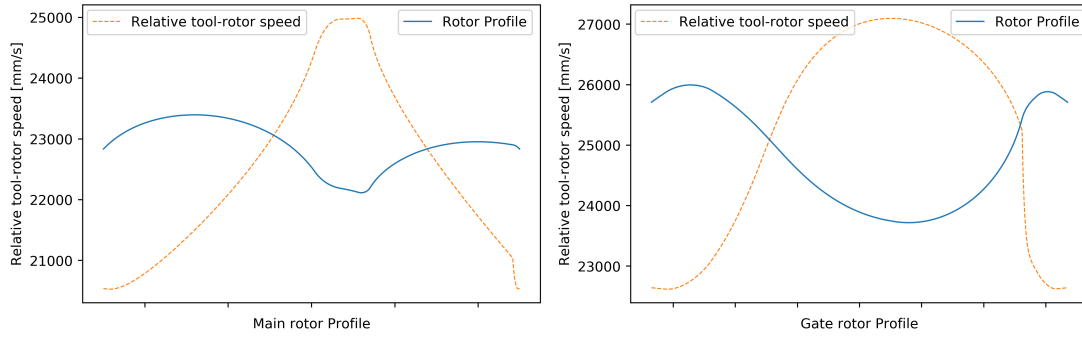
Putting Equations 6.3 in 6.2 and 6.5 in 6.4, 6.1 can be computed as in Equation 6.6.

$$\vec{V}_{rel} = \omega_t \begin{bmatrix} y_h(i - \cos \Sigma) - z_h \sin \Sigma \\ -x_h(i - \cos \Sigma) - C \cos \Sigma \\ -x_h \sin \Sigma + C \sin \Sigma - p i \end{bmatrix} \quad (6.6)$$

where  $i = \frac{\omega_r}{\omega_t}$ .

This expression for the relative velocity between tool and rotor at each point along the meshing line can be used to evaluate relative speeds (magnitude of relative velocity). With an appropriate normalization, it can then be used along with relative tool wear term  $TW_{rel}$  for tool wear estimation along the profiles. The relative speed at each profile coordinate is plotted over the main rotor profile in Figures 6.1. It can be noticed that the points near the root of the main rotor and gate rotor profiles have higher tool-rotor relative speeds. This would affect the points near these regions to have relatively higher

wear compared to those toward tips of the profiles.



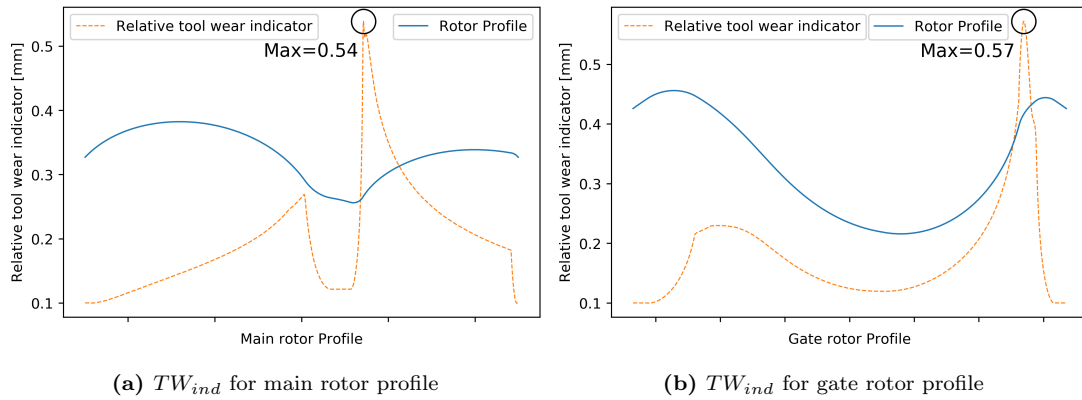
(a) Relative speeds between main rotor and its tool represented across the rotor profile coordinates (b) Relative speeds between gate rotor and its tool represented across the rotor profile coordinates

**Figure 6.1:** Relative speeds between benchmark N-Profile rotors and their respective tools with setting  $\Sigma=45^\circ$ ,  $C=200$  mm,  $\omega_t=1500$  rpm,  $\omega_r=15$  rpm

Assuming the tool wear to be linearly affected by relative speeds, normalization can be done with respect to the minimum relative speed across the profile. Hence a profile point which would have  $x$  times higher relative speed than the minimum relative speed, would be prone to having  $x$  times more tool wear on top of the relative tool wear measure  $TW_{rel}$ . The relative tool wear term hence can be modified to include the effect of relative speeds across the profile in the following way (Equation 6.7). The updated term could be simply called tool wear indicator  $TW_{ind}$ .

$$TW_{ind} = TW_{rel} \frac{\|\vec{V}_{rel}\|}{\min(\|\vec{V}_{rel}\|)} \quad (6.7)$$

The tool wear indicator calculated and plotted across the benchmark N-Profile is presented in Figure 6.2. It makes it clear that the sharper corners of profile and the profile parts having higher relative speeds w.r.t tool turn out to have a higher value of  $TW_{ind}$ . This framework has been applied to profiles developed in this study to evaluate their manufacturability in a relative sense.



(a)  $TW_{ind}$  for main rotor profile

(b)  $TW_{ind}$  for gate rotor profile

**Figure 6.2:** Relative tool wear indicators ( $TW_{ind}$ , Equation 6.7) for benchmark N-Profile rotors with  $\delta=0.1$  mm, represented across the rotor profile coordinates

The relative tool wear ( $TW_{rel}$ ) if plotted across the profile, which does not account

for the effect of relative velocity, the result is as indicated in Figure 6.3.

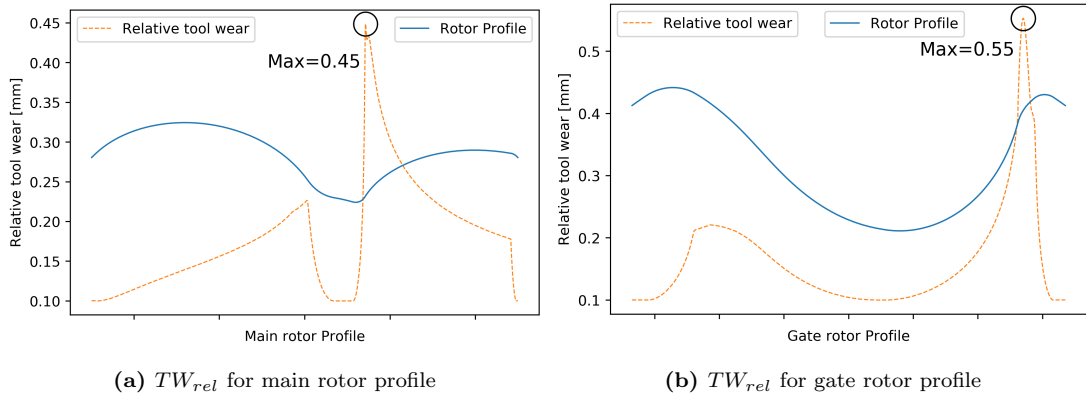


**Figure 6.3:** Relative tool wear ( $TW_{rel}$ ) for benchmark N-Profile rotors with  $\delta=0.1$  mm, represented across the rotor profile coordinates

The difference between maximum values of  $TW_{rel}$  and  $TW_{ind}$  for the same profile make it obvious that if the effect of relative velocity is considered in manufacturability, it entails that the male rotor root radius should wear at least 20% more compared to its tip than that predicted by the model proposed by Stosic (2006b). There could be a way to validate this experimentally by observing a batch of rotors being manufactured. This validation was not done during this study. Hence little can be said firmly about the correctness of the assumption of adding the effect of relative tool-rotor velocity in the manufacturability study. However, from the literature on grinding technology such as Malkin and Guo (2008), it can be claimed that the relative velocity between the tool and piece affects grinding rate in conjunction with the feed rate. The relative velocity is a way estimate the velocity of the material being removed from the piece after being chipped off. Refer Chapter 3 of this book for more details on this.

But when it comes to comparing the manufacturability of two profiles through relative tool wear ( $TW_{rel}$ ), the comparison with or without the relative velocity consideration has only a minor difference. That is, comparison of two profiles based on either  $TW_{rel}$  or  $TW_{ind}$  will hardly affect the conclusion of a comparison. This is because the normalizing factor in Equation 6.7 is almost similar for all kinds of profiles being compared in this study. It depends primarily on the relative velocity distribution across profile which is shown in Figure 6.1. Since this changes only slightly for the optimized profiles, the normalizing factor affects all the profiles more or less equally. Hence the use of any factor  $TW_{rel}$  or  $TW_{ind}$  for comparing the manufacturability of two profiles hardly leads to a different conclusion. For this study,  $TW_{ind}$  has been preferred to compare manufacturability of various profiles developed during this study.

### 6.3 Manufacturability of Developed Profiles

The quantification of manufacturability in terms relative tool wear indicator calculated across the rotor profile or tool profile is demonstrated to be possible. The results presented for the manufacturability of benchmark N-Profile are consistent with the

known and qualitative facts about manufacturability such as higher tool wear indicator value near sharper corners and at regions of high tool-rotor relative speed as well as higher cutting angle. The same framework is hence applied in this section to evaluate manufacturability of the profiles developed in this study. These include homotopy profiles from fourth chapter as well as the K-BETA profiles from fifth chapter.

Special emphasis is put on homotopy profiles that modified gate rotor tips to reduce blow hole but used homotopy at the same time to flatten the tips to reduce their curvature for practical reasons. These fine changes in design can be evaluated numerically with the framework developed in this chapter. Usually, the plots similar to Figure 6.2 can be generated for different profiles and the point of maximum relative tool wear indicator value can be compared to judge if manufacturability is improved or reduced relatively and also by how much. The point of maximum relative tool wear value is more logical to compare instead of the average across all points since the frequency of redressing cycles for the tool are governed by the point that wears most and not by the average wear across the profile.

### 6.3.1 Comparison of H-Rack Profiles and N-Profile

The H-Rack profiles from section 4.3.1 which replace curve  $A - B$  on N-Rack with a homotopy between hyperbola and parabola does not likely fall in the region which affects manufacturability much. In this design, the more wear prone regions of the profile such as tips were unchanged. Hence manufacturability is not supposed to be affected much. The relative tool wear indicator diagrams for H-Rack profile from Figure 4.6 are presented in Figure 6.4.

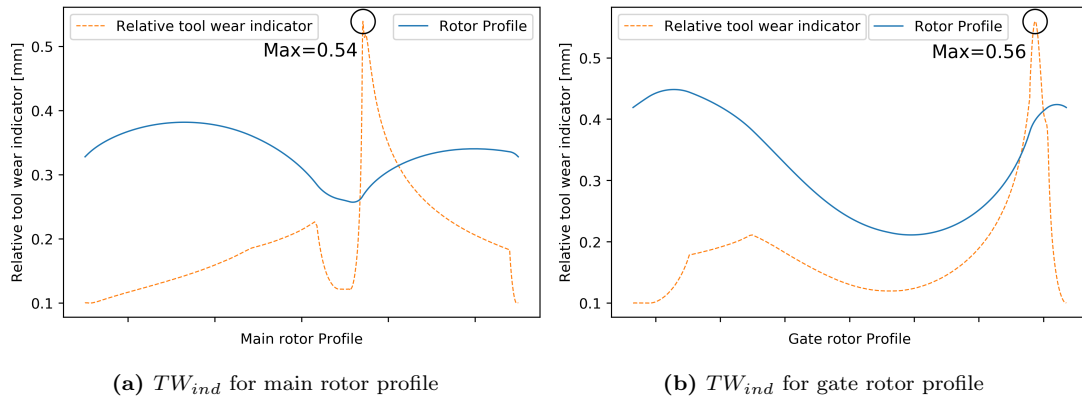


**Figure 6.4:** Relative tool wear indicators ( $TW_{ind}$ , Equation 6.7) for homotopy profile (Figure 4.6) with  $\delta=0.1$  mm, represented across the rotor profile coordinates

It can be observed that the maximum relative tool wear indicator values for N-Profile and H-Profile remain same, 0.54 mm and 0.56/0.57 mm. However, due to the different curves along the long edge of rack, there is a small difference to be observed in relative tool wear characteristics on the long edges of the lobes. Comparing the tool wear at other radius root of main rotor in Figures 6.4a and 6.2a makes this obvious. The value of  $TW_{ind}$  at these peaks are 0.225 mm and 0.275 mm respectively. This indicates that though there are some minor changes, practically (in terms of

the maximum value of the indicator) this H-Profile is equally manufacturable as the benchmark N-Profile.

The other H-Profiles from section 4.3.2 which specifically modified tips of the N-Rack using homotopy between ellipse and line are much more likely to have direct impact on manufacturability. To recall the arguments in section 4.3.2, it was observed that reducing the radius of N-Rack tip circle  $E-F$  reduces blow hole area significantly (Figure 4.7) and this can lead to improvement in adiabatic efficiency by  $\sim 0.5\%$  if the interlobe clearances are small. However such sharpening of the tip was known to cause practical problems in manufacturing and inspection of the profiles. With the quantitative framework to evaluate manufacturability, the relative tool wear indicator diagram for the sharp tip N-Profile (1.5 mm radius of  $E-F$  against 2.5 mm in the benchmark profile) is presented in the Figure 6.5.

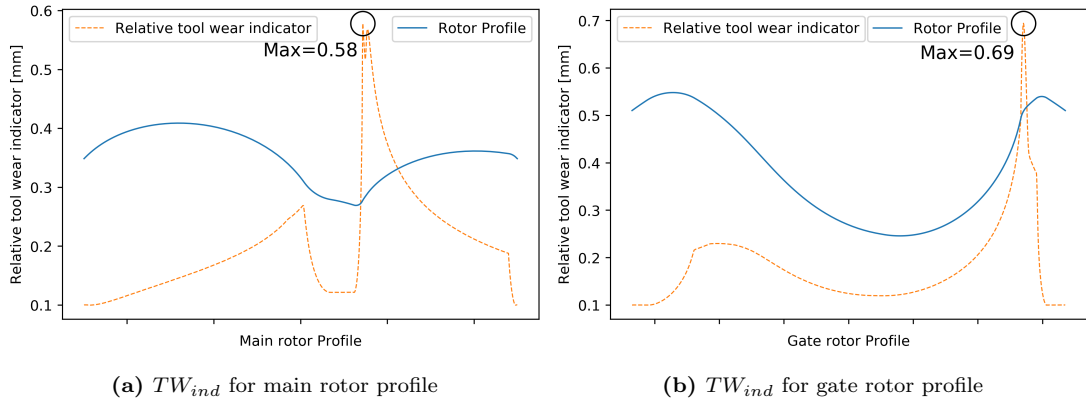


**Figure 6.5:** Relative tool wear indicators ( $TW_{ind}$ , Equation 6.7) for N-Profile with radius of  $E-F$  1.5 mm (Figure 4.7) with  $\delta=0.1$  mm, represented across the rotor profile coordinates

Comparing the maximum values of relative tool wear index from Figure 6.5 and Figure 6.2 which are both N-Profiles but with different radii of tip  $E-F$ , it is observed that the maximum  $TW_{ind}$  values went up from 0.54 mm to 0.58 mm for main rotor and 0.57 mm to 0.69 mm for gate rotor. This is a compromise of 7.4% and 21% in manufacturability of main and gate rotor respectively on account of the sharpening of the tip by 1 mm.

In order to work around this impact on manufacturability while trying to keep the benefit of performance, homotopy between an ellipse and a line was implemented at the  $E-F$ . In Figures 4.10 and 4.11, it was visually demonstrated that the homotopy could reduce the blow hole while maintaining a flatter tip. This effect can be quantitatively demonstrated and proved with the relative tool wear index. The relative tool wear indicator diagram for the H-Profile with a homotopy at  $E-F$  is presented in Figure 6.6.

Since the homotopy was used in such a way that the radius of curvature at the tip after flattening was brought down to the same levels as the benchmark profile (2.5 mm), results in Figure 6.6 confirm that the manufacturability is also maintained at the level of benchmark profile. The main and gate rotor maximum relative tool wear indices for H-Profile are almost same as that of the benchmark N-Profile (Figure 6.2) 0.53/0.54

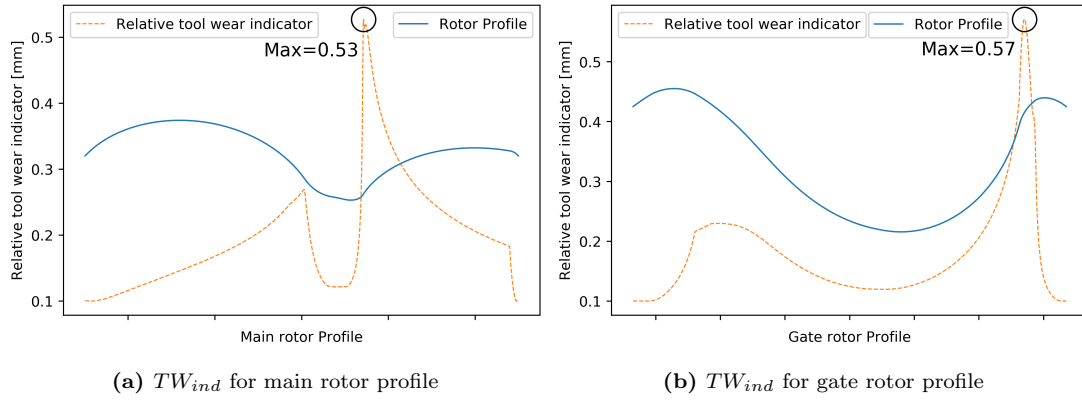


**Figure 6.6:** Relative tool wear indicators ( $TW_{ind}$ , Equation 6.7) for H-Profile with homotopy at  $E - F$  (Figure 4.10) with  $\delta=0.1$  mm, represented across the rotor profile coordinates

mm and 0.57 mm; while preserving the performance improvement of 0.29-0.56% (Table 4.12).

### 6.3.2 Comparison of K-BETA Profiles and N-Profile

Out of the three K-BETA profiles discussed in the last chapter, only K-BETA1 turned out to be beneficial in terms of the energy efficiency. It has a peculiar feature of inclined gate rotor top land which modifies the curvature of gate rotor tips. This modification is expected to affect the manufacturability to some extent and the framework developed hereby may be applied to know that. Since the other two K-BETA profiles did not have any performance advantage, their manufacturability is not discussed.

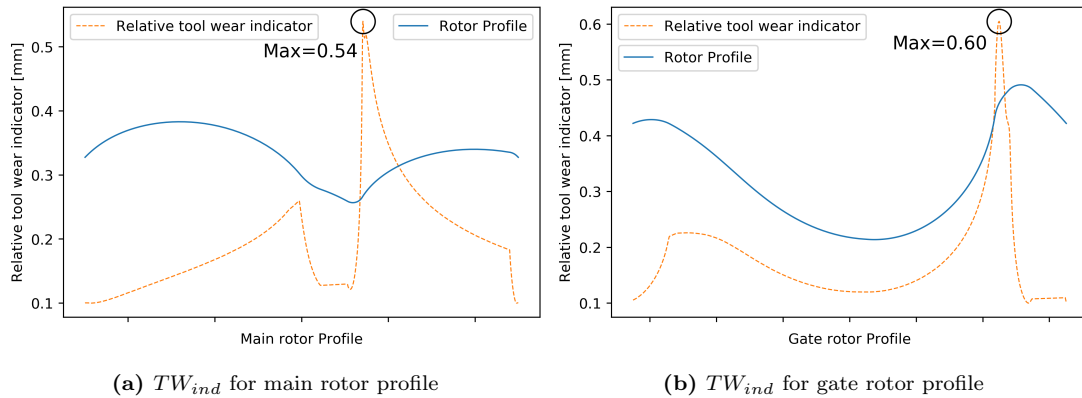


**Figure 6.7:** Relative tool wear indicators ( $TW_{ind}$ , Equation 6.7) for K-BETA1 profile (Figure 5.3) with  $\delta=0.1$  mm, represented across the rotor profile coordinates

In Figure 6.7, the relative tool wear indicator diagrams for the K-BETA1 main and gate rotors are presented. The manufacturability of main rotor is almost same as that of the benchmark N-Profile (0.54 mm maximum  $TW_{ind}$ ). But the manufacturability of gate rotor, as anticipated, dropped by almost 5.3% (maximum  $TW_{ind}$  increased from 0.57 mm to 0.60 mm) due to the increased curvature as an effect of the inclined tip.

## 6.4 Summary

The relative tool wear model by Stosic (2006b) has been adopted with additional considerations to relative speed between tool and rotor to quantify manufacturability of rotor profiles. This tool wear index can be evaluated for various rotor profiles and in this chapter, it has been used to compare manufacturability of the more energy efficient profiles designed in this study such as H-Rack profiles from Chapter 4 and K-BETA profiles from Chapter 5 with benchmark N-Profile.

Generally, it is observed that the the tool wear is maximum at main rotor root and gate rotor tips where radii of curvature on the profile are small as well as tool-rotor relative speed is high. A case has been made that by comparing the maximum values of tool wear index across the profiles, their manufacturability can be compared quantitatively.

Following this line of argument, H-Rack profile wherein homotopy was used to minimise blow hole while trying to curb the minimum radius of curvature on the profile was shown to have similar tool wear index as that of benchmark N-Profile.

The K-BETA1 profile however had to make a trade-off in manufacturability on account of increased curvature at the gate rotor tip due to inclination. Though this reduction in drag loss led to up to 0.8% saving in shaft power consumption, it was calculated to increase relative tool wear index by 5.3% which is a compromise in manufacturability of this profile.



## Chapter 7

# Conclusions and Future Scope

ALL the improvements in developed profiles are summed up to demonstrate the cumulative gain in energy efficiency that is achieved along with some trade-off in manufacturability. The two key ideas that drove this development were homotopy and reduction of oil drag through tip designs. Each feature of the new profile has been studied and presented individually as well as evaluated in isolation throughout the course of this thesis. Put together, the new profile is capable of 1.5 to 2.5% improvement in energy efficiency at a minimal compromise in manufacturability (5% in terms of relative tool wear index). Along with the summary of key contributions of this study, future scope of the research and development of newer and more efficient rotor profiles has been discussed.

### Contents

7.1	Total Improvements in the New Profile . . . . .	114
7.2	Contributions of this Study . . . . .	117
7.3	Future Scope . . . . .	118

## 7.1 Total Improvements in the New Profile

This section presents both the summary of this study and its conclusions in terms of tangible and real improvements in energy efficiency achieved with the new profile development. Since it stands the key objective of this study, the total gains in energy efficiency against trade-off in manufacturability (quantified with with a modified scale devised in this study) are believed to be the net outcome of this study.

The H-Rack modifications consisted of deploying homotopy at two regions on N-Rack;  $\mathcal{H}(\textit{Hyperbola}, \textit{Parabola})$  on the long edge of rack and  $\mathcal{H}(\textit{Ellipse}, \textit{Line})$  on the high pressure side tip. Each modification led to improvements in adiabatic efficiency (Table 4.6 and 4.8) of about  $\sim 0.5\%$  each given that the suitable operating conditions for the profiles are maintained (such as smaller interlobe clearances, avoiding over-flooding of oil and lower speeds of operation). Independent of the H-Rack features, K-BETA1 profile which had a inclined gate rotor top land was experimentally shown to have 0.8% lower shaft power on account of lower oil drag compared to the flat gate rotor top land profile (Table 5.1).

Combining these three features into one rack profile which would be based on N-Rack is presented in the Figure 7.1, which could be referred to as the ‘Kirloskar Profile’ or ‘K-Profile’. The representation in Figure 7.1 is not drawn to scale but it indicates all minute details of the rack such as-

- $A - B$  is a homotopy between hyperbola and parabola (Figure 4.12)
- $G - H$  is a homotopy between ellipse and line (Figure 4.13)
- $F - D$  is an inclined straight line which creates the inclined gate rotor top land (Figure 5.6)
- $F - G$  is a small vertical straight line of width  $c$  added between the inclination  $F - D$  following it, to improve the manufacturability
- The rest of the details are same as that of N-Rack

The K-Profile can be evaluated in SCORPATH or SCORG along with the benchmark N-Profile at various operating conditions to see what are the total improvements in terms of energy efficiency. Similar to all the previous comparisons in this study, it has been evaluated for an oil injected air application. The effect of oil drag loss saving due to tip modification is however derived from the experimental results and work of Abdan (2023). That additional saving in shaft power is added to the advantage of K-Profile at different speeds and pressures, whose relationships with oil drag are explored in depth in the works of Abdan (2023).

For example, it was measured experimentally that the K-BETA1 modification leads to 0.8% saving in shaft power at 38 m/s main rotor tip speed. And it known that the relationship of the oil drag is close to linear with the speed whereas it changes little with discharge pressure. Hence at half the speed (19 m/s main rotor tip speed), the saving in shaft power is assumed to be half of 0.8%, i.e., 0.4%. The comparison of

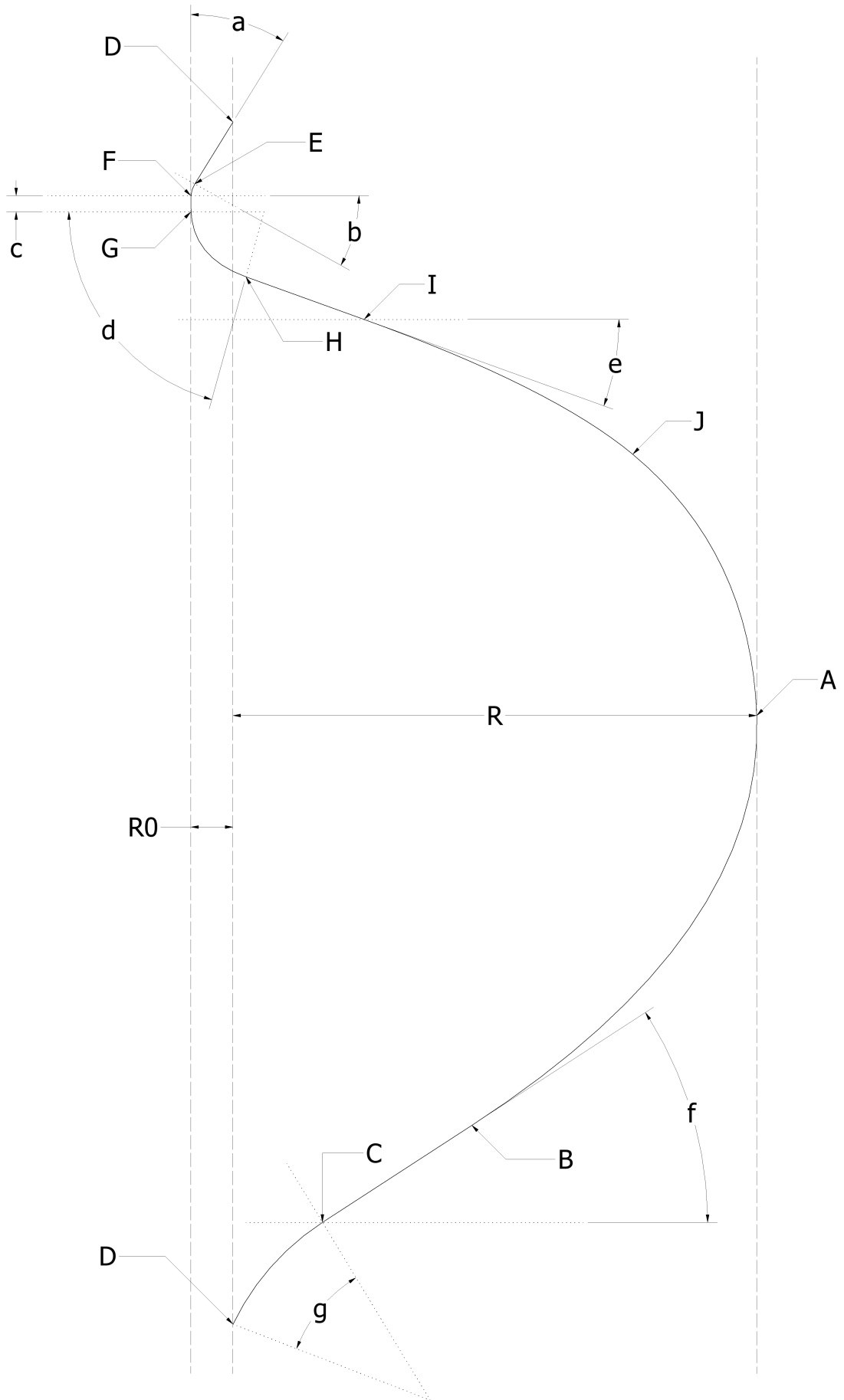


Figure 7.1: The complete K-Rack (H-Rack plus K-BETA1 features) sketch

adiabatic efficiencies of benchmark N-profile and retrofitted K-Profile is presented in Tables 7.1, 7.2 and 7.3 for three different pressure ratios- low, medium and high.

Main rotor tip speed	Adiabatic efficiency of N-Profile	Adiabatic efficiency of K-Profile	% Improvement
18 m/s	80.4 %	82.0 %	1.6 %
26 m/s	83.0 %	84.4 %	1.4 %
34 m/s	82.6 %	83.9 %	1.3 %
42 m/s	80.8 %	82.2 %	1.4 %

**Table 7.1:** Adiabatic efficiencies of K-Profile in comparison to the retrofitted benchmark N-Profile; 1 bar suction and 6.5 bar discharge with internal clearances set to 35 micron

Main rotor tip speed	Adiabatic efficiency of N-Profile	Adiabatic efficiency of K-Profile	% Improvement
18 m/s	78.3 %	80.2 %	1.9 %
26 m/s	82.3 %	83.8 %	1.5 %
34 m/s	82.8 %	84.2 %	1.4 %
42 m/s	81.6 %	83.1 %	1.5 %

**Table 7.2:** Adiabatic efficiencies of K-Profile in comparison to the retrofitted benchmark N-Profile; 1 bar suction and 8.5 bar discharge with internal clearances set to 35 micron

Main rotor tip speed	Adiabatic efficiency of N-Profile	Adiabatic efficiency of K-Profile	% Improvement
18 m/s	67.7 %	69.9 %	2.2 %
26 m/s	74.2 %	75.9 %	1.7 %
34 m/s	76.3 %	77.9 %	1.6 %
42 m/s	76.5 %	78.2 %	1.7 %

**Table 7.3:** Adiabatic efficiencies of K-Profile in comparison to the retrofitted benchmark N-Profile; 1 bar suction and 14.5 bar discharge with internal clearances set to 35 micron

The K-Profile behaves same as N-Profile in its characteristics across speed and pressure ratios. Profile's adiabatic efficiency deteriorates at higher pressure ratios and it forms a sort of inverted U-curve w.r.t. speed. Both these characteristics are similar for N and K-Profile. However, adiabatic efficiency of K-Profile deteriorates less with pressure especially at lower speeds. Notice 2.2% improvement at 14.5 pressure ratio versus 1.6% improvement at 6.5 pressure ratio.

At the point of optimum adiabatic efficiency which is around  $\sim 30$  m/s for 8.5 pressure ratio, the K-Profile is 1.5% more energy efficient than N-Profile. Along with these comparisons, it is also to be noticed in which operating conditions should the compressor be run to maximally utilize the profile advantages. Across all pressures, the improvements are always better at lower speeds. This indicates that the features of K-Profile tend to be more advantageous at lower speeds than at higher speeds.

On the other hand, the inclination feature of gate rotor tends to be more advantageous at higher speeds of operation since oil drag is simply more dominant at high

speeds. For example, at 8.5 pressure ratio (see Table 7.2) the difference between adiabatic efficiency at main rotor speeds 18 m/s and 42 m/s is 3.3% and 2.9% for N-Profile and K-Profile respectively. So in a way, K-Profile allows for wide range of operation with lesser deterioration of adiabatic efficiency than N-Profile. This is a beneficial feature when manufacturers wish to cater wide range of operating speeds with economical (smaller) sizes of compressors. In these cases, tip speeds of the rotors tend to be high.

The features of homotopy at the tip which helps reduce blow-hole area without compromising manufacturability too much, is only advantageous when the interlobe clearances are small. Hence, to take advantage of this feature of K-Profile, trying to achieve as small as practically possible interlobe clearance is recommended. While homotopy helped mitigate impact on manufacturability due to this feature, some of it is definitely compromised with the inclination feature. As discussed in the last chapter, this impact is mainly on gate rotor and the increased curvature leads to 5.3% increase in maximum relative tool wear indicator value for the K-Profile. Hence, this is a trade-off in manufacturability for the gain in energy efficiency.

## 7.2 Contributions of this Study

This study has achieved the goal of improving state of the art rotor profiles by adopting an interdisciplinary approach to draw in an useful concept from pure mathematics. The idea of homotopy has already found applications outside topology such as in solving non-linear differential equations (Liao, 2004) and computer graphics (Dym et al., 2015). The concept of homotopy is simple yet powerful and found to be not only suitable but rewarding for use in profiling through this research. The improvements in profiles achieved from it are already presented here but it has a far reaching potential for applications in mechanical engineering wherein general shape optimization problems are involved. This study may serve as such an opening for further research possibilities and innovations in engineering using homotopy. Author considers this as a key contribution to science from this study.

In terms of the more specific subject of this endeavor, rotor profiling, a total 1.5-2.5% improvement in energy efficiency (which is  $\sim$ 8-12% reduction in inefficiency) has been achieved at the pre-determined operating range and conditions for a typical screw compressor. In spite of the variation in these conditions, the methods and know-how developed hereby are believed to be robust enough to generate at least 1-2% advantage over the state of the art rotor profiles. This advantage is directly reflected in lesser carbon footprint of the machines as well as more business opportunities for the sponsors of this study. Author believes this to be one of the key contribution to engineering from this study.

On a more technical note, the quantification of manufacturability in terms of relative tool wear with considerations to relative speeds between tool and rotor used not only to evaluate manufacturability of various profile designs but also to trigger fine tuning of certain profile features can also be considered as a key contribution of this study.

The experimental study of relationship between certain profile characteristics such

as displacement and sealing line length along with certain operational characteristics such as oil drag and noise (due to bad torque characteristics) explored in this study helped not only to corroborate certain already known facts but also to validate more precise methods of oil drag calculation in screw machines.

Some such methods and approaches were also explored in the course of this study, which did not prove to be very useful in the scope of this study; but they open up new and exciting opportunities for the future studies in rotor profiling. These have been carefully placed in two appendices of this thesis. They too are in part key contributions of this study whose full potentials may be revealed only in the future studies.

### 7.3 Future Scope

From this study onward, there are few more regions of rack which may benefit from application of homotopic curves. One of them is the main rotor tip which is a conjugate of curve  $J - A$  on K-Rack and curve  $H - A$  on the N-Rack. This particular curve affects the blow-hole area similar to and in association with the high pressure side rack tip  $E - F$  in N-Rack and  $G - H$  in K-Rack. It has already been demonstrated in this study how the  $G - H$  on K-Rack has benefited from application of homotopic curves. Hence, same can be done for the main rotor tip.

Another important finding of this study has been that the impact of profile modifications on improvements is highly dependent on the working and operational conditions. Hence, it is learned that a good profile design is driven by consideration of factors such as what clearances can be achieved in the machine, what is going to be the speed of operation, what is the quantity of oil in the system, etc. If anything, deeper understanding of the physics of compression process in screw machines and capability to model the impact of even the smallest phenomena in the chamber would lead to better profile designs. Hence improvements in profiles are linked to these developments too which are likely to come in future.

The two appendices allude to two potentially useful approaches to further improve rotor profiles. These are outcomes of this study but not pursued because of the limits on scope and timeline. The first appendix builds a formalism for strictly analytical approach to finding best suited curves at certain parts of the profile. This is also termed as the ‘Euler-Lagrange approach to optimization’ or the ‘optimization in function spaces’, which are methods from variational calculus applied to rotor profiling. The challenge however with this approach is that the differential equations that arise as a result of this formulation are highly non-linear and exotic in nature. They can not directly be solved by any generally known analytical, semi-analytical or numerical method. But it holds a promise to mathematically reveal the best possible curve for certain region of the rack. A further work on formulating this approach in a more solution friendly way or exploration of techniques to solve such highly complex differential equations may lead to development of better profiles.

The second appendix explores potential application of artificial intelligence in rotor profiling. There has been a pilot study of the feasibility of this approach during the

course of this study which is presented in this appendix. In its most basic form, neural networks can be trained to predict the energy efficiency of rotor profiles given inputs such as a few geometric inputs. These trained networks can be used to boost the speed of profile optimization algorithms since neural networks are much faster than the physics based solvers of profile performance. However, neural networks are highly dependable on their training on large datasets which themselves are time consuming to generate if good enough accuracy of predictions is desired. Also the neural networks only mimic the physics of the process based on vast data so it requires careful consideration to make sense of its results. Hence in its current form, the data set scaling and accuracy are major challenges to this approach. If these are addressed in near future, the ‘machine intelligence’ hence developed may also be used backwards for generating profiles with desired energy efficiency and other criteria such as manufacturability.



## Appendix A

# Euler-Lagrange Approach to Profile Optimization

A strictly analytical approach to find equations of the optimal curves for profiles was attempted to explore. This approach of optimisation in function spaces is based on a purely geometric premise that the best shape of rotors will crudely maximize the inter-teeth volume and minimize the leakage paths. Since both of these are functions of the curves chosen to make up the profile, one can see it as a problem of mapping real valued functions, which are equations of the chosen shapes, to real numbers which are the amount of volume and leakage area calculated for the particular profile.

The approach of optimization in the function spaces (Sasane, 2016) is a mathematical answer to exactly this kind of problems. It involves setting up the objective functions such as inter-teeth volume and sealing line length in terms of the analytical profile curve equation  $f(x)$  and then writing an Euler-Lagrange equation which is a differential equation; solution of which will give a function  $f(x)$  that minimizes the objective function. If successfully applied, there is a possibility to get theoretically the best possible trade-off of the competing profile features such as sealing line length-displacement or sealing line length-blowhole area. This is a purely analytical approach in a sense that it works with a map between all possible curves between two points and the numerical properties associated with it.

Obviously, the rack coordinate system was chosen to formulate this approach as it is in this coordinate system that all the transformations are more neat than others. This feature is supposed to make the formulation of this approach more likely to be solvable. Hence, assuming the definition of a curve  $y = f(x)$  between two points  $A$  and  $B$  on the rack, the solution to meshing condition (rack to rotor) in terms of the function  $f(x)$  is given as-

$$\theta(x, f(x), f'(x)) = \frac{r - x + f(x)f'(x)}{rf'(x)} \quad (\text{A.1})$$

where  $r$  is the pitch radius of the rotor and  $f'(x)$  is a derivative of the function  $f(x)$ .

The transformed curve equation on the rotor  $(x_1, y_1)$  written in terms of the function

$f(x)$  and the meshing condition  $\theta$  is as follows-

$$\begin{aligned}x_1(x, f(x), f'(x)) &= x \cos(\theta) - (f(x) - r\theta) \sin(\theta) \\y_1(x, f(x), f'(x)) &= x \sin(\theta) + (f(x) - r\theta) \cos(\theta)\end{aligned}\tag{A.2}$$

Similarly, a transformation can be written for pairing rotor  $(x_2, y_2)$  as a function of  $f(x)$ . Now the objective functions such as inter-teeth area and sealing line length can be written as some form of integrals of these curves  $(x_1, y_1)$  and  $(x_2, y_2)$ . Inter-teeth area is simply the area under these curves and the sealing line length is a arc length of the sealing line which is generated by rotational transformation of the transformed curves. Hence, the objective function of area ( $O_A$ ) can be written as-

$$\begin{aligned}O_A = \int_{x_A}^{x_B} &\left[ \sin \theta \cos \theta \left( x - 2xf(x) \frac{d\theta}{dx} + xr\theta \frac{d\theta}{dx} - f(x)f'(x) + rf(x) \frac{d\theta}{dx} \right) \right. \\&+ \cos^2 \theta \left( f(x) - f(x)^2 \frac{d\theta}{dx} + 2f(x)r\theta \frac{d\theta}{dx} - r\theta - r^2\theta^2 \frac{d\theta}{dx} \right) \\&\left. + \sin^2 \theta \left( -x^2 \frac{d\theta}{dx} - xf'(x) + xr \frac{d\theta}{dx} \right) \right] dx\end{aligned}\tag{A.3}$$

and the objective function for sealing line length ( $O_L$ ) can be written as-

$$O_L = \int_{x_A}^{x_B} \left[ 1 + \left( -r \frac{d\theta}{dx} + \frac{df(x)}{dx} \right)^2 \right] dx\tag{A.4}$$

The  $\theta$  or  $\frac{d\theta}{dx}$  terms in objective function expressions haven't been substituted because that makes the equations very lengthy to look at. But it must be noted that  $\theta$  and  $\frac{d\theta}{dx}$  are also functions of  $x$ ,  $f(x)$  &  $f'(x)$ . And the term  $\frac{d\theta}{dx}$  is as follows-

$$\frac{d\theta}{dx} = \frac{f(x)f''(x) + f''(x)^2 - 1}{rf'(x)} - \frac{(r - x + f(x)f'(x))f''(x)}{rf''(x)^2}\tag{A.5}$$

Based on these objective functions which are basically integrals and their integrands being functions of  $x$ ,  $f(x)$  &  $f'(x)$ , theoretically, the Euler-Lagrange equation can be applied to them. Given an objective function  $O$  in the form of an integral-

$$O = \int_A^B \mathcal{L}(x, f(x), f'(x)) dx\tag{A.6}$$

the Euler-Lagrange equation for minimizing  $O$  is given as-

$$\frac{\partial \mathcal{L}}{\partial f} - \frac{d}{dx} \frac{\partial \mathcal{L}}{\partial f'} = 0\tag{A.7}$$

What's interesting here is that the Euler-Lagrange equations can be written for integrands in objective functions in Equations A.3 & A.4; but they turn out to be very complicated and long to be handled easily. In fact, the resulting second order differential equations have some exotic terms which have differentials as arguments of the trigonometric functions. This makes these differential equations non-linear in

nature and most probably insolvable by any analytical method. More so, I doubt these exotic non linear differential equations will be readily solvable by any commonly known numerical method as well.

An alternative formulation of the transformation and meshing condition through a change of coordinate system that preserves the input curve equation as they are without adding trigonometric or any other non-linear operators in the evaluation leading to objective function may give some hope to solve the resulting Euler-Lagrange equation. But this seems unlikely at the first glance and may require a more rigorous pursuit of this approach. Some efforts to review methods for solving such highly non-linear and complex differential equations numerically may also turn out to be beneficial.



## Appendix B

# Application of Artificial Intelligence in Rotor Profiling

Artificial Intelligence (AI) is emerging as promising tool for advancements in state of the art design and optimization techniques. Twin screw compressor technology is matured in all aspects of design and manufacturing. But the potential application of AI or Machine Learning (ML) has not yet been explored in this domain. This study has attempted at training an Artificial Neural Network (ANN), which is a class of AI/ML techniques, to predict the energy efficiencies of twin screw compressors for different rotor profile shapes. Neural networks are capable of learning from data to identify complex or non-linear underlying patterns between inputs and outputs arising from the physics of the process. Such a capability can be useful in many ways such as designing robust design and optimization frameworks, automating parts of the design process flows and getting deeper insights into the physics of compression process.

Starting with a limited scope, the N-Profile was chosen as the profile system to generate multiple retrofitted profiles by varying only five profile curve parameters. Generally, the energy efficiency of a screw compressor with a certain rotor profile is calculated by solving the chamber model which is a thermodynamic simulation (Hanjalic and Stosic, 1997) of the compression process. The SCORPATH thermodynamic solver (Stosic, 1993) was used in this study to calculate the effect of different profile shapes on specific power which is a measure of compressor's energy efficiency. It is one of the quickest and versatile chamber models, hence used to most effectively generate vast data-sets required for the training of ANN.

This study attempted to check if an ANN can be successfully trained with large enough data of different profiles and their respective energy efficiencies to capture the physics of the compression process and predict the energy efficiencies for given profiles with reasonable accuracy. It has been found that the ANN is able to learn the pattern associated with profile shapes and their energy efficiency to a fair degree. But increasingly large data-sets are required for training the ANN to achieve a higher accuracy of prediction. This work stands as a pilot study to explore further possibilities for use of these techniques in rotor profiling and/or screw compressor design and optimization.

Machine learning algorithms and their application is a vast topic on its own. Setting

up an ANN for certain task has 3 steps- data generation, training and testing. Choice of a right training algorithm, choosing just the right size of the data-set for training, fine-tuning of the model itself, etc. require an in depth technical attention and analysis. For the purpose of this pilot study, the most commonly used ANN training algorithm and training model parameters were chosen from literature. A comprehensive analysis of the nuances of training the model and their effect on performance of the model were simply out of the scope of this study.

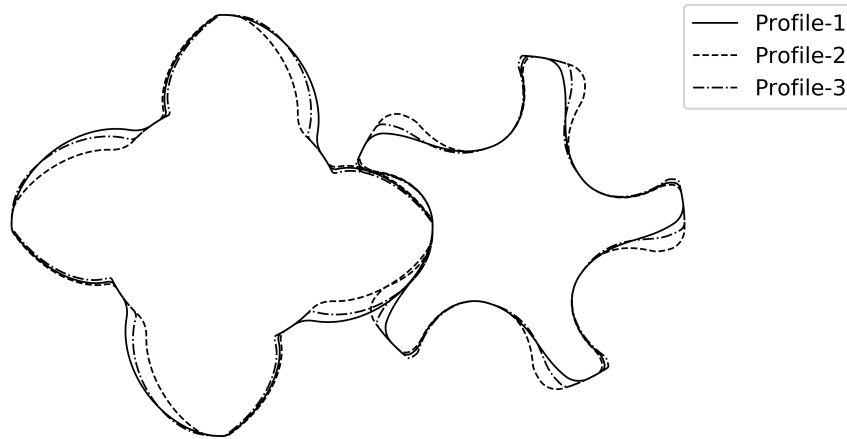


**Figure B.1:** Three retrofitted 4/5 N-Profiles with different set of profile input parameters ( $R1$ ,  $R2$ ,  $R3$ ,  $R4$  &  $n$ )

For data generation, 5 N-Profile inputs -  $R1$ ,  $R2$ ,  $R3$ ,  $R4$  &  $n$  were varied by fixing the lobe combination, center distance as well as main and gate rotor addendum. The 3-D characteristics of rotors such as length, wrap angle and other design parameters such as port positions are also not varied. For the purpose of thermodynamic evaluation of a screw compressor, additional inputs are required such as speed of the rotors, pressure ratio, inlet temperature, oil injection parameters, etc. These inputs too are kept constant for all the profiles. Hence this ANN was tasked to predict the energy efficiency for different screw compressor rotors with no change except their rotor profile shape in the end plane. Figure B.1 depicts an example of different profile shapes generated in end plane of rotors with same inner and outer diameters as well as rest of the design and operational parameters. Such are the different profiles for which the ANN was tasked to predict the energy efficiencies.

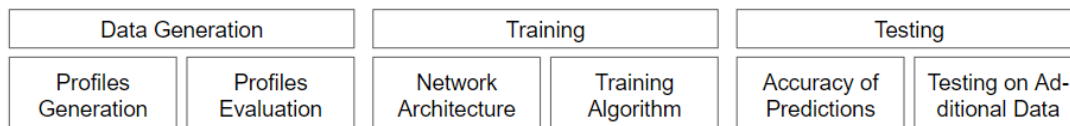


**Figure B.2:** The general framework and steps of setting up an artificial neural network model

For training an ANN, a huge data-set is required. The size of this data-set should be enough to capture as many variations in shapes of the profiles as possible for the ANN to be better at predicting specific powers for a wide range of shapes. For this, a

reasonable range of each input parameter was decided through experience with rotor profile generation. In these five ranges for five input parameters, 8 to 10 uniformly spaced values of each parameter were picked. For every possible combination of these 8 to 10 values for 5 different input parameters, a total of  $\sim 50000$  N-Profiles were designed using a computer code. Not all of these 50000 profiles were valid, since for some combinations of these parameters reversals or non-tangency at nodes may arise in profiles. Such invalid profiles were filtered out using a computer code that automatically checks for reversals and other discrepancies in the generated profiles. Upon these rejections, a data-set of  $\sim 30000$  valid profiles was fed to SCORPATH's chamber model with the same operating conditions for all profiles. The resulting specific powers for each profile were saved against respective set of input parameters. This pretty much completes the data generation part for setting up the ANN model.

The neural networks are inspired by the way neurons fire in a human brain during any neurological activity. Interested readers are advised to refer standard texts on these techniques such as (Géron, 2019) for more details. A neuron in the context of an ANN is a node which can take on numerical values. A typical ANN consists of multiple interconnected layers of neurons which are individually fired or not fired based on the associated activation function with the network. During training process, based on the training data, a training algorithm tries to find the set of weights and biases for each neuron and its connections such that the error between target value (fed with the training data) and the neural network prediction is minimized. This is an iterative process and a good quality of data ensures good training of the model.

The ANN developed for the purpose of predicting specific powers for the rotor profiles has an input layer with five neurons which take on the values of the five input parameters. There is only one hidden layer with ten neurons fully connected to the input layer. And finally there is a single output neuron which is specific power (a measure of energy efficiency). In case of more number of input parameters or inclusion of non-geometric parameters in optimization (such as speed of rotors, pressure ratio, etc.), a network architecture with more than one hidden layer might be required. In case of the inclusion of more input parameters, the size of training data would also grow multiplicatively. This is one of the challenges in scaling the learning of ANN to a wider range of input parameters.

As for the choice of training algorithm, 'Bayesian Regularization' was a preferred choice due to its better generalization outside the training data than other algorithms. Following that, testing serves the purpose of checking how well the trained model performs outside the trained data. Since the model is trained to minimize the error between known targets and model predictions, model performance is always good in training data. For testing purpose, the ANN must only be given the input values (profile parameters) and its prediction must be compared with the expected/known output (which in this case is the specific power). Hence, for testing the ANN, a chunk of data from the originally generated data-set was set aside before feeding it to the model for training. This kept aside data can serve as the testing data-set post training.

Hence out of the close to 30000 profile data points, only ~24000 randomly chosen data profiles were used for training the model and the remaining were later used for testing the performance of the trained model.

The ANN is basically tasked to predict the specific power for given profile as closely as possible to the specific power for the same profile calculated by solving chamber model. To evaluate how well it does this job, the specific power predictions and the calculated specific powers can be plotted on a graph. Ideally, there will be a perfect correlation between these two quantities marked by 100% accuracy of ANN prediction. The linear correlation coefficients  $R$  or  $R^2$  could be good measures of the performance of ANN. Another way to evaluate the performance of ANN is by looking at the %errors between predicted and target specific powers for the testing data points.

For the ANN under discussion, 80% data points were randomly picked up for training and the remaining 20% were used for testing. During training, the training algorithm had to pass over the entire training data-set approximately 600 times (epochs) to find the best combination of weights and biases for constituent neurons in the network. This is a time intensive procedure taking several minutes to do so. At the end of the training, the model could predict the specific powers with more than 99% accuracy for the maximum number of data points in the training data-set. A  $R$  value of 0.9930 was achieved for the training data-set which indicates that the ANN was able to fit well over the training data.

Whatsoever might be the performance in training, it is not considered a good model unless it predicts well outside the training data. A good model generalizes well outside the training data. Hence the ANN was evaluated on the testing data-set of ~6000 data-points. Similar correlation plot is generated in Figure B.3 which shows that the ANN works very well within the testing data too, with a correlation factor of  $R=0.9932$ .

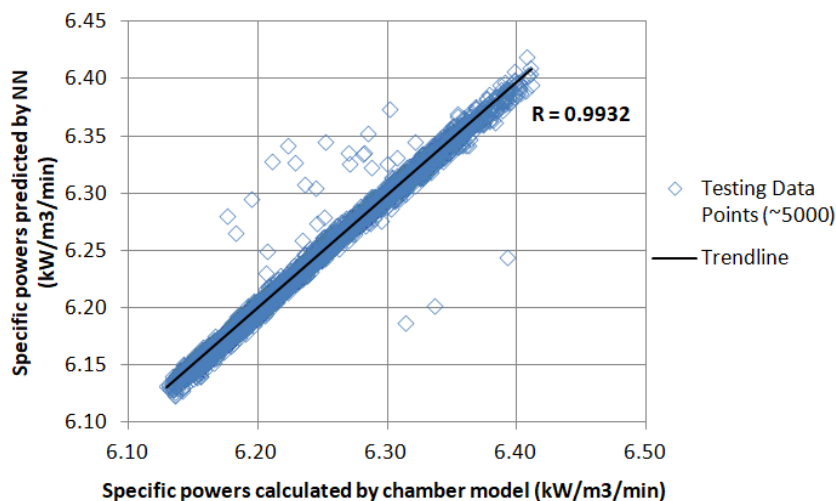


**Figure B.3:** Plot of the specific powers predicted by ANN against those calculated by solving the chamber model for all the profiles in testing data-set

Mind that the data in testing data-set is previously unseen by the model and it still is able to predict the specific powers for these profiles with tremendous accuracy. If

the %error between predicted specific powers and target specific powers is calculated, only 30 out of the  $\sim 6000$  profiles have prediction errors greater than 0.3%. That is, more than 99.5% profiles in the test data had their specific powers predicted by the ANN within 0.3% accuracy. More so, more than 90% profiles had their specific power predictions within 0.1% of the thermodynamically calculated specific power.

The trained NN is able to predict the specific power based on input values relatively quickly than the physics based solver. This is possible because the ANN is essentially working with linear expressions of the form  $wx + b$  at each neuron whereas the physics based solver works with differential equations and their numerical solutions. The SCORPATH solver used in this study is one of the fastest chamber models which does one thermodynamic calculations in approximately 0.3 seconds. The ANN trained on the data from SCORPATH can predict the specific powers as quickly as 12 millisecond. Obviously, the speed is gained but at the cost of versatility; since data-based ANN model can not predict for anything outside its own scope whereas the physics based model can adapt.

This study can be summarized as following-

- ANN are capable of predicting the specific powers for different rotor profile shapes (with limited variation of only inputs) with an accuracy of more than 99%.
- The higher accuracy of prediction is linked with size of the data-set. Scaling the model to include more input parameters would inflate the required training data-set by multiple orders.
- The trained ANN can predict the specific power (data-based prediction) 25000 times faster than it takes for the calculation of the specific power in a solver (physics based calculation).
- The ANN only mimics the physics based solver over the range of training data. It needs to be updated in case of any fundamental change in the physics based model or the range of inputs.

It is hereby demonstrated in a limiting sense that a computer program could learn predict energy efficiency for different profile shapes through rigorous virtual experimenting with them. This approach however is computationally very extensive in its current form. The data-set of 50000 profiles used in this study has relatively very few variables (only 5); still it takes several hours to generate and calculate performances of all these profiles. On top of that, the chamber model for simulating a compression process might be frequently updated based on experiments or a better understanding of the physics of the process. In such cases, the knowledge base for training would need to be updated too.

However, in light of these promising results, neural networks and artificial intelligence on the large pose as promising candidates for a further application in profiling. If the challenges such as data-set scaling and accuracy are properly addressed in near future, the ‘machine intelligence’ developed by NN may be used backwards for generating profiles with desired energy efficiency and other criteria. Scope of the current

research can also be expanded by application of another class of generative AI algorithms, namely Conditional Generative Adversarial Networks (CGAN) (Mirza and Osindero, 2014) to rotor profiling. These class of algorithms use deep convolutional neural networks (CNN) which generate images based on certain conditional parameters. If these models are trained on images of different rotor profiles and the conditional parameter are set to the desirable parameters associated with these profiles, such algorithms should in theory be able to generate rotor profiles on their own based on the desirable parameters which could be energy efficiency or manufacturability. This would be a radically different approach to rotor profile generation and optimization. The initial study presented hereby builds confidence in the potential of these class of techniques and opens a strong future scope for them.

# List of Publications

The academic contributions made during the time this study was carried out are listed below:

## Patent

- “Improved screw compressor rotor with homotopic curves”, IN Patent App. 2022-21019595. (*under examination*)

## Journal Article

- “Experimental validation of the screw compressor oil drag model for various rotor profiles”, 2023 Proceedings of the Institution of Mechanical Engineers, Part E: Journal of Process Mechanical Engineering, SAGE Publications Sage UK: London, England.

## Conference Papers

- “Application of path homotopy in twin screw compressor rotor profile design”, proceedings of the 12<sup>th</sup> International Conference on Compressors and their Systems (Compressors 2021), 6th-8th September 2021, London, United Kingdom. *Published in IOP Conference Series: Materials Science and Engineering, Volume 1180, P. 012004.*
- “Training neural networks to predict the energy efficiency of screw rotor profiles”, proceedings of the 2022 International Compressor Engineering Conference, 10th-14th July 2022, Purdue University, USA. *Published on Purdue e-Pubs, <https://docs.lib.purdue.edu/icec/2777>.*
- “Experimental investigation of the effect of oil injection flow rate on the performance of oil-injected twin-screw compressor”, proceedings of the 2022 International Compressor Engineering Conference, 10th-14th July 2022, Purdue University, USA. *Published on Purdue e-Pubs, <https://docs.lib.purdue.edu/icec/2775>.*
- “Contribution of modern rotor profiles to energy efficiency of screw compressors”, proceedings of the 11<sup>th</sup> International Conference on Screw Machines (ICSM 2022),

7th-8th September 2022, Dortmund, Germany. *Published in IOP Conference Series: Materials Science and Engineering, Volume 1267, P. 012006.*

- “On performance optimization for oil-injected screw compressors using different evolutionary algorithms”, proceedings of the 11<sup>th</sup> International Conference on Screw Machines (ICSM 2022), 7th-8th September 2022, Dortmund, Germany. *Published in IOP Conference Series: Materials Science and Engineering, Volume 1267, P. 012021.*

# Bibliography

Abdan, S.

2023. *Investigation of Mechanical Losses in Oil-flooded, Twin-screw Air Compressors*. PhD thesis, City, University of London.

Abdan, S., S. Patil, N. Stosic, A. Kovacevic, and I. Smith

2023. Experimental validation of the screw compressor oil drag model for various rotor profiles. *Proceedings of the Institution of Mechanical Engineers, Part E: Journal of Process Mechanical Engineering*, P. 09544089231163514.

Abdan, S., N. Stosic, A. Kovacevic, I. Smith, and N. Asati

2021. Estimation of radial shaft seal, oil drag and windage loss in twin screw oil injected compressor. In *IOP Conference Series: Materials Science and Engineering*, volume 1180, P. 012010. IOP Publishing.

Abdan, S., N. Stosic, A. Kovacevic, I. Smith, and N. Asati

2022. Oil drag loss in oil-flooded, twin-screw compressors. *Proceedings of the Institution of Mechanical Engineers, Part E: Journal of Process Mechanical Engineering*, P. 09544089221115493.

Amosov, P., N. Bobrikov, I. Svarc, and A. Vernii

1977. *Vintovie kompresornie mashinii-Spravochnik (Screw Compression Machines-Handbook)*. Mashinstroenie, Leningrad, Russia.

Andreev, P. A.

1961. *Vintovie kompresornie mashinii (Screw Compression Machines)*. SUDPROM Leningrad, Russia.

Armstrong, M. A.

2013. *Basic topology*. Springer Science & Business Media.

Astberg, A.

1984. Screw rotor machine and rotor profile therefor. US Patent 4,435,139.

Bammert, K.

1982. Intermeshing screw rotor machine with specific thread profile. US Patent 4,350,480.

Bowman, J. L.

1983. Helical screw rotor profiles. US Patent 4,412,796.

Box, M.

1965. A new method of constrained optimization and a comparison with other methods. *The Computer Journal*, 8(1):42–52.

Bradski, G.

2000. The opencv library. *Dr. Dobb's Journal: Software Tools for the Professional Programmer*, 25(11):120–123.

Cavatorta, P. and U. Tomei

2014. Screw compressor having male and female rotors with profiles generated by enveloping a rack profile. US Patent 8,702,409.

Chen, C.-H.

1995. Screw compressor with rotors having hyper profile. US Patent 5,454,701.

Dmitriev, O., E. Tabota, and I. A. EurIng

2015. A miniature rotary compressor with a 1: 10 compression ratio. In *IOP Conference Series: Materials Science and Engineering*, volume 90, P. 012055. IOP Publishing.

Dym, N., A. Shtengel, and Y. Lipman

2015. Homotopic morphing of planar curves. In *Computer Graphics Forum*, volume 34, Pp. 239–251. Wiley Online Library.

Edstrom, S. E.

1992. A modern way to good screw rotors. *Proceedings of the 1992 International Compressor Engineering Conference*, Paper 832.

EDUBCA

Accessed December 2022. Uncertainty formula. **url:** <https://www.educba.com/uncertainty-formula/>.

Fleming, J. S., Y. Tang, and H. Anderson

1994. Twin screw compressor performance and its relationship with rotor cutter blade shape and manufacturing cost. *Proceedings of the 1994 International Compressor Engineering Conference*, Paper 1050.

Fleming, J. S., Y. Tang, and G. Cook

1998. The twin helical screw compressor part 2: a mathematical model of the working process. *Proceedings of the institution of mechanical engineers, Part C: journal of mechanical engineering science*, 212(5):369–380.

Fujiwara, M., K. Kasuya, T. Matsunaga, and M. Watanabe

1984. Computer modeling for performance analysis of rotary screw compressor. *Proceedings of the 1984 International Compressor Engineering Conference*, Paper 503.

Géron, A.

2019. *Hands-on machine learning with Scikit-Learn, Keras, and TensorFlow: Concepts, tools, and techniques to build intelligent systems*. O'Reilly Media, Inc.

- Gohman, X. I.  
1886. *Teorija zacepljenij, obobwennaja i razvitaja putem analiza (Theory of Gearing, Generalized and Developed by Analysis)*. Odessa, Russia.
- Gräßer, M. and A. Brümmer  
2017. Influence of water and oil clearance flow on the operational behavior of screw expanders. *Proceedings of the Institution of Mechanical Engineers, Part E: Journal of Process Mechanical Engineering*, 23(1):38–46.
- Gray, L., T. Stratman, B. Conley, B. Ransdell, and D. Peana  
2018. Complex screw rotors. US Patent App. 15/760,086.
- Guggenheimer, H. W.  
1977. *Differential Geometry*. Dover Publications, Inc., New York, USA.
- Guo, C. and Y. Tang  
2003a. Influence of process parameters on screw rotor profiles. *Machining science and technology*, 7(1):105–118.
- Guo, C. and Y. Tang  
2003b. Screw rotor profile manufacturability. *Machining science and technology*, 7(1):53–64.
- Hanjalic, K. and N. Stosic  
1993. Scorpath—screw compressors rotor profiling and thermodynamics. *User Manual*.
- Hanjalic, K. and N. Stosic  
1997. Development and optimization of screw machines with a simulation model—part ii: Thermodynamic performance simulation and design optimization. *Journal of fluids engineering*, 119(3):664–670.
- Haslinger, J. and R. A. Mäkinen  
2003. *Introduction to shape optimization: theory, approximation, and computation*. SIAM.
- Hauser, J., M. Beinert, and D. Huettermann  
2016. High pressure, single stage rotor. US Patent App. 14/600,997.
- Hauser, J., A. Bruemmer, and K. Kauder  
2008. Rotor profile generation and optimization of screw machines using nurbs. *Proceedings of the 2008 International Compressor Engineering Conference*, Paper 1861.
- Hauser, J. and A. Brümmer  
2011. Geometrical abstraction of screw compressors for thermodynamic optimization. *Proceedings of the Institution of Mechanical Engineers, Part C: Journal of Mechanical Engineering Science*, 225(6):1399–1406.

- Helpertz, M.  
2003. *Methode zur stochastischen Optimierung von Schraubenrotorprofilen*. PhD thesis, Technische Universität Dortmund.
- Hough, D., S. J. Morris, and A. D. Barber  
1987. Screw rotor machines with specific tooth profiles. US Patent 4,636,156.
- Huang, C.-Y.  
2015. *New Twin Screw Compressor Design by Deviation Function Method*. PhD thesis, UCLA.
- Jones, E., T. Oliphant, P. Peterson, et al.  
2001–. SciPy: Open source scientific tools for Python. **url:** <http://www.scipy.org/>.
- Kauder, K., M. Helpertz, B. Reusch, and S. Berlik  
2002. Optimisation methods for rotors of twin-screw compressors. *VDI BERICHTE*, 1715:29–50.
- Kim, J. S. and J. H. Lee  
2004. Rotor profile for screw compressors. US Patent 6,779,993.
- Kovacevic, A., N. Stosic, E. Mujic, and I. K. Smith  
2005. Design integration for screw compressors. *ASME International Mechanical Engineering Congress and Exposition*, 42118:29–33.
- Kovacevic, A., N. Stosic, and I. Smith  
2007. *Screw compressors: three dimensional computational fluid dynamics and solid fluid interaction*. Springer Science & Business Media.
- Krigar, H.  
1878. Screw blower. DE Patent 4121A.
- Lee, H.-T.  
1990. Screw-rotor machine with an ellipse as a part of its male rotor. US Patent 4,890,992.
- Lee, H.-T., Z.-H. Fong, and Y.-R. Wu  
2006. Mechanism of the screw rotor. US Patent App. 10/961,056.
- Liao, S.  
2004. On the homotopy analysis method for nonlinear problems. *Applied Mathematics and Computation*, 147(2):499–513.
- Litvin, F. L.  
1989. *Theory of gearing*. NASA Reference Publication 1212, USA.
- Lysholm, A.  
1943. A new rotary compressor. *Proceedings of the Institution of Mechanical Engineers*, 150(1):11–16.

- Lysholm, A.  
1967. Screw rotor machine. US Patent 3,314,598.
- Lysholm, A. and B. G. K. William  
1938. Rotary compressor. US Patent 2,111,568.
- Mäkinen, R. A., J. Périaux, and J. Toivanen  
1999. Multidisciplinary shape optimization in aerodynamics and electromagnetics using genetic algorithms. *International Journal for Numerical Methods in Fluids*, 30(2):149–159.
- Malkin, S. and C. Guo  
2008. *Grinding technology: theory and application of machining with abrasives*. Industrial Press Inc.
- Menssen, E.  
1977. Screw compressor with involute profiled teeth. US Patent 4,028,026.
- Mirza, M. and S. Osindero  
2014. Conditional generative adversarial nets. *arXiv preprint arXiv:1411.1784*.
- Mould, R., G. Richmond, and D. Thrall  
1982. Computer aided manufacture of original equipment manufacturer screw compressor rotors. *Proceedings of the 1982 International Compressor Engineering Conference*, Paper 390.
- Patil, S.  
2022. Improved screw compressor rotor with homotopic curves. IN Patent App. 202221019595.
- Patil, S., M. Davis, N. Stosic, A. Kovacevic, and N. Asati  
2022. Contribution of modern rotor profiles to energy efficiency of screw compressors. Presented at the 11<sup>th</sup> International Conference on Screw Machines (ICSM 2022), TU Dortmund.
- Patil, S., N. Stosic, A. Kovacevic, I. Smith, and N. Asati  
2021. Application of path homotopy in twin screw compressor rotor profile design. In *IOP Conference Series: Materials Science and Engineering*, volume 1180, P. 012004. IOP Publishing.
- Persson, J. E.  
1968. Screw rotor machines and profiles. US Patent 3,414,189.
- Radzevich, S. P.  
2019. *Geometry of surfaces: a practical guide for mechanical engineers*. Springer Nature: Cham, Switzerland.

- Read, M., N. Stosic, and I. Smith  
2017. Operational characteristics of internally geared positive displacement screw machines. In *ASME International Mechanical Engineering Congress and Exposition*, volume 58417, P. V006T08A032. American Society of Mechanical Engineers.
- Rinder, L.  
1979. *Schraubenverdichter (Screw Compressor, in German)*. Springer-Verlag, Wien, Austria.
- Rinder, L.  
1987. Screw rotor profile and method for generating. US Patent 4,643,654.
- Robert, N. H.  
1952. Helical rotary engine. US Patent 2,622,787.
- Sakun, I. A.  
1960. *Screw Compressors (in Russian)*. Mashgiz Moscow, Russia.
- Sangfors, B.  
1984. Computer simulation of the oil injected twin screw compressor. *Proceedings of the 1984 International Compressor Engineering Conference*, Paper 502.
- Sasane, A.  
2016. *Optimization in function spaces*. Courier Dover Publications.
- Sauls, J.  
1998. An analytical study of the effects of manufacturing on screw rotor profiles and rotor pair clearances. *VDI BERICHTE*, 1391:231–242.
- Sauls, J.  
2000. Application of manufacturing simulation for screw compressor rotors. *Proceedings of the 2000 International Compressor Engineering Conference*, Paper 1475.
- Sauls, J.  
2002. Comparison of screw rotor profiles from a manufacturing perspective. *Proceedings of the 2002 International Compressor Engineering Conference*, Paper 1580.
- Schibbye, C. B.  
1979. Screw-rotor machine with straight flank sections. US Patent 4,140,445.
- Schibbye, L.  
1970. Improvements in and relating to rotary positive displacement machines of the intermeshing screw type and rotors therefor. GB Patent App. 3,421,766 A.
- Sheth, D. and S. Malkin  
1990. Cad/cam for geometry and process analysis of helical groove machining. *CIRP annals*, 39(1):129–132.

Singh, P. J. and J. L. Bowman

1988. Calculation of blow-hole area for screw compressors. *Proceedings of the 1986 International Compressor Engineering Conference*, Paper 786.

Singh, P. J. and A. D. Onuschak

1984. A comprehensive, computerized method for twin-screw rotor profile generation and analysis. *Proceedings of the 1984 International Compressor Engineering Conference*, Paper 501.

Stosic, N.

1993. Scorpath - screw compressor optimal rotor profiles and thermodynamics. **url:** <http://www.staff.city.ac.uk/~ra600/DISCO/DISCO%20SCORPATH.htm>.

Stosic, N.

1998. On gearing of helical screw compressor rotors. *Proceedings of the Institution of Mechanical Engineers, Part C: Journal of Mechanical Engineering Science*, 212(7):587–594.

Stosic, N.

2006a. Evaluating errors in screw rotor machining by tool to rotor transformation. *Proceedings of the Institution of Mechanical Engineers, Part B: Journal of Engineering Manufacture*, 220(10):1589–1596.

Stosic, N.

2006b. A geometric approach to calculating tool wear in screw rotor machining. *International Journal of Machine Tools and Manufacture*, 46(15):1961–1965.

Stosic, N. and K. Hanjalic

1997. Development and optimization of screw machines with a simulation model—part i: Profile generation. *Journal of fluids engineering*, 119(3):659–663.

Stosic, N., K. Hanjalic, J. Koprivica, N. Lovren, and M. Ivanovic

1986. Cad of screw compressor elements. *Strojarstvo Journal Zagreb*, 28:181.

Stosic, N., I. Smith, and A. Kovacevic

2005. *Screw compressors: mathematical modelling and performance calculation*. Springer Science & Business Media.

Stosic, N., I. Smith, A. Kovacevic, and K. Venumadhav

2000. Retrofit ‘n’ rotors for efficient oil-flooded screw compressors. *Proceedings of the 2000 International Compressor Engineering Conference*, Paper 1480.

Stosic, N., I. K. Smith, and A. Kovacevic

2002. Screw compressor: A strong link in the development chain. *Tehnicki Vjesnik*, 9(3):39–44.

- Stosic, N., I. K. Smith, and A. Kovacevic  
 2003a. Opportunities for innovation with screw compressors. *Proceedings of the Institution of Mechanical Engineers, Part E: Journal of Process Mechanical Engineering*, 217(3):157–170.
- Stosic, N., I. K. Smith, and A. Kovacevic  
 2003b. Optimisation of screw compressors. *Applied Thermal Engineering*, 23(10):1177–1195.
- Stosic, N., I. K. Smith, A. Kovacevic, and E. Mujic  
 2011a. Geometry of screw compressor rotors and their tools. *Journal of Zhejiang University-SCIENCE A*, 12(4):310–326.
- Stosic, N., I. K. Smith, A. Kovacevic, and E. Mujic  
 2011b. Review of mathematical models in performance calculation of screw compressors. *International Journal of Fluid Machinery and Systems*, 4(2):271–288.
- Stosic, N. R.  
 1997. Plural screw positive displacement machines. International Patent WO1997043550A1.
- Stosic, N. R.  
 2017. Reduced noise screw machines. US Patent 9,714,572.
- Su, S.-H. and C.-H. Tseng  
 2000. Synthesis and optimization for rotor profiles in twin rotor screw compressors. *Journal of mechanical design*, 122(4):543–552.
- Svígler, J.  
 2010. *A treatise on the theory of screw machines*. Západočeská univerzita.
- Tang, Y.  
 1995. *Computer aided design of twin screw compressors*. PhD thesis, University of Strathclyde.
- Tang, Y.  
 2007. Meshing helical rotors. US Patent 7,163,387.
- Tang, Y. and J. Fleming  
 1994. Clearances between the rotors of helical screw compressors: their determination, optimization and thermodynamic consequences. *Proceedings of the institution of mechanical engineers, Part E: journal of process mechanical engineering*, 208(2):155–163.
- Utri, M., A. Brümmer, and J. Hauser  
 2018. Comparison of thermodynamic efficiency between constant, dual and multiple lead rotors for an industrial air screw compressor. In *IOP conference series: materials science and engineering*, volume 425, P. 012025. IOP Publishing.

- Vaidya, A.  
2019. Screw rotor with high lobe count. US Patent 10,436,196.
- Weih, G.  
2019. Rotor pair for a compression block of a screw machine. US Patent 10,400,769.
- Wilfred, B. and N. H. Robert  
1963. Rotary compressors. US Patent 3,073,514.
- Wu, Y.-R. and Z.-H. Fong  
2008. Improved rotor profiling based on the arbitrary sealing line for twin-screw compressors. *Mechanism and Machine Theory*, 43(6):695–711.
- Wu, Y.-R. and Z.-H. Fong  
2009. Optimization design of an explicitly defined rack for the generation of rotors for twin-screw compressors. *Mechanism and Machine Theory*, 44(1):66–82.
- Yates, R. C.  
1947. *A Handbook on Curves and their Properties*. JW Edwards, USA.
- Zaytsev, D. and C. I. Ferreira  
2005. Profile generation method for twin screw compressor rotors based on the meshing line. *International Journal of Refrigeration*, 28(5):744–755.
- Ziviani, D., I. H. Bell, X. Zhang, V. Lemort, M. De Paepe, J. E. Braun, and E. A. Groll  
2020. Pdsim: Demonstrating the capabilities of an open-source simulation framework for positive displacement compressors and expanders. *International Journal of Refrigeration*, 110:323–339.